SPINOCEREBELLAR ATAXIA TYPE 2:

ATAXIN-2 MECHANISMS AND BLOOD BIOMARKERS

by

Nesli Ece Şen

B.S., Molecular Biology and Genetics, Bilkent University, 2012

Submitted to the Institute for Graduate Studies in

Science and Engineering in partial fulfillment of

the requirements for the degree of

Master of Science

Graduate Program in Molecular Biology and Genetics

Boğaziçi University

2015

To my grandparents Gülşen and Mahmut Bekler;

my first teachers who inspired me to explore.

ACKNOWLEDGEMENTS

I would like to express my sincere gratitude to my thesis supervisor Prof. A. Nazlı Başak for her endless support, encouragement and invaluable guidance, both scientifically and personally, throughout this work. I am also deeply thankful to my co-advisor Prof. Georg Auburger and also Suzana Gispert for providing me the opportunity of an excellent academic and experimental training at Goethe University.

I would like to extend my thanks to Prof. Esra Battaloğlu, Prof. Sibel Ertan and Assist. Prof. İbrahim Yaman for their precious contributions to this thesis.

The presence of all NDAL members has brought nothing but happiness, strength and improvement to my life, I am more than grateful to every single one of them. I am also thankful for the hospitality and friendship provided by all Auburger Lab members.

I respectfully acknowledge the Suna and İnan Kıraç Foundation, Boğaziçi University Research Funds and Goethe University Research Funds for their generous financial support that renders our research possible.

I cordially thank the patients and family members from the large SCA2 pedigree for their hospitality during the sample collection in Balıkesir, and their overall cooperation.

Last but not least, I am eternally grateful to my beloved family, especially my mother Sibel Bekler Keçeci and grandparents Gülşen and Mahmut Bekler; my role-model, and the first teachers I had. They have not only taught me how to read and write, but also to be determined for what I really desire and to never give up.

ABSTRACT

SPINOCEREBELLAR ATAXIA TYPE 2:

ATAXIN-2 MECHANISMS AND BLOOD BIOMARKERS

Spinocerebellar Ataxia Type 2 is an autosomal dominant movement disorder caused by trinucleotide expansions in the *ATXN2* gene (>34 CAG repeats). Intermediate expansions of 26-39 repeats are considered as risk factors for several other neurodegenerative disorders, such as ALS, PD and HSP. Ataxin-2 localizes to the rough-ER, binds to the 3'-UTRs of mRNA molecules together with PABPC1 and modulates ribosomal translation. Under stress conditions, ataxin-2 controls the assembly of stress granules, where it sequesters mRNAs and vital proteins that regulate cellular growth and proliferation. Although ataxin-2 is known to contribute to many cellular processes, its exact function is not entirely understood. In order to elucidate ataxin-2 function and the expansion-related pathogenesis and to identify blood biomarkers of SCA2, the transcriptome profiles of *Atxn2* knock-out mice and SCA2 patients from a large pedigree were examined. A cluster of genes, whose products are normally secreted to the extracellular fluids, emerged among the 100 most significantly downregulated genes in the mouse transcriptome data. Significant upregulations of Apo-AI, Hemopexin and SERPINA1 proteins were found in *Atxn2*-KO mouse liver. Candidate blood RNA biomarkers were inferred from the whole blood transcriptome data of SCA2 patients via either direct unbiased filtration or by focusing on neurodegeneration-associated genes. Independent validations of the candidate genes revealed significant upregulations in *ETV7*, *SERINC2*, and *ATXN1*, along with downregulations in *DACT1*, *MATR3*, and *PHTF2* in patient blood. Gene Set Enrichment Analysis of the patient transcriptome data presented an enrichment in the Parkinson's disease pathway, key components of which were further analyzed in the context of *ATXN2* knock-down neuroblastoma cells. This thesis exhibits insights into the native function and expansion-induced pathogenesis of ataxin-2 by investigating the downstream effects of *ATXN2* deficiency and expansions on global and gene-specific transcription profiles.

ÖZET

SPİNOSEREBELLAR ATAKSİ TİP 2:

ATAKSİN-2 MEKANİZMASI VE KAN BİYO-BELİRTEÇLERİ

Spinoserebellar ataksi tip 2, *ATXN2* genindeki trinükleotid artışı (>34 tekrar) sonucu görülen otozomal dominant geçişli bir hareket bozukluğudur. Tekrar sayısının 26-39 arasında olması ALS, PH, HSP gibi bir takım başka nörodejeneratif hastalıklar için de risk oluşturur. Ataksin-2 proteini granüllü ER'da bulunur, mRNA moleküllerinin 3'-UTR uçlarına PABPC1 ile bağlanarak ribozomal translasyonu kontrol eder ve stres koşulları altında translasyonu baskılanmış mRNAların ve hücre büyüme/bölünmesini kontrol eden proteinlerin hapsedildiği stres granüllerinin oluşumunu düzenler. Ataksin-2'nin birçok mekanizmada etkin olduğu bilinse de, kesin görevi henüz tam olarak anlaşılamamıştır. Bu tez çerçevesinde Ataksin-2'nin işlevini ve tekrar-artışının neden olduğu patogenezi anlamak ve SCA2 hastalığı için kan biyo-belirteçleri bulmak amacıyla, *Atxn2* knock-out farelerde ve geniş bir SCA2 ailesinden alınan hasta örneklerinde transkriptom analizi yapıldı. Fare transkriptom verisinde en fazla azalma gösteren faktörler arasında normal şartlarda hücre dışı-sıvılara salgılanan bir grup protein gözlemlendi. Bu proteinlerden Apo-AI, Hemopexin ve SERPINA1 *Atxn2*-KO fare karaciğerinde anlamlı artışlar gösterdi. Kan biyo-belirteci olmaya aday genler SCA2 hastalarının transkriptom verilerinden ya tarafsız filtreleme ya da nörodejenerasyonla ilgili genlere odaklanma yaklaşımlarıyla elde edildi. Bu aday genlerin bağımsız yöntemlerle doğrulanması sonucu, *ETV7*, *SERINC2* ve *ATXN1* genlerinde anlamlı artışlar ve *DACT1*, *MATR3* ve *PHTF2* genlerinde anlamlı azalmalar görüldü. Hastaların transkriptom verileri kullanılarak yapılan Gen Seti Zenginleştirme Analizi Parkinson hastalığı yolağında toplu bir artış ortaya koydu. Bir sonraki aşamada bu yolağa dahil olan başlıca genler *ATXN2* knock-down nöroblastoma hücrelerinde incelendi. Tezde, yabanıl ataksin-2 ile mutasyona uğramış ataksin-2'nin hücre düzeyindeki etkileri gözlemlenerek, farklı mekanizmalarda etkin olduğu bilinen ataksin-2 proteininin normal işlevi ve tekrar-artışına bağlı patogenezine ışık tutulmaktadır.

TABLE OF CONTENTS

ACKNOWLEDGEMENTS iv
ABSTRACT v
ÖZET vi
LIST OF FIGURES x
LIST OF TABLES xii
LIST OF SYMBOLS xiv
LIST OF ACRONYMS/ABBREVIATIONS xvi
1. INTRODUCTION 1
1.1. Classification of Neurodegenerative Disorders 1
1.2. Spinocerebellar Ataxias and Common Mechanisms 5
1.3. Clinical Features of SCA2 9
1.4. SCA2 Genetics and Ataxin-2 Mechanism 13
1.4.1. Ataxin-2 Function and Mechanisms of Pathogenicity 17
1.4.2. Implication of *ATXN2* in Other Neurodegenerative Disorders 22
1.5. Biomarkers of SCA2 26
2. PURPOSE 28
3. SUBJECTS AND MATERIALS 29
3.1. SCA2 Patients and Healthy Controls from a Large Turkish Pedigree 29
3.1.1. Equipment and Solutions for DNA Isolation and PCR Amplification 31
3.1.2. Equipment and Solutions for Agarose Gel Electrophoresis and Gel Extraction 31
3.2. *Atxn2* Knock-Out Mouse Line 32
3.3. *Atxn2* Knock-Down SH-SY5Y Line and Cell Culture Equipment 33
3.4. Equipment and Solutions for RNA Isolation, DNaseI Treatment and cDNA Synthesis 34
3.5. qRT-PCR Equipment and Taqman Assays 35
3.6. Equipment and Solutions for Protein Isolation, Quantitation and SDS-PAGE 37

3.7. Quantitative Immunoblotting Equipment, Solutions and Antibodies 38
3.8. Software, Online Tools and Databases 40
3.9. General Laboratory Equipment, Chemicals and Kits 41
4. METHODS 46
4.1. SCA2 Patient Peripheral Blood Samples 47
4.1.1. Blood Collection, Transport and Storage 47
4.1.2. DNA Isolation and *ATXN2* Poly-Q Repeat Size Determination 47
4.2. *Atxn2* Knock-Out Mouse Tissue Samples 49
4.3. *ATXN2* Knock-Down SH-SY5Y Cell Culture 49
4.3.1. Generation of *ATXN2* Knock-Down Cell Line 49
4.3.2. General Culture Conditions, Freezing and Thawing 49
4.3.3. Time-Course Starvation Experiments 51
4.4. RNA Isolation 53
4.5. DNaseI Treatment and cDNA Synthesis 54
4.6. Expression Analyses with Quantitative Real Time-PCR 55
4.7. Protein Isolation and Quantitation 56
4.8. SDS-PAGE and Quantitative Immunoblot Analyses 57
4.9. High-Throughput Transcriptome Analyses 59
4.9.1. Microarray Analysis of *Atxn2*-KO Mice 59
4.9.2. Deep RNA-Sequencing Analysis of SCA2 Patients 60
4.10. Gene Set Enrichment Analysis 60
4.11. Statistical Analyses 61
5. RESULTS 62
5.1. Identification of Cerebellum and Liver Biomarkers in *Atxn2*-KO Mice 63
5.1.1. High-Throughput Expression Analysis Results 63
5.1.1.1. Network of Secreted Factors Among Differentially Downregulated Genes 63
5.1.2. Secretion Network Protein Levels in *Atxn2*-KO Mice 64
5.1.3. Expression Analysis of ER-Associated Genes in *Atxn2*-KO Mice 68
5.1.4. Expression Analysis of Secretion Network Genes in *Atxn2*-KO Mice 69
5.2. Identification of Blood Biomarkers in SCA2 Patients 72

5.2.1. Genotypes of the SCA2 Pedigree 72
5.2.2. High-Throughput Deep RNA-Sequencing Analysis Results..... 73
5.2.2.1. Candidate Genes Acquired by Unbiased Filtering 74
5.2.2.2. Neurodegeneration-Associated Genes as Candidates..... 78
5.3. Characterization of the Interplay between Ataxin-2 and Mitochondrial Factors 82
5.3.1. Enrichment of the Parkinson's Disease Pathway Genes in SCA2 Patients..... 82
5.3.2. Expression Analysis of the Mitochondrial Genes in *Atxn2*-KO Mice 84
5.3.3. Expression Analysis of the Mitochondria- and Ataxin-2-Associated Genes in *ATXN2*-KD SH-SY5Y Cells..... 86
6. DISCUSSION 90
6.1. Cerebellum and Liver Biomarkers in *Atxn2*-KO Mice..... 92
6.1.1. Potential Dysregulation of the ER-Golgi Secretory Pathway..... 93
6.2. Blood Biomarkers in SCA2 Patients 95
6.3. Gene Set Enrichment Analysis 98
6.4. The Relationship between Ataxin-2 and the Mitochondrial Factors 99
7. CONCLUSION..... 103
APPENDIX A: SUPPLEMENTARY TABLES 105
APPENDIX B: PUBLICATIONS..... 113
REFERENCES 114

LIST OF FIGURES

Figure 1.1. Classification of the CNS disorders based on the most distinctive clinical phenotype and the anatomical location of the lesion. 2

Figure 1.2. Currently known repeat expansion units. 4

Figure 1.3. Graphical visualization of the spatial neuronal loss in different poly-Q SCAs. 7

Figure 1.4. The anatomical structure of the cerebellar cortex. 10

Figure 1.5. MRI scan of a SCA2 patient showing cerebellar atrophy in the midsaggital section. 11

Figure 1.6. The correlation of AO with CAG repeat expansion size in *ATXN2*. 15

Figure 1.7. Known functional domains of ataxin-2 protein. 18

Figure 1.8. Recruitment of microRNAs to the 3'-UTRs of target mRNAs mediated by the interaction between ataxin-2 and PABP. 19

Figure 1.9. *ATXN2*-associated disease mechanisms. 20

Figure 1.10. Signaling cascade leading to the sequesteration of TORC1 into stress granules by the yeast ortholog of ataxin-2, Pbp1. 21

Figure 1.11. Association of the intermediate-length poly-Q expansions in *ATXN2* with distinct neurodegenerative disorders. 23

Figure 3.1. The large SCA2 pedigree from Balıkesir, Turkey. 30

Figure 4.1. Flow charts summarizing the methods performed with *Atxn2*-KO mouse tissues, SCA2 patient blood samples and *ATXN2*-KD SH-SY5Y cells. 46

Figure 4.2. A schematic view of the counting chamber. 52

Figure 4.3. Layout of the 6-well plates designed for the time-course starvation experiments of NT and *ATXN2*-KD SH-SY5Y cells. 53

Figure 5.1. Summary of the results obtained throughout this thesis. 62

Figure 5.2. The interaction network among the 100 most downregulated genes in *Atxn2*-KO mice cerebellum. 64
Figure 5.3. Fold-change differences of the biomarker candidates at the protein level in *Atxn2*-KO mice cerebellum. 66
Figure 5.4. Fold-change differences of the biomarker candidates at the protein level in *Atxn2*-KO mice liver. 67
Figure 5.5. Expression levels of the ER-associated factors, *Syvn1* and *Sel1l,* in *Atxn2*-KO mice cerebellum. 69
Figure 5.6. Expression levels of the ER-associated factors, *Syvn1* and *Sel1l,* in *Atxn2*-KO mice liver. 69
Figure 5.7. Expression levels of the candidate biomarker genes in *Atxn2*-KO mice cerebellum. 71
Figure 5.8. Expression levels of the candidate biomarker genes in *Atxn2*-KO mice liver. 71
Figure 5.9. Expression levels of the candidate biomarker genes in SCA2 patients showing no statistical significance. 76
Figure 5.10. Expression levels of the candidate biomarker genes in SCA2 patients showing a trend towards significance. 77
Figure 5.11. Expression levels of the candidate biomarker genes in SCA2 patients showing statistically significant dysregulations. 78
Figure 5.12. The interaction network of the significantly dysregulated ALS- and ataxia-associated genes in SCA2 patients. 79
Figure 5.13. Expression levels of the ALS- and ataxia-associated genes in SCA2 patients showing no statistical significance. 81
Figure 5.14. Expression levels of the *MATR3* and *ATXN1* genes in SCA2 patients showing significant dysregulations. 82
Figure 5.15. Highly significant enrichment in the Parkinson's disease pathway. 84
Figure 5.16. Significant downregulations of the mitochondrial genes in *Atxn2*-KO mice cerebellum and liver. 85
Figure 5.17. Expression analysis results of the mitochondria- and ataxin-2-associated genes after time-course starvation of NT- and *ATXN2*-KD SH-SY5Y cells. 89

LIST OF TABLES

Table 1.1. List of the repeat-expansion disorders. 5

Table 3.1. Blood donors from the large SCA2 pedigree. 29

Table 3.2. Solutions and chemicals used in the amplification of *ATXN2* CAG repeat tract. 31

Table 3.3. Primers used in the amplification of *ATXN2* CAG repeat tract. 31

Table 3.4. Materials used in agarose gel electrophoresis. 32

Table 3.5. General information regarding *Atxn2*-KO mouse line. 32

Table 3.6. General information regarding naïve SH-SY5Y cell line. 33

Table 3.7. Target and control shRNA constructs used in the knock-down protocol. 33

Table 3.8. Materials used in the cell culture experiments. 34

Table 3.9. Reagents and kits used for total RNA isolation from different sample types. 34

Table 3.10. Contents of the kits used in DNaseI treatment and reverse transcription of the isolated total RNA. 35

Table 3.11. Materials used in Taqman gene expression assays. 35

Table 3.12. Human Taqman assays. 36

Table 3.13. Murine Taqman assays. 37

Table 3.14. Materials used in protein isolation, quantitation and SDS-PAGE. 37

Table 3.15. Contents of the lysis buffers used in protein isolation. 38

Table 3.16. Contents of the stock solutions used in SDS-PAGE. 38

Table 3.17. Materials used in quantitative immunoblots. 38

Table 3.18. Primary antibodies used in quantitative immunoblots. 39

Table 3.19. Secondary antibodies used in quantitative immunoblots. 39

Table 3.20. Software, tools and databases utilized. 40

Table 3.21. General laboratory equipment. 41

Table 3.22. General chemicals used in various experiments. 44

Table 3.23. Commercially available kits used in various experiments. 45

Table 4.1. Content of the *ATXN2* CAG repeat amplification PCR mix. 48

Table 4.2. PCR conditions for *ATXN2* CAG repeat amplification. 48

Table 4.3. Contents of the different media used in *ATXN2*-KD SH-SY5Y culture experiments. 50

Table 4.4. Content of the reaction mix for qRT-PCR with Taqman probes. 55

Table 4.5. Cycling conditions of the qRT-PCR with Taqman probes. 55

Table 4.6. Contents of the resolving and stacking gels casted in SDS-PAGE. 58

Table 5.1. Summary of the quantitative immunoblot analyses in *Atxn2*-KO mice cerebellum and liver. 65

Table 5.2. Genotype information of the blood donors from the Turkish SCA2 pedigree. 73

Table 5.3. List of the differentially expressed candidate biomarker genes in SCA2 patients. 74

Table 5.4. List of the differentially expressed ALS and ataxia-associated genes in SCA2 patients. 80

Table A1. List of all known spinocerebellar ataxias. 105

Table A2. Significantly upregulated pathways in the blood RNA-sequencing data of SCA2 patients. 107

Table A3. Significantly downregulated pathways in the blood RNA-sequencing data of SCA2 patients. 112

LIST OF SYMBOLS

*	Asterix
#	Number
%	Percent
^	Power
<	Less than
>	Greater than
bp	Basepairs
cm	Centimeter
g	Gram
g	Gravitational force
h	Hour
kb	Kilobase
kDa	Kilo Dalton
M	Molar
mg	Milligram
min	Minute
ml	Milliliter
mm	Millimeter
mM	Millimolar
ng	Nanogram
^{o}C	Celsius degree
pH	Power of Hydrogen
pmol	Picomole
rpm	Revolution per minute
sec	Seconds
T	Trend
U	Unit
V	Volt

α	Alpha
β	Beta
Δ	Delta
µg	Microgram
µl	Microliter
µm	Micrometer
µM	Micromolar

LIST OF ACRONYMS/ABBREVIATIONS

3'	Three prime end
3-D	Three dimensional
5'	Five prime end
A	Adenine
A2BP1	Ataxin-2 binding protein 1
AA/BA	Acrylamide/Bisacrylamide mix
AD	Alzheimer's disease
ADCA	Autosomal dominant cerebellar ataxia
AFF2	AF4/FMR2 family, member 2
AFG3L2	AFG3 ATPase family member 3-like 2
Ala	Alanine
ALS	Amyotrophic lateral sclerosis
ALS2	Alsin
ALSoD	Amyotrophic Lateral Sclerosis Online Database
alt.	Alternatively spliced exon
AMPA	α-amino-3-hydroxy-5-methyl-4-isoxazolepropionate
ANG	Angiogenin
ANOVA	Analysis of variance
AO	Age of onset
Apo	Apolipoprotein
APS	Ammonium persulfate
AR	Androgen receptor
ARCA	Autosomal recessive cerebellar ataxia
Asp	Aspartate
AT	Ataxia telangiectasia
ATM	Ataxia telangiectasia mutated
ATN1	Atrophin-1
ATP	Adenosine-tris-phosphate

ATXN	Ataxin
b-actin	Beta Actin
BEAN1	Brain expressed, associated with NEDD4, 1 , SCA31
BPB	Bromophenol blue
BPES	Blepharophimosis, ptosis and epicanthus inversus
BSA	Bovine serum albumin
C	Cytosine
C9orf72	Chromosome 9 open reading frame 72
Ca^{2+}	Calcium Ion
CACNA1A	Calcium channel, voltage-dependent, alpha 1A subunit
CBD	Corticobasal degeneration
CCD	Cleidocranial dysplasia
CCDC88C	Coiled-coil domain containing 88C
CCHS	Congenital central hypoventilation syndrome
cDNA	Complementary DNA
CHMP2B	Charged multivesicular body protein 2B
Chr.	Chromosomal locus
CJD	Creutzfeldt-Jakob disease
CNS	Central nervous system
CNT	Control
CO_2	Carbondioxide
CpG	C-phosphate-G
Ct	Cycle threshold
Cu	Copper
D	Aspartate
DACT1	Dishevelled-binding antagonist of beta-catenin 1
DCP2	Decapping protein 2
DCTN1	Dynactin 1
DDX6	DEAD/H-box helicase 6
DEAD	Asp-Glu-Ala-Asp
DM	Myotonic dystrophy
DMPK	Dystrophia myotonica-protein kinase
DMSO	Dimethyl sulfoxide

DNA	Deoxyribonucleic acid
DNase I	Deoxyribonuclease I
dNTP	Deoxyribonucleotide triphosphate
DRPLA	Dentatorubral pallidoluysian atrophy
DTT	Dithiothreitol
E	Glutamate
ECL	Enhanced chemiluminescence
EDTA	Ethylenglycoltetraacetic acid
EEF2	Eukaryotic translation elongation factor 2
EGF	Epidermal growth factor
EGFR	Epidermal growth factor receptor
EIF	Eukaryotic initiation factor
ELOVL	Elongation of very long chain fatty acids protein
EPM1	Progressive myoclonic epilepsy 1
ER	Endoplasmic reticulum
ES	Enrichment score
EtOH	Ethanol
ETS1	E-twenty-six family 1
ETV7	ETS family variant 7
FAM	6-Carboxyfluorescein
FCS	Fetal calf serum
FBXW8	F-box and WD repeat domain containing 8
FDR	False discovery rate
FGF14	Fibroblast growth factor 14
FIG4	Polyphosphoinositide phosphatase
FMR1	Fragile X mental retardation 1
FRAXA	Fragile X syndrome
FRAXE	Fragile site, folic acid type, rare, fra(X)(q28) E
FRDA	Friedreich ataxia
FTD	Frontotemporal dementia
FTDP-17	FTD and parkinsonism linked to chr. 17
FUS	Fused in sarcoma
Fwd	Forward primer

FWER	Family-wise error rate
FXN	Frataxin
FXTAS	Fragile X-associated tremor/ataxia syndrome
G	Guanine
GABA	Gamma-aminobutyric acid
GAPDH	Glyceraldehyde 3-phosphate dehydrogenase
GHITM	Growth hormone inducible transmembrane protein
Gln	Glutamine
Glu	Glutamate
GSS	Gerstmann–Sträussler–Scheinker syndrome
GWAS	Genome wide association study
GSEA	Gene Set Enrichment Analysis
H	Histidine
H_2O	Water
dH_2O	Distilled water
HBSS	Hank's Balanced Salt Solution
HCl	Hydrochloric acid
HD	Huntington's disease
HDAC1	Histone deacetylase 1
HDL2	Huntington’s-disease-like 2
HEK293	Human embryonic kidney 293
HeLa	Cervical cancer cells derived from Henrietta Lacks
HEPES	4-(2-hydroxyethyl)-1-piperazineethanesulfonic acid
HFG	Hand–foot–genital syndrome
hnRNP	Heterogeneous nuclear ribonucleoproteins
HPE5	Holoprosencephaly 5
HPRT1	Hypoxanthine-guanine phosphoribosyltransferase 1
Hpx	Hemopexin
HRP	Horseradish peroxidase
HSP	Hereditary Spastic Paraplegia
HTT	Huntingtin
ISSX	X-linked infantile spasm syndrome
ITPR1/InsP3R1	Inositol trisphosphate receptor 1

JPH3	Junctophilin 3
KCNC3	Voltage-gated potassium channel subunit Kv3.3
KCND3	Voltage-gated potassium channel subunit Kv4.3
KD	Knock-down
KO	Knock-out
KRAB	Krueppel-associated box
LBD	Lewy body dementia
LC	Liquid chromatography
LRRK2	Leucine-rich repeat kinase 2
Lsm	Like Sm
LsmAD	Like Sm-associated domain
MATR3	Matrin 3
ME31B	Maternal expression at 31B
MEM	Modified eagle medium
MgCl2	Magnesium Chloride
miRNA	Micro RNA
MJD	Majado-Joseph disease
MRGH	Mental retardation with growth hormone deficiency
MRI	Magnetic resonance imaging
mRNA	Messenger RNA
MS	Mass spectrometry
mTOR	Mammalian target of rapamycin
Mttp	Microsomal triglyceride transfer protein
NaCl	Sodium chloride
ND	Neurodegenerative disorder
NEAA	Non-essential amino acids
NES	Normalized enrichment score
NMDA	N-Methyl-D-aspartate
No.	Number
NOM	Nominal
NOP56	Nucleolar protein 5A, 56 kDa
NT	Non-target
OD	Optical density

OPA1	Optic atrophy 1
OPMD	Oculopharyngeal muscular dystrophy
OPTN	Optineurin
p62/SQSTM1	Sequestosome 1
PABPC1	Poly(A)-binding protein, cytoplasmic 1
PABPN1	Poly(A)-binding protein, nuclear 1
PAGE	Polyacrylamide gel electrophoresis
PAIP	Poly(A)-binding protein interacting protein
PAM2	Poly(A)-binding protein interacting motif 2
PARK2	Parkin
PARK7	Parkinson disease protein 7, DJ-1
P-bodies	Processing body
PBP1	Pab binding protein 1
PBS	Phosphate buffered saline
PCR	Polymerase chain reaction
PD	Parkinson's disease
PDYN	Prodynorphin
PFN1	Profilin 1
PHTF2	Putative homeodomain transcription factor 2
PiD	Pick's disease
PINK1	PTEN-induced putative kinase 1
PMSF	Phenylmethylsulfonyl fluoride
Plin3	Perilipin 3
Poly(A)	Polyadenine
Poly-Q	Polyglutamine
PPP2R2B	Protein phosphatase 2, regulatory subunit B, beta
PRKCG	Protein kinase C, gamma
PSP	Progressive supranuclear palsy
PVDF	Polyvinylidene fluoride
Q	Glutamine
qRT-PCR	Quantitative real time-PCR
PAS	Per-Arnt-Sim kinase
R	Arginine

RAI1	Retinoic acid induced 1
RBFOX1	RNA-binding protein Fox-1
RBP4	Retinol binding protein 4
rER	Rough endoplasmic reticulum
Rev	Reverse primer
RIPA	Radioimmunoprecipitation assay
RISC	RNA-induced silencing complex
RNA	Ribonucleic acid
RNP	Ribonucleoprotein
RPMI	Roswell park memorial institute
RPKM	Reads per kilobase mapped reads
rRNA	Ribosomal RNA
S	Serine
SBMA	Spinal bulbar muscle atrophy
SC	Sample collection
SCA	Spinocerebellar ataxia
SDS	Sodium dodecyl sulfate
SEL1L	Sel-1 suppressor of lin-12-like
SEM	Standard error of the mean
SETX	Senataxin
SERINC2	Serine incorporator 2
SERPINA1	Serpin peptidase inhibitor, clade A, member 1
SG	Stress granule
shRNA	Small hairpin RNA
SH-SY5Y	Neuroblastoma cells subcloned from SK-N-SH cells
SMA	Spinal muscular atrophy
Snf1	Sucrose non-fermenting 1
SNP	Single nucleotide polymorphism
SOD1	Superoxide dismutase 1
SPAST	Spastin
SPD	Synpolydactyly
SPG11	Spatacsin
SPTBN2	Spectrin, beta, non-erythrocytic 2

SRP	Signal regocnition particle
SYVN1	Synovial apoptosis inhibitor 1
T	Thymidine
TARDBP/TDP43	Transactive response DNA binding protein 43 kDa
TBC1	Tre-2/USP6, BUB2, cdc16
TBE	Tris/Borate/EDTA
TBP	TATA box binding protein
TBS	Tris buffered saline
TBS-T	Tris buffered saline-Tween
TGM6	Transglutaminase 6
TMEM240	Transmembrane protein 240
TNR	Trinucleotide repeat
TORC1	Target of rapamycin complex 1
Tris	Tris(hydroxymethyl)-aminomethane
TTBK2	Tau tubulin kinase 2
TTR	Transthyretin
U	Uracil
UBE3A	Ubiquitin protein ligase E3A
UBQLN2	Ubiquilin 2
UPR	Unfolded protein response
UPS	Ubiquitin-proteasome system
UTR	Untranslated region
UV	Ultraviolet
VABP	VAMP-associated protein B
VCP	Valosin containing protein
VDBP	Vitamin D binding protein
VDCC	Voltage-dependent Calcium channel
WT	Wild type
Y	Tyrosine
ZBRK1	BRCA1-interacting KRAB zinc finger protein 1
Zn	Zinc
ZNF9	Zinc finger domain 9

1. INTRODUCTION

Neurodegenerative disorders (NDs) are a large group of neurological diseases caused by the loss or malfunctioning of the neurons. Progressive and asynchronous degeneration of the neurons highly affects the daily life quality of the patients, and may eventually be fatal if cognition or the execution of the vital functions, such as respiration and heart rate, is impaired. It has been reported that neurodegenerative and neuropsychiatric disorders can be responsible for 3.3% of the deaths due to noncommunicable conditions worldwide, following cardiovascular and respiratory problems (61.1%), and cancer (21.7%) (Statistical Annex, World Health Report 2004 by World Health Organization). Along with the improvements in cardiovascular disease and cancer therapeutics, the population size of individuals above 65 years-old in developed countries is growing faster than that of the whole population. Thus, it is anticipated that the ratio of elderly to the whole population will double in the up-coming generations, raising the percentage of neurodegenerative and neuropsychiatric disorder-associated deaths, as aging is the main risk factor for the development of most NDs (Przedborski *et al.*, 2003). Advancements in the medical science over the past century and the consequent increase in the average life expectancy of mankind renders this group of disorders a pivotal phenomenon to be dealt with.

1.1. Classification of Neurodegenerative Disorders

There are a few hundred NDs defined so far, presenting with a variety of clinical features depending on the specific subset of affected neurons, mechanism of pathology and environmental factors. Clinical and pathological overlaps of different features are quite common and further complicate the classification of these disorders. One way of categorizing NDs is based on the combination of most distinctive clinical phenotype and the anatomical location of the lesion. Using this method, central nervous system (CNS) disorders are first grouped into four according to the site of lesion: cerebral cortex, basal ganglia, brain stem and cerebellum, and spinal cord. Further subcategorization is done for each group depending on other clinical features the disease might present (Figure 1.1).

Cerebral cortex diseases may be dementing or non-dementing. Basal ganglia diseases are either hypokinetic or hyperkinetic. Brain stem and cerebellum diseases are well classified into cerebellar cortical atrophy and olivopontocerebellar atrophy, although there are some cerebellar disorders that do not fit to any of these subcategories. Spinal cord diseases are amyotrophic lateral sclerosis, spinal muscular atrophy and Friedreich's ataxia. In some cases, functional and anatomical connection of distant cell populations in the nervous system may lead to multiple lesions in separated regions, as closer parts remain intact. The disease, in such a case, would be classified in both corresponding categories. On the contrary, there exists a group of disorders that are considered to be neurodegenerative only due to their course, with no known causative pathogenesis whatsoever, thus cannot be placed in any of these categories (Przedborski *et al.*, 2003).

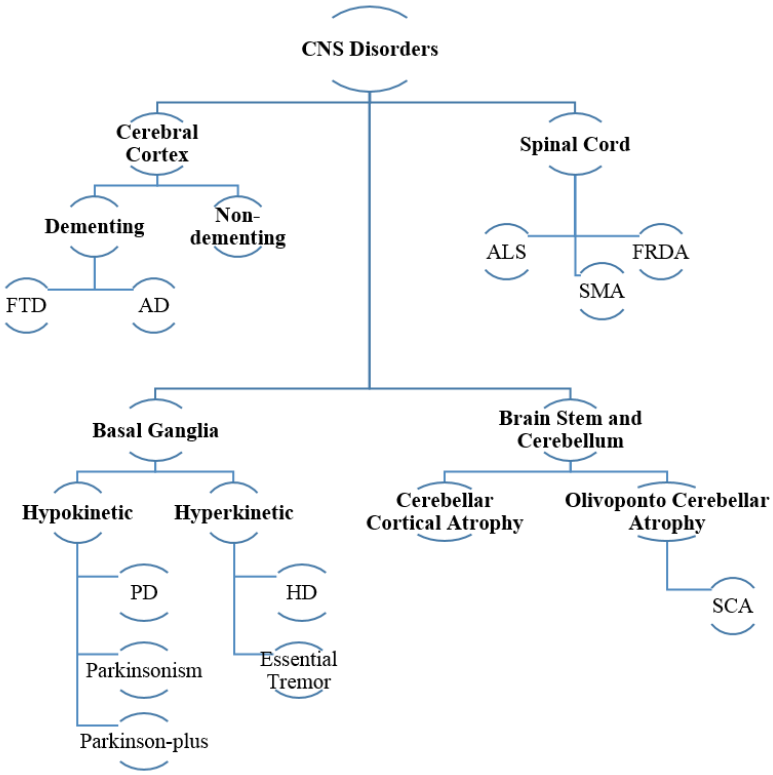

Figure 1.1. Classification of CNS disorders based on the most distinctive clinical phenotype and the anatomical location of the lesion (Przedborski *et al.*, 2003).

A different and rather recently adopted way to classify NDs is based on their molecular characteristics. Such a categorization has been made possible by the leap in the research on molecular and genetic basis of diseases over the past few decades. Disorders

that have been classified into distinct groups previously depending on the clinical and anatomical hallmarks, may now fall into the same category and be collectively called '-opathies', provided that they share the same mode of pathogenesis with or without a genetic cause. An example is the group of disorders defined as proteinopathies, all resulting from the toxic misfolding and aggregation of various proteins, including prion diseases (CJD, GSS), synucleinopathies (PD, PSP, and LBD), tauopathies (CBD, FTDP-17, and PiD), etc… Other than the causative patho-mechanism, genetic factors also distinguish NDs into separate groups. Many disease-causing mutations have been identified in various genes, some in fact being the proteinopathy or channelopathy genes. Among all the mutations identified so far, simple repeat expansion mutations arise as a common feature of many NDs (Hekman and Gomez, 2015; Mirkin, 2007).

The inheritance of nearly 30 disorders have been currently explained with repeat expansion mutations. Figure 1.2 shows a spatial representation of the known repeat expansions within their respective genes. The length of one repeat unit may vary from trinucleotides up to 12-nucleotides. Expansions are seen not only in the exonic coding region, but may also occur at intronic or regulatory regions such as the promoter, 5'- or 3'-UTRs. In contrast to most genetic mutations that are considered to be fixed and inherited in a stable manner, repeat expansions have a dynamic nature. Most repeat regions are rather less expansion-prone in the presence of an interrupting unit or below a certain repeat number threshold. However, when the interrupting unit is lost and the repeat size reaches or goes beyond the threshold value, the region overcomes the innate genome correction mechanisms and becomes more and more prone to further expansions in consequent parent-to-child transmissions. An effect known as anticipations takes place across generations, as growing repeat sizes with each transmission result in an earlier disease onset and a more severe disease course. The longer a repeat region, the higher becomes its potential to further expand and become more deleterious in the next progeny. Hence, anticipation also leads to increased penetrance of the mutation in addition to increased expressivity (McMurray, 2010; Mirkin, 2007).

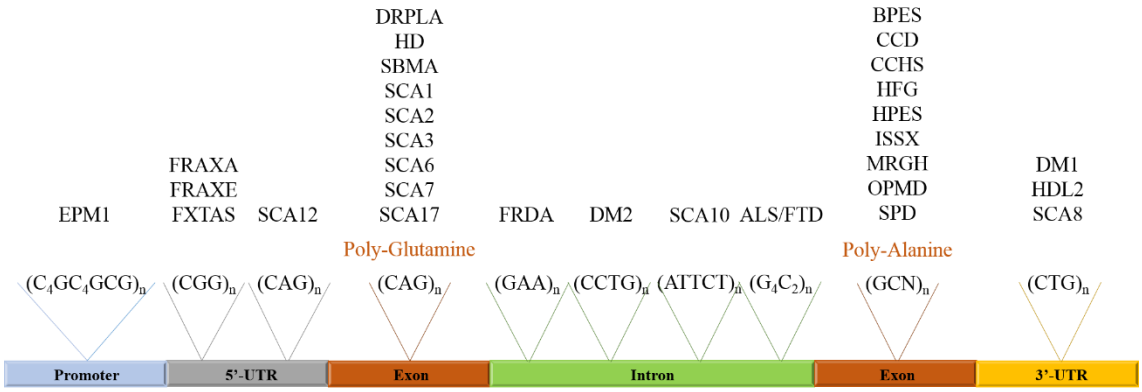

Figure 1.2. Currently known repeat expansion units (DeJesus-Hernandez *et al.*, 2011; Mirkin, 2007; Pulst *et al.*, 1996; Renton *et al.*, 2011).

Trinucleotide repeats (TNRs) are the dominating group among the currently known repeat expansion mutations. More than 25 NDs today are known to be caused by a TNR expansion in various genes. Similar to all repeat expansion mutations, TNR expansions can be located at regulatory or coding regions of a gene. Along with ten different neurodegenerative and neuropsychiatric disorders (DRPLA, HD, SBMA, OPMD, HDL2, FRAXA, FRAXE, FXTAS, FRDA, DM1), spinocerebellar ataxias (SCAs) predominate this group, with eight different types (SCA1, 2, 3, 6, 7, 8, 12, 17) (Table 1). In six of these SCAs, the repetitive trinucleotide unit is CAG which codes for glutamine (Gln, Q). Such disorders, caused by an expansion in the exonic poly-glutamine repeat tract, are collectively called poly-glutamine (poly-Q) diseases. In addition to six SCA types, HD, SBMA and DRPLA also belong to this group. The threshold between normal and pathogenic alleles greatly varies among poly-Q disorders (Table 1). The presence of interrupting CAA trinucleotides, which also code for glutamine amino acid, among the CAG repeats has been shown to provide more stability at this locus, and reduce the likelihood of an expansion (Choudhry *et al.*, 2001). As in most TNR diseases, anticipation is observable in poly-Q diseases, especially when the expansion is transmitted paternally across generations (Rüb *et al.*, 2013).

Table 1.1. List of the repeat-expansion disorders (Al-Mahdawi *et al.*, 2006; Brais *et al.*, 1998; Knight *et al.*, 1993; Kobayashi *et al.*, 2011; McMurray, 2010; Reddy *et al.*, 2013; Rüb *et al.*, 2013; Sato *et al.*, 2009; Todd and Paulson, 2010).

Disease	Gene	Chr.	Repeat Unit	Location	Repeat # (Normal)	Repeat # (Disease)
SCA1	*ATXN1*	6p22	CAG	exon	6 – 44	49 – 91
SCA2	*ATXN2*	12q24	CAG	exon	14 – 32	33 – >200
SCA3	*ATXN3*	14q32	CAG	exon	12 – 44	52 – 89
SCA6	*CACNA1A*	19p13	CAG	exon	3 – 18	20 – 33
SCA7	*ATXN7*	3p21	CAG	exon	4 – 35	36 – 460
SCA17	*TBP*	6q27	CAG	exon	25 – 44	47 – 63
DRPLA	*ATN1*	12p13.31	CAG	exon	7 – 34	49 – 88
HD	*HTT*	4p16.3	CAG	exon	6 – 34	36 – 121
SBMA	*AR*	Xq12	CAG	exon	9 – 36	38 – 62
SCA12	*PPP2R2B*	5q31	CAG	5'-UTR	< 32	51 – 78
OPMD	*PABPN1*	14q11.2	GCN	exon	< 6	8 – 17
HDL2	*JPH3*	16q24.2	CTG	exon (alt.)	6 – 28	> 41
FRAXA	*FMR1*	Xq27.3	CGG	5'-UTR	20 – 45	55 – 220
FRAXE	*AFF2*	Xq28	GCC	5'-UTR	6 – 25	> 200
FXTAS	*FMR1*	Xq27.3	CGG	5'-UTR	20 – 45	55 – 220
FRDA	*FXN*	9q21.11	GAA	intron	5 – 30	70 – >1000
SCA8	*ATXN8OS*	13q21	CTG	3'-UTR	15 – 50	71 – 1300
DM1	*DMPK*	19q13.32	CTG	3'-UTR	5 – 38	50 – >1500
SCA10	*ATXN10*	22q13	ATTCT	intron	10 – 29	800 – 4500
SCA31	*BEAN*	16q22	TGGAA	intron		> 110
SCA36	*NOP56*	20p13	GGCCTG	intron		3 – 8
ALS/FTD	*C9Orf72*	9p21.2	GGGGCC	intron	2 – 19	250 – >2000
DM2	*ZNF9*	3q21.3	CCTG	intron	< 30	75 – 11000

1.2. Spinocerebellar Ataxias and Common Mechanisms

Spinocerebellar ataxias (SCAs) are the autosomal dominant group of progressive cerebellar atrophies with incoordination of limb movements, gait ataxia and dysarthria as the primary and common symptoms (Ramachandra and Kusuma, 2015). The term autosomal dominant cerebellar ataxia (ADCA) is also used to define these diseases. SCAs are divided into three major groups based on their clinical presentations; ADCAI

comprises mixed cerebellar ataxia symptoms with additional neurological problems such as seizures, areflexia, and deficiency in sensory and cognitive systems, ADCAII shows cerebellar ataxia with retinopathy which has only been observed in SCA7 so far, and ADCAIII group presents pure cerebellar ataxia symptoms. Currently, 36 genetic loci have been identified for the 40 clinically differentiated types of SCAs. In 28 of these loci, the causative genes have been identified, the pathogenic roles of eight loci still remain unsolved (Supplementary Table S1) (Kobayashi *et al.*, 2011; McMurray, 2010; Rüb *et al.*, 2013; Sato *et al.*, 2009; Todd and Paulson, 2010). The worldwide prevalence of all SCAs combined is around 4 in 100.000, although geographical variability is observed in some subtypes due to the residency of a founder population in a defined region. SCA3 is the most common type worldwide preceding SCA1, SCA2, SCA6, SCA7 and SCA8 (Ramachandra and Kusuma, 2015).

Poly-Q domain expansions are shown to be the common genetic cause of some SCAs, therefore recurrent mechanisms of pathology are also shared among these subtypes at the anatomical and molecular levels. Neuronal cell loss in the cerebellum, and additional damage to the extra-cerebellar tissues, especially at later stages of the disease, greatly overlaps in all poly-Q SCAs. The most shared atrophy among all poly-Q SCAs is observed at the Purkinje cell layer and Fastigial nuclei in the cerebellum, giant Betz neurons in the primary motor cortex of the cerebrum, substantia nigra in the midbrain and superior olive in the pons. Many other regions of the cerebellum, midbrain and pons is affected to different degrees in different disease subtypes (Figure 1.3) (Seidel *et al.*, 2012).

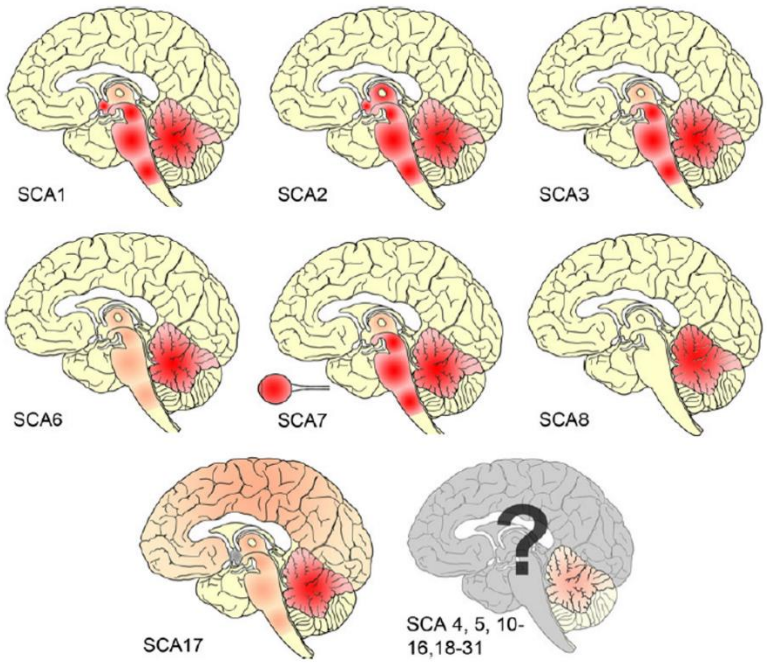

Figure 1.3. Graphical visualization of the spatial neuronal loss in different poly-Q SCAs. The focal points of cell loss is demonstrated by intensity of the red color in the midsaggital sections through cerebrum, brain stem and cerebellum (Seidel *et al.*, 2012).

Primary effects of the expansion at the molecular level manifest as toxic RNA foci and aberrant folding of the expanded protein, altered subcellular localization of which enhances the formation of intracellular protein aggregates. Major secondary effects of these abnormalities occur as transcriptional dysregulations, disruption of the Ca^{2+} homeostasis, mitochondrial dysfunction and problems in degradation pathways. The variability in the prominence of these secondary effects in different SCAs depend on the particular function of the responsible protein for each type.

Since most of the expansion-bearing proteins in SCA pathogenesis are associated with transcription and the regulation of RNA metabolism either directly or indirectly, some poly-Q SCAs are counted as a part of 'transcriptionopathies' (Matilla-Dueñas *et al.*, 2014). Transcriptional changes in different gene sets were observed in poly-Q SCAs, however dysregulation of the genes involved in calcium homeostasis was a common feature. A decrease in the expression of Ca^{2+}-dependent proteins, which is normally quite high due to their roles in Purkinje cell survival and function, was observed in various poly-Q SCAs

and also in other poly-Q diseases (Czeredys *et al.*, 2013; Egorova *et al.*, 2015; Hansen *et al.*, 2013; Lin *et al.*, 2000; Saegusa *et al.*, 2007; Tian *et al.*, 2015). Deletions and missense mutations in *ITPR1* Ca^{2+} receptor have been found as the genetic cause of two SCA types (SCA15 and SCA16), which are classified as 'channelopathies', together with several other ion channel dysfunction-mediated disorders.

Mitochondrial dysfunction is also a common pathogenic mechanism in poly-Q SCAs. Aside from its well-established role in calcium homeostasis, enhanced fission of the mitochondria, accumulated reactive oxygen species in the cytoplasm, subsequent activation of the stress response and the increase in caspase pathways all contribute to the pathology (Wang *et al.*, 2011). Several mitochondrial mutations have also been directly linked to a number of ataxia cases (Gorman *et al.*, 2015; Jobling *et al.*, 2015; Park *et al.*, 2014).

Yet another common impairment leading to poly-Q SCAs occur in the degradation pathways due to intracellular aggregations formed by expanded proteins. Although these aggregates intend to be protective by eliminating the toxic component from the environment, an overload of work arises for the proteosomal degradation machinery. The densely packed stress granules induced by oxidative stress or altered homeostasis are hallmarks of not only poly-Q SCAs, but also of the majority of NDs. They generate large chunks of material that is problematic for the conventional degradation pathways of the cell: ubiquitin-proteosome system (UPS) and autophagy. UPS is responsible for the degradation of most proteins, while autophagy is employed in the degradation of terminally aggregated proteins and cellular organelles. Targeting of the substrate proteins to both systems depends on the ubiquitin tags. Proteins targeted to UPS undergo ATP-dependent degradation by the proteasome machinery, and if not, they are covered with autophagosomes, double-membrane-coated vesicles, and subjected to lysosomal digestion (Lilienbaum, 2013). Ubiquitin is often found to be part of the intracellular aggregates in a number of NDs (Goldbaum and Richter-Landsberg, 2004). SQSTM1, also known as p62, is an autophagy receptor identifying targets to degrade in the cytoplasm, and is a component of the stress granules, besides the fact that it has an established role in the

pathogenesis of various NDs (Fecto *et al.*, 2011; Gal *et al.*, 2007; Hiji *et al.*, 2008; Homma *et al.*, 2014; Lim *et al.*, 2015).

Lastly, irregularities in neuronal excitability and excitotoxicity are also shared among different types of SCAs; glutamate toxicity caused by the instability of the glutamate transport (*spectrin* mutations), altered regulation of cellular excitability (*FGF14* mutations) and activation of unfolded protein response (UPR) via increased frameshifting mistake during translation (*eEF* mutations) have all been shown as direct causes of distinct SCA types (Hekman and Gomez, 2015).

1.3. Clinical Features of SCA2

Spinocerebellar Ataxia Type 2 (SCA2) is an autosomal dominant neurodegenerative disorder and is a rather frequent type among ADCAs; it accounts for 13% of all ADCAs, while SCA1 counts for 6% and SCA3 for 23% (Geschwind *et al.*, 1997). SCA2 is somewhat more frequent in Cuba, Spain, Italy and Turkey, and less in Brazil, Finland and Japan (Cellini *et al.*, 2001; Juvonen *et al.*, 2005; Lopes-Cendes *et al.*, 1997; Matsumura *et al.*, 2003; Pujana *et al.*, 1999). A small town in Cuba, called Holguin, is where SCA2 is the most common worldwide. A founder haplotype with approximately 1000 individuals descendent from the same ancestor is resident in this town inducing a prevalence of 500/100.000 and an incidence of 18 per year (Lastres-Becker *et al.*, 2008b). The mean age of onset (AO) of the disease is in the third decade, however there are cases that manifest as early as <10 years, or late as >60 years of age. Anticipation is an observed phenomenon of SCA2; the repeat length further expands especially during paternal transmission, which results in an earlier disease onset and a more severe disease course with a rapid progression in the progeny (Rüb *et al.*, 2013). Average disease duration is around 10 years, although some extreme cases have been reported ranging from six to 50 years of survival in Cuba and North America. Currently, there is no cure for this disease directly targeting the causality. A variety of treatments are utilized to alleviate the symptoms. Levodopa, a dopamine precursor mainly used in PD treatment, is given to the patients to cure the parkinsonism symptoms, such as rigidity, bradykinesia and tremor.

Magnesium supplement is applied for muscle cramps. Deep brain stimulation has been reported to improve early onset postural tremor (Lastres-Becker *et al.*, 2008b). The latest stem cell technologies are also under intense utilization to regenerate Purkinje neurons from the patient induced-pluripotent stem cells or to employ mesenchymal stem cells in the innate regeneration machinery, although further improvements in this field are still needed for an effective treatment to be made public (Nakamura *et al.*, 2014; Wang *et al.*, 2015).

The initial symptoms of SCA2 are incoordination of gait and limbs, postural rigidity, dysarthria, loss of velocity saccades, tremor, myoclonus and hyperreflexia, which turns into hyporeflexia in a short time. As the disease progresses, challenges in vital autonomic tasks present as dysphagia and dysfunction of the cardiac, gastrointestinal and exocrine systems. These systematic symptoms are accompanied by distal amyotrophy, and cognitive deficiencies such as short-term memory loss, frontal executive dysfunctions, emotional instability and attention loss (Lastres-Becker *et al.*, 2008b). The severity of these symptoms increase as the disease progresses, rendering the patient bed-ridden and in need of special care. The eventual decease of the patients is mostly due to problems in crucial autonomic functions, such as respiration.

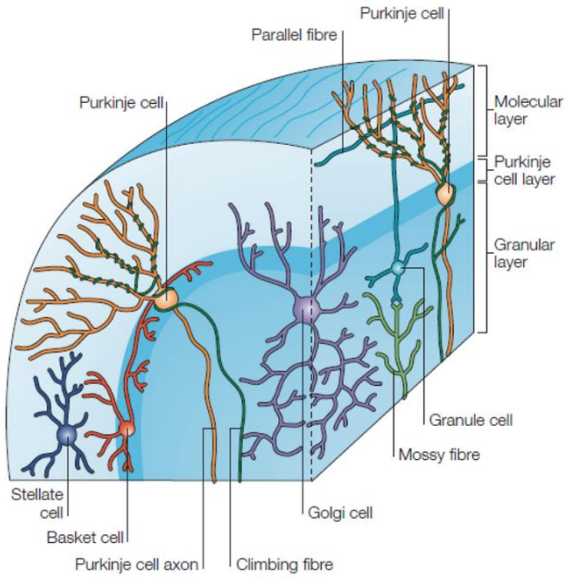

Figure 1.4. The anatomical structure of the cerebellar cortex (Apps and Garwicz, 2005).

Early saccade slowing is a differentiating symptom of SCA2 that separates it from other cerebellar ataxias (Wadia and Swami, 1971), and is explained by the early degeneration of the pontine and brainstem in addition to Purkinje cell loss at the cerebellum (Scherzed *et al.*, 2012). The cerebellum is divided into three cortical layers: molecular, Purkinje and granular (Figure 1.4). Purkinje cells are located in the middle layer and extend their dendrites towards the uppermost molecular layer where they receive input from the climbing fibers. With the extensively large axonal projections, Purkinje cells are the only output neurons of the cerebellar cortex and a crucial component of cerebellar information processing (Apps and Garwicz, 2005). The most prominent patho-anatomical feature of SCA2 is the early degeneration of Purkinje neurons in both hemispheres of the cerebellum (Figure 1.5), accompanied by secondary findings throughout the disease course, such as thinning of the granular neurons in the cerebellum, degeneration of substantia nigra in the midbrain, loss of spinal cord motor neurons especially in the cranial and cervical layers, and frontotemporal and thalamic atrophy at the very end stages of the disease (Lastres-Becker *et al.*, 2008b). Degeneration of the cerebellar and midbrain regions explains the uncoordinated movements and parkinsonism symptoms such as rigidity and tremor, subsequent loss of motor neurons contribute to distal amyotrophy, as frontotemporal atrophy and the general enlargement of the ventricles in the cerebrum would account for the executive function loss, emotional instability and attention problems. The severe atrophy observed in thalamus is exclusive to SCA2 and not commonly seen in other NDs, possibly underlying the dysregulations of the autonomic tasks.

Figure 1.5. MRI scan of a SCA2 patient showing cerebellar atrophy in the midsaggital section (Chakor and Bharote, 2012). Red arrows indicate atrophy.

Alongside the severe degeneration in the cerebellum, the remaining Purkinje cells also show an abnormal phenotype with reduced dendritic spines and a peripheral dying-back, also called axonopathy, can be observed in the granular layer of the cerebellum. SCA2 also differs from other SCAs in terms of the lack or scarcity of inclusion bodies in the nucleus. Intranuclear inclusion bodies are completely absent in the Purkinje neurons, however cytoplasmic aggregates are seen not only in the Purkinje cells, but throughout the brain (Lastres-Becker *et al.*, 2008b).

Purkinje cells are especially susceptible to death, as they are among the largest, so-called 'magnocellular' neurons, dealing with a high metabolic activity, bearing a massive dendritic spine network receiving abundant excitatory input at every instant. Magnocellular neurons are known to contain large amounts of intracellular membranes in the form of rough-ER (rER), called Nissl bodies, in order to cope with extensive protein synthesis, folding, and quality control. Therefore, impaired homeostasis of the protein synthesis and degradation affects these magnocellular neurons to a greater extend, such as Purkinje cells and motor neurons, prior to other neuronal subtypes. Purkinje cells, with their enlarged dendritic arborizations and fairly long axonal extensions, suffer greatly from the subcellular imbalance in the degradation of proteins. Protein synthesis is known to occur at the farthest points of the neurons, even as far as synaptic buttons. However, the turn-over of these proteins mainly occurs in the cell soma. Especially in the case of distal protein aggregates, autophagic degradation via lysosomal fusion is crucial for the elimination of inclusions and is only achieved in the cell body. Thus, larger neurons with more distal projections suffer more from the toxic protein aggregates located far away from the cell soma, even though the retrograde transportation mechanisms are not necessarily damaged. Still, problems in the retrograde transport of intracellular protein aggregates or the damaged organelles is known to be a common pathological mechanism shared among many NDs, either due to a genetic mutation or as a sporadic case (Wong and Holzbaur, 2015).

Similar to altered proteostasis, magnocellular neurons are also more susceptible to problems in Ca^{2+} homeostasis than other types of neurons. Purkinje cells express a lot of

Ca^{2+} dependent proteins and enzymes taking roles in Ca^{2+} intake, processing and secondary signaling. Ca^{2+} channels are also significantly important in the foundation and maintenance of the neural connections in the cerebellum between Purkinje cells and climbing fibers during development. One of the two possible ways of Ca^{2+} intake for a Purkinje cell is the activation of InsP3R1 (a.k.a. ITPR1) channel on the ER and release of intracellular Ca^{2+} (Egorova *et al.*, 2015). Since ER is the major source of intracellular Ca^{2+} stores, and Purkinje cells are known to contain excess amount of rER structures, any alteration in the Ca^{2+} metabolism instantly affects the stability of Purkinje neurons.

1.4. SCA2 Genetics and Ataxin-2 Mechanism

The responsible genetic locus for SCA2 co-segregating with the disease phenotype was identified as Chr.12q23-24.1 in Cuban ADCA pedigrees, and the particular disease phenotype has been referred to as SCA2, since it is the second example of a locus association to an ADCA, after SCA1 (Gispert *et al.*, 1993; Orr *et al.*, 1993). The causative gene in this region, later named to be *ATXN2*, was then identified by three groups independently utilizing positional cloning, CAG expansion-specific probes and poly-Q-specific antibodies (Imbert *et al.*, 1996; Pulst *et al.*, 1996; Sanpei *et al.*, 1996). The ubiquitous expression of *ATXN2* was detected in brain, heart, muscle and placenta, also high levels in pancreas and liver (Imbert *et al.*, 1996; Sanpei *et al.*, 1996). At the cellular level, *ATXN2* is expressed highly in the Purkinje cells and large neurons in substantia nigra, moderately expressed in globus pallidus and amygdaloid neurons of the basal ganglia and pyramidal neurons of the hippocampus (Nechiporuk *et al.*, 1998).

ATXN2 gene spans ~130 kb of genomic DNA and has 25 exons. An alternative start codon is found 120 codons downstream of the conventional start site (Sanpei *et al.*, 1996). Exons 10 and 21 are subject to alternative splicing, both of which are located distant from the domains with a known function (Sahba *et al.*, 1998). A trinucleotide CAG expansion was found in the 5'-end of the *ATXN2* coding region which was later determined to be located at exon 1 (Sahba *et al.*, 1998). Two novel SNPs, that established two haplotypes, were identified in exon 1, lying 106 and 117bp upstream of the CAG repeat tract: CC and

GT, respectively. All expanded alleles segregated with the CC haplotype, which was also seen in 30% of the normal alleles. Majority of the normal alleles segregating with the CC haplotype either have a pure CAG tract, or the CAA interruption closer to the 5'-end of the repeat tract is lacking. Thus, the dynamic expansion shows an occurrence tendency towards the 5'-end of the repeat region (Choudhry *et al.*, 2001).

ATXN2 gene shows no sequence similarity, except for the CAG repeats, with a known gene other than the *ATXN2*-related protein (A2RP) (Pulst *et al.*, 1996). *ATXN2* is conserved among five mammalian species and chicken (Imbert *et al.*, 1996). The nucleotide sequence similarity is quite high between human and mouse homologs (89%). However the mouse homolog contains only one CAG triplet at the corresponding locus to human poly-Q tract, which suggests that the main function of *ATXN2* is not exclusive to this region (Nechiporuk *et al.*, 1998).

In humans, the trinucleotide repeat tract is most frequently composed of 22 repeats interrupted by CAA triplets in such a pattern: $(CAG)_8$-CAA-$(CAG)_4$-CAA-$(CAG)_8$. Loss of the two CAA units in between promotes instability, rendering it more prone to expansions. More than 34 CAG repeats in this domain is considered pathogenic for SCA2, while intermediate-length repeats between 26-39 have been associated with increased risk for other NDs, such as ALS and PD, a subject to be discussed in the following sections. The most commonly seen pathogenic alleles for SCA2 are around 37-39 repeats, while some extreme cases with >200 repeats have been reported (Babovic-Vuksanovic *et al.*, 1998; Mao *et al.*, 2002). Although loss of CAA interruptions enhances expansion via meiotic instability, pathogenic alleles may also contain CAA interruptions, transmitting stably to the next generation (Charles *et al.*, 2007). Presence of a CAA interruption is argued to have no alteration on the molecular pathogenicity, as it also codes for glutamine amino acid and does not alter protein structure (Costanzi-Porrini *et al.*, 2000). However, conversion of a CAG unit to CAA reduces RNA-mediated toxicity without an effect on the protein in *ATXN3*, another SCA gene containing a poly-Q domain (Todd and Paulson, 2010).

An obvious effect of the repeat size exists on the age of onset (AO) and severity of the symptoms. AO is inversely correlated with the repeat size; the longer the CAG repeat

tract, the earlier becomes the manifestation with stronger symptoms and a rapid progression (Almaguer-Mederos *et al.*, 2010). Figure 1.6 shows the correlation between AO and repeat size according to the survival likelihood analysis of Cuban SCA2 patients. Individuals with 34 CAG repeats are inferred to have only 50% likelihood of developing the disease in their late 60s, while the same percentage of disease likelihood converges to earlier ages as the repeat size increases. Nearly certain disease onset at around 50s and 40s is predicted for individuals carrying 40 and 45 CAG repeats, respectively (Figure 1.6).

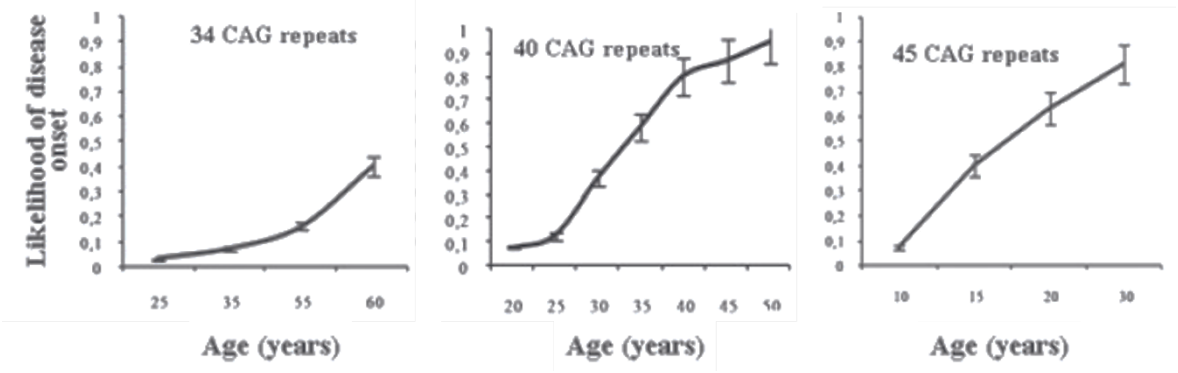

Figure 1.6. The correlation of AO with CAG repeat expansion size in *ATXN2* (Almaguer-Mederos *et al.*, 2010).

Anticipation contributes greatly to inter-generational variation in AO and disease severity. It is typically observed during paternal transmission of the pathogenic allele rather than maternal, and may bring disease onset as much as 30 years earlier (Mao *et al.*, 2002). Such paternal transmissions leading to a massive CAG repeat tract in the progeny has been reported a number of times where fathers with ~40 CAG repeats (AO: 22-30 years-old) transmitted the pathogenic allele to their offspring with massive expansions; 202, 230 and 500 CAGs (AO: 2-10 months-old) (Babovic-Vuksanovic *et al.*, 1998; Mao *et al.*, 2002).

Despite the existence of a significant correlation between repeat size and disease onset, a large portion of AO variation among individuals with the same repeat length remains unsolved. This variability is higher among individuals with rather shorter pathogenic repeats, between 36-40 units. When the expansion size is larger or smaller than

this interval, the variation among individuals decreases, and the disease shows similar manifestations by means of AO and symptoms. Repeat sizes of 33 and 34 consistently result in manifestation at >60 years of age, and 45 repeats almost always show an AO of <20 years-old, whereas, in the case of 37 repeats, distinct ages of onset as different as 20 and 60 years-old is observed (Cancel *et al.*, 1997; Geschwind *et al.*, 1997; Moretti *et al.*, 2004; Pulst *et al.*, 1996; Riess *et al.*, 1997).

The correlation between AO and the repeat size of an individual is a complex issue, and is under the influence of other modifying genetic, epigenetic and environmental factors. The first line of evidence regarding AO variability was that homozygosity for the CAG repeat in *ATXN2* gene is not a modifier of AO (Sanpei *et al.*, 1996). Conversely, another study reported a severe disease with an earlier AO in homozygous SCA2 patients (Ragothaman and Muthane, 2008; Spadafora *et al.*, 2007). The potential modifying effect of a genetic polymorphism in other poly-Q domain carrying genes was investigated with the initial hypothesis that poly-Q proteins are known to interact with each other and co-localize at the intracellular inclusion bodies. A correlation between the AO variation and the presence of a large $(CAG)_n$ allele of *RAI1* (retinoic-acid induced 1), which functions in neuronal differentiation during early development, was demonstrated in 4.1% of the previously unexplained AO variation cases (Hayes *et al.*, 2000). Similarly, the presence of long normal alleles of the *CACNA1A* gene, also a CAG repeat containing gene, the full expansion of which is known to cause the SCA6 phenotype, is proposed to decrease AO of SCA2 patients and explain 5.8% of the AO variation. *CACNA1A* is argued to be a good candidate modifier of AO in SCA2, since it is localized in the cytoplasm where ataxin-2 is present, unlike other poly-Q proteins that are mostly found in the nucleus, and is not only highly expressed in the Purkinje cells, but also is an important factor for their firing activity (Pulst *et al.*, 1996).

In addition to genetic modifiers, epigenetic modifications around the *ATXN2* locus are also implicated in ataxin-2 toxicity and AO variation in SCA2 patients. The promoter of the *ATXN2* gene is located in exon 1 and contains a CpG rich segment without a TATA box (Aguiar *et al.*, 1999). Both hyper- and hypomethylation states were observed in the promoter of *ATXN2* gene in SCA2 patients, and none of the patients showed a full-methylation pattern at all CpG sites. The hypermethylation state in *ATXN2* promoter is

associated with the expanded pathogenic allele, which may be an outcome of the cells' effort to reduce *ATXN2* expression and expansion-mediated toxicity (Laffita-Mesa *et al.*, 2012). Allele specific *de novo* hypermethylation of the *ATXN2* promoter is reported to result in a delayed AO and a milder disease phenotype (Bauer *et al.*, 2004). Hypomethylation of this locus, on the other hand, contributed to intrafamilial anticipation of the disease, without a variation in CAG repeat number between two generations (Laffita-Mesa *et al.*, 2012).

1.4.1. Ataxin-2 Function and Mechanisms of Pathogenicity

Ataxin-2 is a ~140 kDa cytoplasmic protein composed of 1312 amino acids when carrying a normal poly-Q allele with 22 CAG repeats (Imbert *et al.*, 1996). High levels of ataxin-2 protein in Purkinje cells and substantia nigra was observed by immunostaining studies. The intensity of the staining showed an increase with age in expansion-free individuals, whilst SCA2 patients exhibited an already higher intensity initially, compared to healthy individuals (Huynh *et al.*, 1999). Ataxin-2 expression has also been observed in other regions of the brain, such as pyramidal neurons of the hippocampus and amygdaloid neurons of the basal ganglia, where *ATXN2* mRNA was also detected via qPCR analyses (Nechiporuk *et al.*, 1998). Even though cytoplasmic micro-aggregates were present in patient cerebella, no inclusion bodies were evident in the nucleus, in contrast to other poly-Q disorders. Within the cell, ataxin-2 shows a rather diffuse distribution in the cytoplasm with a tendency to co-localize with the intracellular membranes, such as Golgi apparatus and ER (Lastres-Becker *et al.*, 2008b).

Except for its poly-Q domain, ataxin-2 shows no major homology with other proteins, but contains several domains with well-established functions (Figure 1.7). Ataxin-2 harbors a Like-Sm (Lsm) and a Lsm-associated domain (LsmAD) proximal to N-terminus where the poly-Q domain is located, and a PAM2 motif towards the C-terminus end. Lsm family proteins regulate RNA metabolism by participating in pre-mRNA splicing, de-capping and mRNA decay (He and Parker, 2000). LsmAD domain contains a Clathrin-mediated trans-Golgi signal composed of YDS (Tyrosine-Aspartate-Serine) amino acids, next to an ER exit signal coded by ERD (Glutamate-Arginine-Aspartate)

amino acids (Albrecht *et al.*, 2004). These two signals are important for the co-localization of ataxin-2 to the Golgi apparatus, and their deletion results in altered subcellular localization. Expansions in the poly-Q domain also lead to impaired ataxin-2 localization *in vitro*, disrupting the morphology of the Golgi complex (Huynh *et al.*, 2003). PAM2 motif covers a segment of 18 amino acids and is shared among various proteins, most of which are involved in RNA metabolism ranging from synthesis to degradation. PAM2 is one of the two known Poly(A)-Binding Protein (PABP)-interacting motifs and recognizes the C-terminal PABC domain of PABP (Albrecht and Lengauer, 2004).

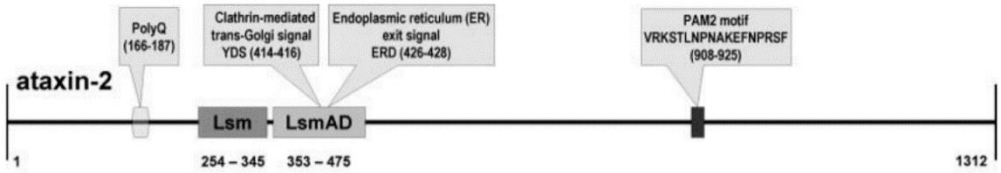

Figure 1.7. Known functional domains of ataxin-2 protein (Albrecht *et al.*, 2004).

Ataxin-2 has direct and indirect mRNA binding features, both of which lead to its association with the poly-ribosome complex (a.k.a. polysome). The direct interaction occurs through the Lsm/LsmAD domain, whereas the interaction of PAM2 motif with PABP, docked onto the poly(A)-tails of mRNAs, is the basis of indirect binding. Deletion of one domain, or the other, does not lead to complete dissociation ataxin-2 from polysome complex, suggesting that these two domains mediate polysome assembly independent from each other (Satterfield and Pallanck, 2006). With the establishment of polysome assembly, ataxin-2 stabilizes the target mRNAs and regulates their translation. Interaction of ataxin-2 with poly(A) nuclease enzyme in the presence of PABP is necessary to prevent over-trimming of the poly(A) tail and maintain the stability of the translation complex (Mangus *et al.*, 2004). Ataxin-2 is also indirectly involved in tissue specific alternative splicing via its interaction with ataxin-2-binding-protein 1 (A2BP1 or RBFOX1), whose Fox-1 domain recognizes a six nucleotide long segment in the alternatively spliced exons (Shibata *et al.*, 2000).

The direct binding capability of Lsm/LsmAD domains to RNA molecules raised the hypothesis that ataxin-2 may be interacting with microRNAs and recruit them to the 3'-UTRs of translating mRNAs (Figure 1.8) (Satterfield and Pallanck, 2006). Indeed, long-

term olfactory habituation in *Drosophila* was later proven to be regulated by Atx2-microRNA complex-mediated translational regulation of certain targets. The previously reported interaction of Atx2 with Me31B family of DEAD box helicases, which are linked to the RISC complex subunit Argonaute, is suggested to be the mode of Atx2 involvement in microRNA-mediated translational regulation. Moreover, Atx2 is shown to co-localize with the translational repressor complex Me31B/RCK/Dhh1p at the stress granules, further strengthening this hypothesis (McCann *et al.*, 2011).

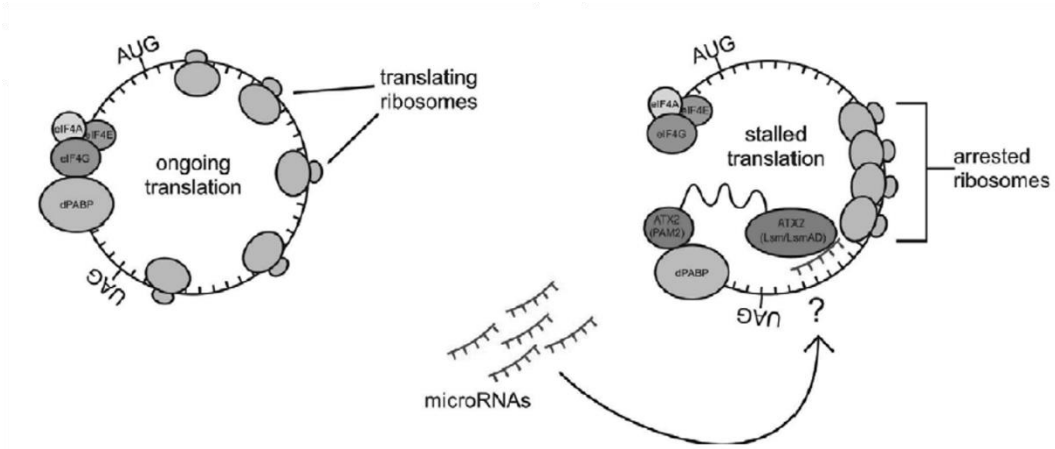

Figure 1.8. Recruitment of microRNAs to the 3'-UTRs of target mRNAs mediated by the interaction between ataxin-2 and PABP (Satterfield and Pallanck, 2006).

Ataxin-2 not only controls their assembly, but also is an important component of the stress granules, which are cytoplasmic clusters of translationally repressed mRNAs and their accompanying RNA-binding proteins (RNPs), densely packed until stress conditions disappear. Through its localization at the stress granules, ataxin-2 interacts with many other RNA stabilizing or destabilizing proteins, such as TDP-43, FUS and Profilin-1, mutations in which are mainly associated with ALS (Elden *et al.*, 2010; Farg *et al.*, 2013; Figley *et al.*, 2014). Such interactions have a modifying impact on disease pathogenesis, since the dissociation of stress granules becomes troublesome when one of these proteins bear a mutation and many other essential proteins and mRNAs remain sequestered in the insoluble aggregates (Figure 1.9) (explained in Section 1.4.2).

Further molecular interaction partners of ataxin-2 include endophilin-A1 and A3, which play a role in the membrane curvature during synaptic vesicle endocytosis (Ralser *et al.*, 2005). This interaction occurs at the ER, and also at the plasma membrane controlling

the endocytic cycling of the epidermal-growth factor receptor (Figure 1.9) (Nonis *et al.*, 2008). Only the expanded form of ataxin-2 interacts with the C-terminus of InsP3R1 on the ER membrane, sensitizing it for activation and causing an over-release of intracellular Ca^{2+} stores (Figure 1.9) (Liu *et al.*, 2009). Only the normal form of ataxin-2, on the other hand, regulates the susceptibility of neuroblastoma cells to apoptotic signals, hence take on a tumor suppressor activity (Wiedemeyer *et al.*, 2003). An indirect interaction of ataxin-2 with the actin filaments through intermediate factors have been shown to regulate filament formation and stability in a dosage-sensitive manner depending on ataxin-2 concentration (Satterfield *et al.*, 2002).

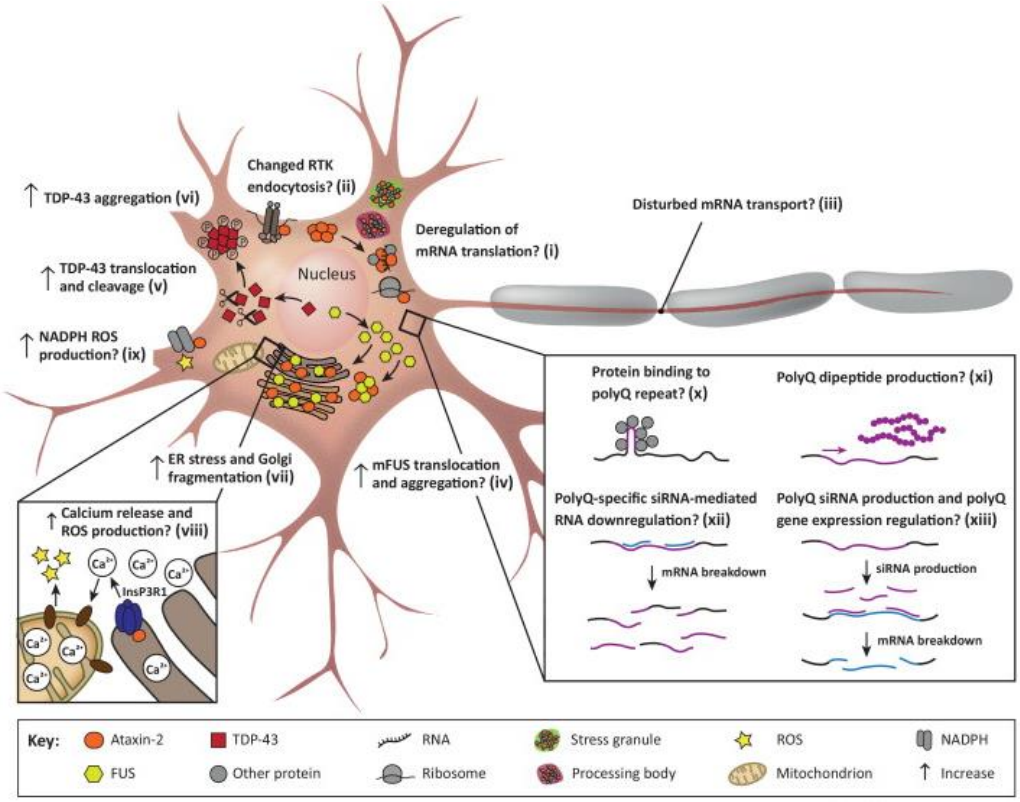

Figure 1.9. *ATXN2*-associated disease mechanisms (Van den Heuvel *et al.*, 2014).

Aside from its widely studied role in RNA metabolism and translational regulation, ataxin-2 also emerges as a key factor in the maintenance of cellular energy dynamics. It is well explained that ataxin-2 is responsible for the formation of stress granules under non-optimum conditions. Low energy sources, as stress-inducers, have recently been shown to activate a signaling cascade in yeast where consecutive phosphorylation reactions result in the activation of ataxin-2 homolog, Pbp1 (Figure 1.10). The active conformation of ataxin-

2 sequesters the TORC1 subunit of mTOR, which is normally involved in the regulation of cell growth and proliferation, into insoluble stress granules (DeMille *et al.*, 2014). The impairment of stress granule dissociation, when ataxin-2 is expanded, may also account for the elimination of mTOR from its ordinary habitat in post-stress conditions and further contribute to toxicity.

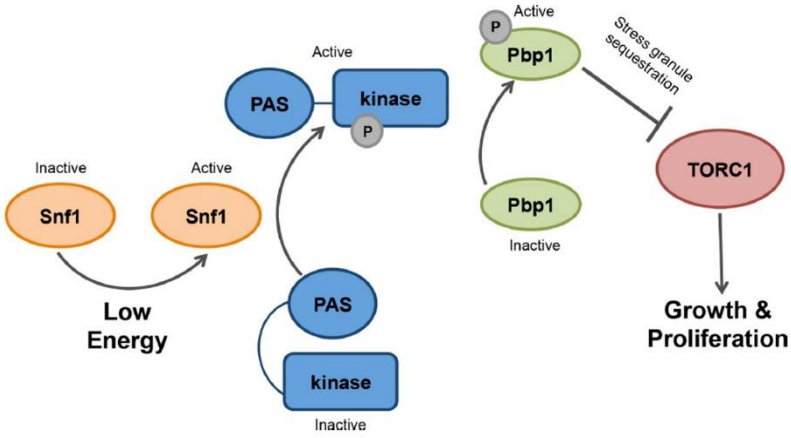

Figure 1.10. Signaling cascade leading to the sequesteration of TORC1 into stress granules by the yeast ortholog of ataxin-2, Pbp1 (DeMille *et al.*, 2014).

In addition to all the above-mentioned mechanisms that are either regulated or indirectly affected by ataxin-2, the mechanisms controlling *ATXN2* expression and the protein function are of equal importance. The transcription of *ATXN2* gene is regulated by a complex of ZBRK1, KRAB-containing zinc-finger transcriptional regulator 1, and ataxin-2. ZBRK1 bindings motifs are found in the promoter region of *ATXN2* via bioinformatics tools, and the physical interaction has been shown experimentally. Ataxin-2 is the first identified co-activator of ZBRK1, regulating its own transcription (Hallen *et al.*, 2011). Another control mechanism over the expression of *ATXN2* was investigated by promoter deletion analyses. Implementation of small deletions to the 5'-UTR revealed a crucial 8 bp segment that shows complete alignment with the E-twenty-six (ETS) family transcription factor recognition motif. Later, ETS1 transcription factor was found to physically interact with the promoter and has been identified as a regulator of *ATXN2* expression (Scoles *et al.*, 2012). The redundancy of *ATXN2* transcripts and the synthesized protein not only have a feedback control on their own transcription, but also are key determinants in the downstream cellular energetics. Alterations in ataxin-2 levels were shown to interfere with the stress granule and p-body formation under stress conditions.

Moreover, the concentration of PABP is also linked to ataxin-2 levels, further explaining the impact of unsteady ataxin-2 concentrations on the assembly of stress granules and translational control (Nonhoff *et al.*, 2007).

The turnover of the long-lived or expanded ataxin-2 is primarily mediated by UPS, as long as the insoluble aggregates do not require elimination by autophagosomes. Two ubiquitin ligases up to now have been identified to interact with ataxin-2: parkin and FBXW8. Parkin, product of the *PARK2* gene, is an E3 ubiquitin ligase, mutations in which are known to cause autosomal recessive juvenile Parkinson's disease (Kitada *et al.*, 1998). Parkin was shown to interact with the N-terminus of both normal and expanded ataxin-2 and mediate its ubiquitination. However, the finding of altered expression levels of *FBXW8*, another E3 ubiquitin ligase, in the cerebellum transcriptome analysis of SCA2 mouse model, led to further *in vivo* and *in vitro* characterization studies of this association. FBXW8 was shown to co-localize with ataxin-2 and parkin, but only *FBXW8* expression levels were affected by expanded ataxin-2 in patient fibroblasts and blood samples, although both E3 ligases were sequestered into cytoplasmic aggregates. This exclusive effect of expanded ataxin-2 on only FBXW8 levels suggest parkin to be a secondary player in the degradation process of ataxin-2 (Halbach *et al.*, 2015).

1.4.2. Implication of *ATXN2* in Other Neurodegenerative Disorders

An interaction network for the 54 human proteins involved in 23 inherited ataxias was generated making use of the yeast 2-hybrid system. Eighteen of the 23 ataxia genes showed interaction either directly or indirectly. In this network, ataxin-2 was shown to have a direct and strong interaction with ataxin-1, the causative protein for SCA1 (Lim *et al.*, 2006). Further studies investigated the relationship between these two proteins and revealed that ataxin-2 could physically interact with ataxin-1 and was a contributor to expanded ataxin-1 toxicity, which was mediated by sequestration of ataxin-2 into intranuclear aggregates (Al-Ramahi *et al.*, 2007). Dysregulations in *ATXN2* level also acted as a modifier of disease onset and severity in SCA3 (Lessing and Bonini, 2008). Furthermore, hypermethylation of the *ATXN2* promoter contributed to an earlier AO by up to eight years, and also to increased severity in SCA3 patients (Laffita-Mesa *et al.*, 2012).

It was well established that more than 34 repeats in the CAG tract of *ATXN2* gene was pathogenic for the manifestation of SCA2, whereas less number of repeats was considered to be safe. However, intermediate-length expansions in the poly-Q domain have been recently related to increased risk for some other neurodegenerative disorders (Figure 1.11). Growing evidence suggests that intermediate-length expansions have a modifying effect over the clinical and molecular features of other disorders like AO, survival duration, disease severity, toxicity of other mutant proteins etc.

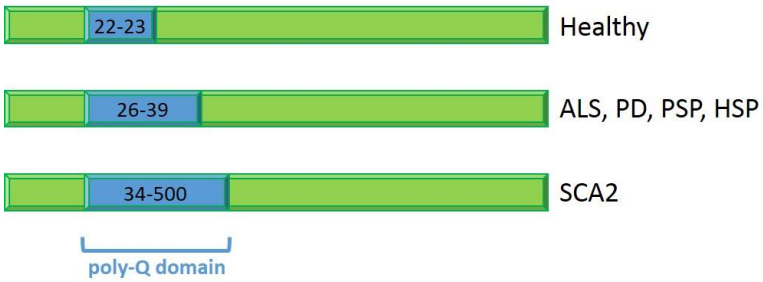

Figure 1.11. Association of the intermediate-length poly-Q expansions in *ATXN2* with distinct neurodegenerative disorders (Charles *et al.*, 2007; Elden *et al.*, 2010; Nielsen *et al.*, 2012; Ross *et al.*, 2011).

The first link of *ATXN2* intermediate allele involvement in another disease was discovered in the context of ALS (Elden *et al.*, 2010). With the discovery of TDP-43 and FUS mutations that explained a remarkable percentage of ALS cases, stress granules became a popular point of mechanism investigation since both TDP-43 and FUS are known RNA-binding proteins that shuttle from nucleus to cytoplasm and co-localize at the stress granules with translationally repressed mRNAs (Li *et al.*, 2013). Ataxin-2 was shown to interact with TDP-43 in an RNA-dependent manner at the stress granules and boost its cytotoxicity. Mislocalization of the ataxin-2/TDP-43 complex was also observed in the spinal cord samples of ALS patients. Following the functional association of ataxin-2 and TDP-43, screening of *ATXN2* gene for possible ALS-causing mutations revealed the significant occurrence of intermediate-length expansions in ALS patients (Elden *et al.*, 2010). Genotyping of this locus was further performed in distinct cohorts worldwide, all of

which confirmed *ATXN2* intermediate allele as a risk factor for ALS, as well as exposing a modifier effect on survival (Chiò *et al.*, 2015; Elden *et al.*, 2010; Lahut *et al.*, 2012; Lee *et al.*, 2011; Liu *et al.*, 2013). The cut-off values defining the "intermediate-length" interval, however, showed variation among different cohorts. In depth sequence analysis of *ATXN2* showed that intermediate alleles contributing to ALS pathogenesis are mostly interrupted by CAA repeats, and the number of interrupting units has an impact on AO (Yu *et al.*, 2011). The intermediate-length expansions in the *ATXN2* gene are found to be significantly enriched in *C9orf72* GGGGCC hexanucleotide repeat expansion, currently the most frequent genetic cause of both familial and sporadic forms of ALS, carriers (Renton *et al.*, 2014; van Blitterswijk *et al.*, 2014).

A similar scenario as TDP-43 also applies to FUS; ataxin-2 is shown to modify FUS toxicity and they are found to co-localize in the motor neuron samples of ALS patients (Farg *et al.*, 2013). An interaction between ataxin-2 and yet another stress granule component Profilin-1, which is also an ALS-causing gene, was again displayed in various disease models (Figley *et al.*, 2014). Mutations in all above-mentioned ALS genes have been shown to alter stress granule dynamics and mediate cell death, and the toxicity they provoke is shown to be modified by ataxin-2 owing to their co-localization. Ataxin-2 is believed to exhibit its modifier effect through (i) rendering the dissociation of stress granules impossible in post-stress conditions, (ii) activating stress-induced caspases, and (iii) enhancing modifications over other stress granule components.

Stress granules are formed under stringent conditions to pause the dispensable metabolic activities and relieve the burden of the cells. Ataxin-2, as previously explained, is involved in the assembly of stress granules, as well as their disassembly when stress disappears. Intermediate-length expansions in ataxin-2 destroys the dissolving ability of stress granules, capturing TDP-43 and FUS in the cytoplasmic aggregates preventing their translocation back to the nucleus. Accumulation mediated by intermediate-length ataxin-2 was observed to enhance the activation of stress-induced caspases, which lead to pathological TDP-43 modifications such as hyper-phosphorylation and cleavage (Hart and Gitler, 2012). Golgi fragmentation induced by ataxin-2/FUS double mutation also leads to the activation of the caspase pathway (Figure 1.9) (Farg *et al.*, 2013). Lastly, components of the stress granules are exposed to many enzymes capable of performing post-

translational modifications, such as proteases, kinases and ubiquitin-modifying enzymes. This increases the chance of a stress granule component of being subjected to a pathological modification that would further lead to alterations in cellular dynamics (Li *et al.*, 2013).

ATXN2 expansions are also pronounced in levodopa-responsive parkinsonism syndromes (Furtado *et al.*, 2002). Observation of anticipation phenomenon in some pedigrees with familial parkinsonism raised the possibility of a repeat expansion involvement in the pathogenesis. Segregation of the expanded allele with the neurological signs in a family suggested that *ATXN2* expansions could be the cause of at least a set of familial parkinsonisms (Payami *et al.*, 2003). A subsequent study further confirmed the presence of CAA-interrupted *ATXN2* expansions in autosomal dominant levodopa-responsive parkinsonism patients, although the associated repeat range was detected to be slightly higher than that of ALS, between 37-39. Two of the patients investigated in this study, also bearing a mutation in the known parkinsonism gene *LRRK2*, interestingly showed an earlier disease onset (Charles *et al.*, 2007). Modifier effect of *ATXN2* intermediate-expansions on the onset of different NDs is also evidenced in a Danish hereditary spastic paraplegia (HSP) cohort. Although the frequency of intermediate *ATXN2* expansions did not differ between patients and controls, this expansion significantly lowered the AO among HSP patients (Nielsen *et al.*, 2012). On the other hand, a strong risk association was established between the *ATXN2* expansion and progressive supranuclear palsy (PSP). Repeat lengths of 30 or more were significantly enriched in PSP patients and hypothesized to contribute to disease development. Even though expansions were detected in FTD, AD and PD patients, no significant frequency difference was found compared to controls (Ross *et al.*, 2011).

Some interesting clinical cases with the manifestation of psychiatric symptoms alongside SCA2 also exist. It is a common feature of ND patients to develop psychotic behavior during the disease course, both due to the degeneration of the respective brain regions and the general depression of the patient. An interesting case with the onset of paranoid type schizophrenia at the age of 22 is reported to manifest SCA2 nearly ten years afterwards (Rottnek *et al.*, 2008). SNP association analyses were performed in an

independent study to assess the risk of *ATXN2* variations on schizophrenia susceptibility. A non-synonymous SNP, that is predicted to increase the stability of the ataxin-2 protein, was found to be significantly associated with schizophrenia (Zhang *et al.*, 2014).

1.5. Biomarkers of SCA2

SCA2 is a monogenic disease, and there exists a definite way of assessing the disease risk for an individual by simply genotyping the CAG tract of the *ATXN2* gene. Hence, biomarker studies regarding SCA2 are more targeted to clinical signs and mostly inspects the progression of the disease from a neuro-physiological approach. The status of nerve conduction abnormalities in the sensory and motor system are proposed to be progression markers of SCA2. Reduction of sensory amplitudes is the earliest observation, even present in pre-symptomatic individuals. Subsequent increase in sensory latency followed by motor nerve involvement divides the clinical progression into three phases (Velázquez-Perez *et al.*, 2010). Metabolite concentration screening in the cerebellum and pons of SCA2 patients may also be utilized as a marker of cellular dynamics. Low levels of neurometabolites N-acetylaspartate and glutamate, and high levels of glial markers and energetic metabolites myoinositol and creatine, are correlated with disease severity, suggesting an effort employed by the cells to compensate damage. Neuro- and energetic metabolite imaging therefore may be a way to monitor neural metabolism at the affected regions and are argued to be good candidates for the evaluation of applied treatments (Adanyeguh *et al.*, 2015).

The only molecular biomarker study for SCA2 so far examines the plasma proteome of ten SCA2 patients compared to age- and sex-matched controls. Authors performed 2D-difference in-gel electrophoresis to detect differentially expressed spots by 1.5-fold, following which LC-MS/MS and Western blot analysis revealed the identity of these proteins and validated the expression change. Nine differentially expressed proteins associated with cognitive impairment (RBP4, TTR), oxidative stress (albumin), calcium-dependent apoptosis (VDCC gamma-3 subunit) and neuropathy (Apo-AI, Apo-E) were

acquired consistent with the previously explained potential mechanisms of pathology contributing to the disease (Swarup *et al.*, 2013).

2. PURPOSE

Due to its autosomal dominant nature, SCA2 generally affects multiple individuals per family, and it may show anticipation between generations with earlier disease onset and faster progression. Although levodopa replacement or deep brain stimulation may alleviate the symptoms in a subset of patients, there is no treatment directly targeting the cause of the disease yet.

The development of effective therapies is only possible with the complete understanding of the causative factor and the precise dissection of the different pathogenic stages. Although ataxin-2 is known to be involved in several different mechanisms, such as transcriptional control, ribosomal translation and stress granule formation, its exact role in the complex network of cellular pathways is yet to be discovered. Identification of a therapeutic target and development of a potent treatment for SCA2, therefore, would only be possible upon complete exploration of both native ataxin-2 function and the basis of expansion-induced pathogenesis. Accordingly, the major aims of this thesis are:

- Examining the downstream effects of *ATXN2* deficiency in order to elucidate the native function of the protein
- Examining the downstream effects of *ATXN2* expansions in order to understand the expansion-induced pathogenesis
- Identifying biomarker candidates for both loss- and gain-of ataxin-2 function
- Developing blood biomarkers of SCA2 that would demonstrate the molecular pathology related to a specific stage of the disease

We believe that unravelling the native ataxin-2 function and the expansion-induced pathogenesis at different stages of the disease would eventually lead to the identification of suitable molecular targets for cause-targeted therapies.

3. SUBJECTS AND MATERIALS

3.1. SCA2 Patients and Healthy Controls from a Large Turkish Pedigree

A large Turkish pedigree from Burhaniye, Balıkesir, consisting of several individuals with a SCA2 clinical diagnosis, was referred to our laboratory by Dr. Gülden Akdal from Dokuz Eylül University Medical School, Neurology Clinic (Table 3.1).

Peripheral blood samples were collected from five disease-manifesting and eight non-symptomatic individuals in this family into EDTA and PAXgene Blood RNA tubes (Figure 3.1).

Table 3.1. Blood donors from the large SCA2 pedigree.

Individual No.	Birth Year	SCA2 Status	AO
#1	1964	Non-symptomatic	
#2	1967	Non-symptomatic	
#3	1961	Manifested	32
#4	1964	Non-symptomatic	
#5	1986	Non-symptomatic	
#6	1988	Manifested	12
#7	1994	Manifested	<10
#8	1965	Non-symptomatic	
#9	1979	Manifested	
#10	1941	Non-symptomatic	
#11	1944	Non-symptomatic	
#12	1947	Manifested	53
#13	1976	Non-symptomatic	

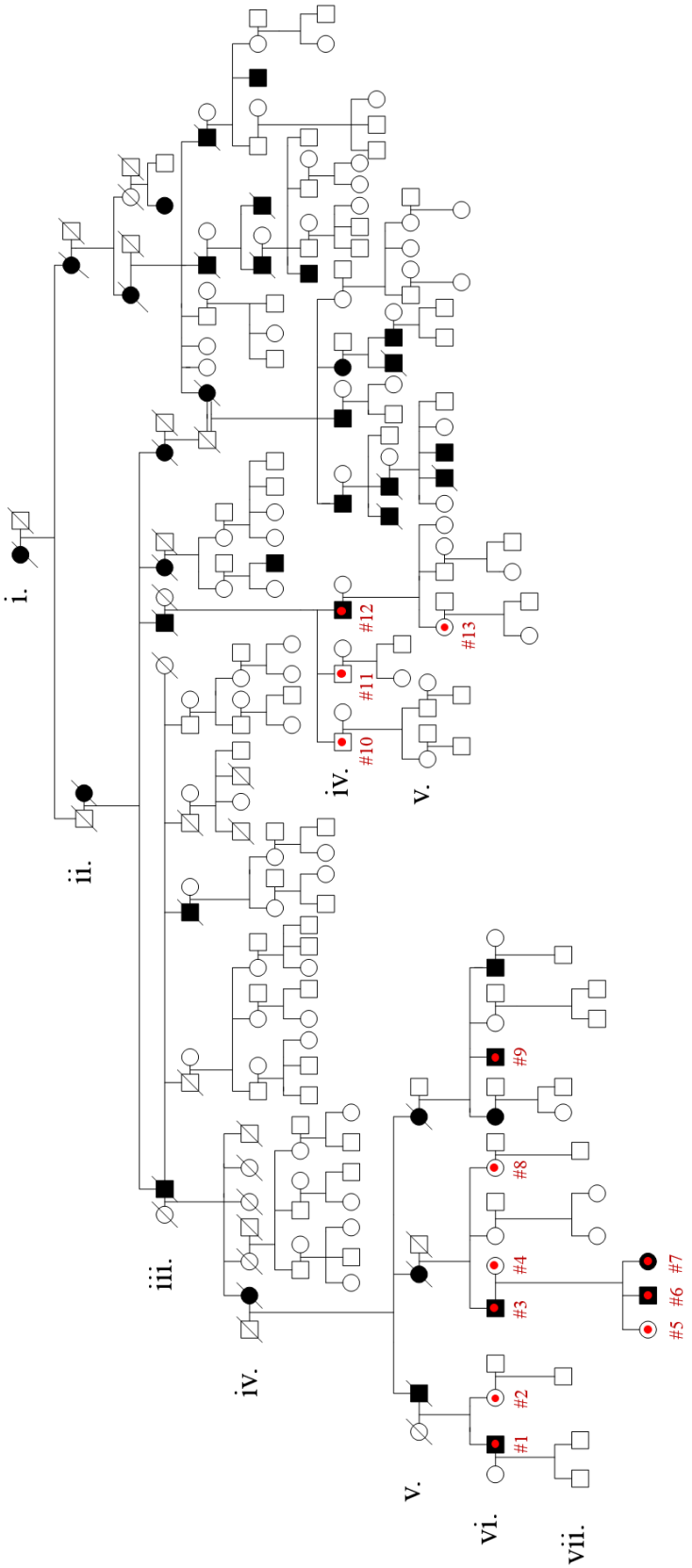

Figure 3.1. The large SCA2 pedigree from Balıkesir, Turkey. Red dot indicates the individuals who were available for blood collection in July 2013.

3.1.1. Equipment and Solutions for DNA Isolation and PCR Amplification

MagNA Pure Compact Nucleic Acid Isolation Kit I and MagNA Pure Compact Instrument were used in DNA extraction from blood samples. Concentration and quality of the isolated DNA were measured with NanoDrop 2000c UV-Vis Spectrophotometer. Content of the FastStart Taq DNA Polymerase dNTPack kit used in PCR amplification and the primer sequences are listed in Tables 3.2 and 3.3, respectively.

Table 3.2. Solutions and chemicals used in the amplification of *ATXN2* CAG repeat tract.

FastStart Taq DNA Polymerase, dNTPack Catalog No: 04738357001, Roche Diagnostics GmbH	
Contents	**Concentration**
FastStart Taq DNA Polymerase	5 U/µl
PCR Reaction Buffer w/ 20 mM $MgCl_2$	10X
PCR Reaction Buffer w/o $MgCl_2$	10X
$MgCl_2$	25 mM
GC Rich Solution	5X
dNTP	10 mM each

Table 3.3. Primers used in the amplification of *ATXN2* CAG repeat tract.

Forward Primer	5'-GGG CCC CTC ACC ATG TCG-3'
Reverse Primer A	5'-CGG GCT TGC GGA CAT TGG-3'
Reverse Primer B	5'-/56-FAM/-CGG GCT TGC GGA CAT TGG-3'

3.1.2. Equipment and Solutions for Agarose Gel Electrophoresis and Gel Extraction

All the solutions, chemicals and laboratory equipment used in agarose gel electrophoresis are listed in Table 3.4. Extraction of the expanded and normal alleles from the gel was performed using the QIAquick Gel Extraction Kit, Qiagen.

Table 3.4. Materials used in agarose gel electrophoresis.

Solution/Chemical/ Equipment		Catalog No.	Company
5X TBE	0.45 M Tris-base	T1503	Sigma-Aldrich
	0.45 M Boric acid	194810	MP Biomedicals, LLC
	10 mM Na_2EDTA	0105-500G	Amresco, Ohio
Agarose Biomax		-	Prona, EU
GelRed Dropper Bottle		103.302-05	Olerup SSP
DNA Ladder, GeneRulerTM 100bp		SM0241	Thermo Scientific
DNA Gel Loading Dye (6X)		R0611	Thermo Scientific
Tank, OWL EasyCast B1		349900	Thermo Scientific
Power Supply, EC300XL2		C1596100710705	Thermo Scientific
GelDoc		-	Biorad

3.2. *Atxn2* Knock-Out Mouse Line

Details regarding the *Atxn2* knock-out (*Atxn2*-KO) mouse line used in the framework of this thesis are shown in Table 3.5.

Table 3.5. General information regarding *Atxn2*-KO mouse line.

Mouse	Method	Background	Phenotype	Reference
Atxn2-knock out (*Atxn2*-KO)	Excision of exon 1	C57BL/6J	• No sign of ataxia or neurological symptoms • Reduced fertility • Insulin resistance • Obesity	(Lastres-Becker *et al.*, 2008a)

3.3. *Atxn2* Knock-Down SH-SY5Y Line and Cell Culture Equipment

Details regarding the naïve SH-SY5Y cell line and shRNA constructs utilized in the knock-down procedure are shown in Tables 3.6 and 3.7, respectively.

Table 3.6. General information regarding naïve SH-SY5Y cell line.

Cell Line	Catalog No.	Type	Company	Reference
SH-SY5Y	94030304	neuroblastoma	European Collection of Cell Cultures Sigma-Aldrich, Taufkirchen, Germany	(Biedler *et al.*, 1978)

Table 3.7. Target and control shRNA constructs used in the knock-down protocol.

shRNA	Catalog No.	Company	Reference
MISSION Non-Target Control TP	SHC002V	Sigma-Aldrich, Taufkirchen, Germany	PhD Thesis Michael Klinkenberg, PhD
MISSION ATXN2 Knock-Down TP	TRCN0000118914	Sigma-Aldrich, Taufkirchen, Germany	PhD Thesis Jessica Drost, PhD

General equipment, solutions and media used in the cell culture experiments with non-target (NT) and *ATXN2* knock-down (*ATXN2*-KD) SH-SY5Y cells are listed in Table 3.8.

Table 3.8. Materials used in the cell culture experiments.

Solution/Chemical/ Equipment	Catalog No.	Company
Roswell Park Memorial Institute 1640 (RPMI)	21875-034	Life Technologies
Hank's Balanced Salt Solution 1X (HBSS)	24020-091	Life Technologies
L-glutamine 200 mM	25030-024	Life Technologies
Fetal Calf Serum Gold (FCS)	A15-151	PAA
Dulbecco's Phosphate Buffered Saline (PBS)	14190-094	Life Technologies
Trypsin-EDTA 0.05%	25300-054	Life Technologies
Puromycin	A1113803	Life Technologies
Distilled H_2O	10977-035	Life Technologies
6-well cell culture plate sterile, with lid	657160	Greiner Bio-One
Cellstar cell culture flasks, 25 cm^2	690175	Greiner Bio-One
Cellstar cell culture flasks, 75 cm^2	658175	Greiner Bio-One
Cell scraper	831.830	Sarstedt
CryoTube Vials	377224	Thermo Scientific
Neubauer counting chamber, 0.0025 mm^2	728.1	Carl Roth
Cell culture bench Lamin Air HB2448	-	Heraeus
Cell culture bench MSC Advantage	-	Thermo Scientific
Centrifuge 5702	-	Eppendorf
Centrifuge MinifugeTM	-	Labnet
CO^2-Incubator HERAcell 240i	-	Thermo Scientific
Nitrogen tank RS Series	-	Welabo
Water bath GFL 1083	-	Gemini BV Laboratory

3.4. Equipment and Solutions for RNA Isolation, DNaseI Treatment and cDNA Synthesis

Reagents and kits used for total RNA isolation from different sample types are shown in Table 3.9.

Table 3.9. Reagents and kits used for total RNA isolation from different sample types.

Sample	Reagent / Kit
WT and *Atxn2*-KO mouse tissue	TRIzol Reagent
Patient and control blood sample	PAXgene Blood RNA Kit v2
NT and *ATXN2*-KD SH-SY5Y cells	QIAshredder and RNeasy Mini Kit

Solutions and enzymes used in DNaseI treatment of the isolated total RNA and reverse transcription into cDNA are listed in Table 3.10.

Table 3.10. Contents of the kits used in DNaseI treatment and reverse transcription of the isolated total RNA.

DNaseI Amplification Grade, Catalog No: 18068-015, Invitrogen	
DNaseI Reaction Buffer	10X
DNaseI Amplification Grade	100 U
EDTA	25 mM
Oligo(dT)$_{20}$ Primer, Catalog No: 18418-020, Invitrogen	
Oligo(dT)$_{20}$ Primer	50 µM
dNTP	10 mM each
Random Primers, Catalog No: 48190-011, Invitrogen	
Random Primer	300 µg
SuperScript III Reverse Transcriptase, Catalog No: 18080-044, Invitrogen	
SuperScript III Reverse Transcriptase	200 U/µl
First Strand Buffer	5X
DTT	0.1 M

3.5. qRT-PCR Equipment and Taqman Assays

General laboratory equipment and solutions used in gene expression analysis via qRT-PCR are listed in Table 3.11.

Table 3.11. Materials used in Taqman gene expression assays.

Solution/Chemical/ Equipment	Catalog No.	Company
Taqman Probes	-	Applied Biosystems
FastStart Universal Probe Master	4914058001	Roche Diagnostics GmbH
MicroAmp Fast Optical 96-well Reaction Plate	4346906	Applied Biosystems
MicroAmp Optical Adhesive Film	4311971	Applied Biosystems
StepOnePlus Real-Time PCR System Thermal Cycling Block	272006429	Applied Biosystems

All the human and murine Taqman probes used in this thesis are listed in Tables 3.12 and 3.13, respectively.

Table 3.12. Human Taqman assays.

Gene	Assay code	Gene	Assay code
ABCD2	Hs00193054_m1	*LIG4*	Hs01866071_u1
ALS2	Hs01066522_m1	*LRRK2*	Hs00968209_m1
ATM	Hs01112355_g1	*MATR3*	Hs00251579_m1
ATXN1	Hs00165656_m1	*MMP9*	Hs00234579_m1
ATXN2	Hs00268077_m1	*MTPAP*	Hs00912730_m1
ATXN3	Hs001026440_g1	*MYCN*	Hs00232074_m1
ATXN7	Hs00165660_m1	*NUP214*	Hs01090093_m1
BCKDHB	Hs00609053_m1	*OPA1*	Hs01047019_m1
C9orf72	Hs00376619_m1	*PABPC1*	Hs01598422_mH
CACNA1B	Hs01053090_m1	*PHTF2*	Hs01111633_m1
CHMP2B	Hs01045897_m1	*PINK1*	Hs00260868_m1
CNOT3	Hs00248115_m1	*PMAIP1*	Hs00560402_m1
CYP26B1	Hs01011223_m1	*PSENEN*	Hs00708570_s1
DACT1	Hs00420410_m1	*RNF152*	Hs00741870_g1
DBT	Hs01066445_m1	*SEC61A1*	Hs01037684_m1
DCP2	Hs00400333_m1	*SERINC2*	Hs00386067_m1
DCTN1	Hs00896389_g1	*SETX*	Hs00209294_m1
DLAT	Hs00898876_m1	*SLC2A4*	Hs00168966_m1
DLD	Hs00164401_m1	*SPAST*	Hs00208952_m1
ERLIN2	Hs00200360_m1	*SPG11*	Hs00276752_m1
FUS	Hs00192029_m1	*SSR2*	Hs00162346_m1
ETS1	Hs00428293_m1	*SSR4*	Hs00196721_m1
ETV5	Hs00927557_m1	*SYVN1*	Hs00381211_m1
ETV7	Hs00903229_m1	*TARDBP*	Hs00606522_m1
FMR1	Hs00924547_m1	*TBC1D3*	Hs00414388_m1
GAD1	Hs01065893_m1	*TBP*	Hs99999910_m1
GALNT14	Hs00226180_m1	*TIMD4*	Hs00293316_m1
GEMIN7	Hs02378886_s1	*TTBK2*	Hs00392032_m1
GHITM	Hs00209205_m1	*UBQLN2*	Hs01128785_s1
GRAMD1C	Hs00214023_m1	*VCPIP1*	Hs00228106_m1
HPRT1	Hs99999909_m1	*ZDHHC20*	Hs00708514_s1
ITPR1	Hs00976045_m1	*ZNF699*	Hs04195321_s1
KLHL11	Hs00216741_m1		

Table 3.13. Murine Taqman assays.

Gene	Assay code
Apoa1	Mm00437568_g1
Atxn2	Mm00485946_m1
Hpx	Mm00457510_m1
Sel1l	Mm01326442_m1
Serpina1a	Mm02748447_g1
Serpina1a/a1c	Mm04207709_gH
Serpina1a/a1b/a1c	Mm04207703_mH
Syvn1	Mm01233557_g1
Tbp	Mm00446971_m1

3.6. Equipment and Solutions for Protein Isolation, Quantitation and SDS-PAGE

General laboratory equipment and solutions used in protein isolation, quantitation and SDS-PAGE experiments are listed in Table 3.14. Contents of the lysis buffers used in protein isolation and stock solutions used in SDS-PAGE are shown in Tables 3.15 and 3.16, respectively.

Table 3.14. Materials used in protein isolation, quantitation and SDS-PAGE.

Solution/Chemical/ Equipment	Catalog No.	Company
Protease Inhibitor Cocktail, Complete Mini, EDTA-free	11836170001	Roche
Protease Inhibitor Cocktail	1861278	Thermo Scientific
Pellet pestles polypropylene	Z359947	Sigma-Aldrich
Kontes Pellet Pestle Cordless Motor		Sigma-Aldrich
Roti-Quant Bradford Solution 5X	K015.1	Carl Roth
BSA Standard	B9001S	New England BioLabs
Precision Plus Protein Standards, all blue	161-0373	Biorad
Precision Plus Protein Standards, dual color	161-0374	Biorad
Blot Absorbent Filter Paper	1703958	Biorad
Mini Trans-Blot Filter Paper	1703932	Biorad
Mini-PROTEAN Tetra Cell	552BR065924	Biorad
Mini-PROTEAN 3 Cell	525BR084014	Biorad
Mini-PROTEAN System Glass Plates short	1653308	Biorad
Mini-PROTEAN System Glass Plates spacer 1.0mm	1653311	Biorad

Table 3.15. Contents of the lysis buffers used in protein isolation.

RIPA Lysis Buffer	50 mM Tris-HCl pH:8.0 150 mM NaCl 1% Igepal CA-630 0.5% Sodium deoxycholate 0.1% SDS 2 mM EDTA	5 ml Tris-HCl 1 M pH:8.0 3 ml NaCl 5 M 1 ml Igepal CA-630 0.5 g Sodium deoxycholate 1 ml SDS (10%) 0.4 ml EDTA 500mM Complete to 100 ml with dH_2O
SDS Lysis Buffer	137 mM Tris-HCl pH:6.8 4% SDS 20% Glycerol	2.74 ml Tris-HCl 0.5 M pH:6.8 4 ml SDS (0.1%) 2 ml Glycerol Complete to 10 ml with dH_2O

Table 3.16. Contents of the stock solutions used in SDS-PAGE.

Running Buffer (10x):	25 mM Tris pH 8.2 192 mM Glycine 0.1% SDS	29 g Tris 144 g Glycine 10 g SDS
Loading Buffer (2x)	250 mM Tris-HCl pH:7.4 20% Glycerol 4% SDS 10% 2-Mercaptoethanol 0.005 % Bromophenol blue 5% dH2O	2.5 ml Tris/HCl 1M pH:6.9 2.0 ml Glycerol 4.0 ml SDS (10%) 0.5 ml 2-Mercaptoethanol 0.5 ml BPB-Solution (0.1%) 0.5 ml dH_2O
Transfer Buffer (10x):	25 mM Tris pH 8.2 192 mM Glycine	30 g Tris 145 g Glycine
TBS (10x)	0.5 M Tris 1.5 M NaCl	60.5 g Tris 87.6 g NaCl

3.7. Quantitative Immunoblotting Equipment, Solutions and Antibodies

General laboratory equipment and solutions used in quantitative immunoblots are listed in Table 3.17.

Table 3.17. Materials used in quantitative immunoblots.

Solution/Chemical/ Equipment	Catalog No.	Company
ImmunoBlot PVDF membrane	1620177	Biorad
Protran Nitrocellulose membrane BA83	10401396	GE Healthcare
SuperSignal West Pico Chemiluminescent Substrate	1856135-6	Thermo Scientific
Super RX medical X-Ray film	Super RX	Fujifilm
Developer G153A+B	HT536	AGFA
Rapid Fixer G354	2828Q	AGFA
Odyssey Classic	-	Li-Cor Biosciences

Primary and secondary antibodies used in immunoblotting are listed in Table 3.18 and 3.19, respectively.

Table 3.18. Primary antibodies used in quantitative immunoblots.

1º Antibody	Catalog No.	Company	Host
α-Tubulin	T9026	Sigma-Aldrich	Ms monoclonal
β-Actin	A5441	Sigma-Aldrich	Ms monoclonal
AGPAT3	ab107574	Abcam	Rb polyclonal
Apo-AI	ARP54279_P050	Aviva	Rb polyclonal
Apo-AII	ABIN 970121	Antikoerper/Aviva	Rb polyclonal
Apo-CI	H00000341-D01P	Abnova	Rb polyclonal
Ataxin-2	611378	BD Biosciences	Ms monoclonal
DACT1	AP21723PU-N	Acris	Rb polyclonal
ETV7	sc-292509	Santa Cruz	Rb polyclonal
Fibrinogen alpha	ab108616	Abcam	Rb polyclonal
Hemopexin	ab90947	Abcam	Rb polyclonal
LSM12 C-terminus	OAAB09407	Aviva	Rb polyclonal
LSM12 Middle	ARP52909_P050	Aviva	Rb polyclonal
SEL1L	ab7898	Abcam	Rb polyclonal
SERPINA1	GWB-92B2C9	GenWay Biotech	Ms monoclonal
SERPINA3	ab129194	Abcam	Rb polyclonal
Serum Albumin	GTX85111	GeneTex	Ch polyclonal
Synoviolin 1	OAAB15823	Aviva	Rb polyclonal
Transferrin	ab1223	Abcam	Rb polyclonal
Transthyretin	LS-B7812 / 50269	LS Bio	Ch polyclonal
VDBP	ab89765	Abcam	Ms polyclonal

Table 3.19. Secondary antibodies used in quantitative immunoblots.

2º Antibody	Catalog No.	Company	Host
α-mouse	926-32210 IRDye 800CW	Li-cor	Goat
α-rabbit	926-32221 IRDye 680RD	Li-cor	Goat
α-chicken	ab6753	Abcam	Rabbit

3.8. Software, Online Tools and Databases

Software, online tools and databases used in the framework of this thesis are listed in Table 3.20.

Table 3.20. Software, tools and databases utilized.

Software/Tool/Database	Source
Adobe Reader XI	Adobe
CLC Main Workbench v5.7	CLC bio
ClustalW	http://www.ebi.ac.uk/Tools/msa/clustalw2/
Endnote X7	Thomson Reuters
GeneCards	http://www.genecards.org/
GSEA/MSigDB web site v5.0	Broad Institute
GraphPad Prism v6.0	GraphPad Software Inc.
GraphPad QuickCalcs Outlier Calculator	http://graphpad.com/quickcalcs/Grubbs1.cfm
Image Lab Software v5.2.1	Biorad
ImageJ v1.48	http://imagej.nih.gov/ij/
ImageStudio v4.0	Li-Cor Biosciences
Mendeley Desktop	Mendeley Ltd.
MS Office	Microsoft
MSigDB	http://www.broadinstitute.org/gsea
NanoDrop 2000 / 2000c Software	Thermo Scientific
NCBI tools	http://www.ncbi.nlm.nih.gov/
Peak Scanner Software v1.0	Life Technologies
Photoshop	Adobe
StepOne Software v2.2.2	Applied Biosystems
STRING v10	http://string-db.org/
UniProt	http://www.uniprot.org/

3.9. General Laboratory Equipment, Chemicals and Kits

General laboratory equipment, chemicals and kits used in the framework of this thesis are listed in Tables 3.21, 3.22 and 3.23, respectively.

Table 3.21. General laboratory equipment.

Equipment	Types	Catalog No.	Company
96-well plate	MicroAmp Fast Optical 96-well Reaction Plate	4346906	Applied Biosystems
96-well plate optic cover	MicroAmp Optical Adhesive Film	4311971	Applied Biosystems
Aluminum foil	Aluminium foil alupro	A0621	Ecopla
Autoclave	Autoclave Tuttnauer 2540EL	-	Systec
	Autoclave Varioklav 400	-	H+P Labortechnik
Balances	TE612	-	Sartorius
	Analytical Balance 474-32	-	Kern & Sohn
	Analytical Balance PE1600	-	Mettler Toledo
	Analytical Precision Balance A120S	-	Sartorius
Centrifuges	2-16K	-	Sigma
	5415 C	-	Eppendorf
	5415 D	-	Eppendorf
	5415 R	-	Eppendorf
Cuvettes	UV-Cuvette micro	759200	Brand
DNA extraction system	MagNA Pure Compact Instrument	3731146001	Roche Diagnostics GmbH
Electrophoretic equipment	OWL EasyCast B1 Tank	349900	Thermo Scientific
	Mini-PROTEAN Tetra Cell	552BR065924	Biorad
	Mini-PROTEAN 3 Cell	525BR084014	Biorad
Filter Paper	Blot Absorbent Filter Paper	1703958	Biorad
	Mini Trans-Blot Filter Paper	1703932	Biorad
Refrigerators	2021D (-20 °C)	-	Arçelik
	HT5786-A (-86 °C)	-	Hettich

Table 3.21. General laboratory equipment (cont.).

Equipment	Types	Catalog No.	Company
Refrigerators	Freezer (-80 °C) Forma900	-	Forma900
	Freezer (-80 °C) HERAfreeze	-	HERAfreeze
	Freezer AEG Arctis	-	AEG Arctis
Gel documentation	GelDoc	-	Biorad
Glass Plates	Mini-PROTEAN System Glass Plates short	1653308	Biorad
	Mini-PROTEAN System Glass Plates spacer 1.0mm	1653311	Biorad
Heat Block	Thermomixer comfort	-	Eppendorf
	Thermomixer compact	-	Eppendorf
Hood	IP44/I	-	Wesemann
Immunoblot documentation	Odyssey Classic	-	Li-Cor Biosciences
Incubators	Drying oven T5025	-	Heraeus
	Drying oven T5028	-	Heraeus
	BD23	-	Binder
	Modell 200	-	Memmert
Magnetic stirrer	Ikamag RCT	-	IKA Werke
	REO basic C	-	IKA Werke
Membranes	ImmunobBlot PVDF membrane	1620177	Biorad
	Protran Nitrocellulose Membranes BA83	10401396	GE Healthcare
Microcentrifuge tubes	1.5-ml Boil-Proof Microtubes	-	Axygen
	0.5-ml Thin Wall Flat Cap PCR tubes	-	Axygen
	8-tube strips	-	Axygen
Micropipettes	Pipet-lite SL10, 20, 100, 1000	-	Rainin
	Finnpipette F1, 1-10 µl, 10-100 µl	-	Thermo Scientific
	Pipetman Classic pipettes, 2 µl, 10 µl, 20 µl, 200 µl, 1000 µl	-	Gilson
Micropipette tips	Universal Fit Filter Tips, 10 µl, 100 µl, 200 µl, 1000 µl	-	Axygen
	TipOne, 10 µl, 200 µl, 1000 µl	-	Starlab
	TipOne, sterile, 10 µl, 20 µl, 200 µl, 1000 µl	-	Starlab
Microscope	DMIL Inverted	090-135-001	Leica
Microwave oven	Intellowave MD554	501283307	Arçelik

Table 3.21. General laboratory equipment (cont.).

Equipment	Types	Catalog No.	Company
Parafilm	Parafilm	PM-996	Bemis
Pestle	Pellet pestles polypropylene	Z359947	Sigma-Aldrich
Pestle Motor	Kontes Pellet Pestle Cordless Motor	-	Sigma-Aldrich
pH meter	pH Bench Meter Microprocessor ATC pH210	-	HANNA Instruments
Pipet Controller	Pipet Boy accu-jet	-	Brand
Power supplies	EC300XL2 Power Supply	C1596100710705	Thermo Scientific
	Power pack Consort E122	-	Consort
Real Time-PCR System	StepOnePlus Real-Time PCR System Thermal Cycling Block	272.006.429	Applied Biosystems
Rotators	2-1175	-	Neolab
	34528E	-	Neolab
	Polymax 1040	-	Heidolph
	RM5	-	CAT
	RollerMixer	-	Ratek
Serological pipets	Non-sterile, 5 ml, 10ml, 25ml	-	Sigma-Aldrich
	Sterile, 5 ml, 10ml, 25ml	-	Sigma-Aldrich
Shakers	Minishaker MS1	-	IKA Werke
Spectrophotometers	NanoDrop 2000c UV-Vis Spectrophotometer	-	Thermo Scientific
	BioPhotometer 6131	-	Eppendorf
Sterile tubes	Cellstar Tubes sterile, 15 ml, 50ml, 50ml brown	-	Greiner Bio-One
Thermal cyclers	TC-312	FTC3102D	Techne
Vortex	REAX top	100420596	Heidolph
	Vortex Genie 2	-	Bender & Hobein
Water bath	WNB10	L307.1074	Memmert
Water purification system	Arium 611UV Ultrapure Water System	-	Sartorius
	Milli-Q Ultrapure Water System	-	Millipore
Wipes	Kim Precision Wipes	5511	Kimberly-Clark
X-ray film	Super RX medical X-Ray film	Super RX	Fujifilm

Table 3.22. General chemicals used in various experiments.

Chemical	Catalog No.	Company
2-Mercaptoethanol	12006	Merck
2-Propanol	33539	Sigma-Aldrich
	100995	Merck
Acrylamide/Bis-Acrylamide 29:1	161-0124	Biorad
Agarose Biomax	-	Prona
Ammonium persulfate	101201	Merck
Boric acid	194810	MP Biomedicals
Bovine serum albumin	A7906	Sigma-Aldrich
	B9001S	New England BioLabs
Bradford Solution (Roti-Quant, 5X)	K015.1	Carl Roth
Bromophenol Blue	B6131	Sigma-Aldrich
Di-sodium EDTA	0105-500G	Amresco
Distilled water (DNase/RNase free)	10977-035	Life Technologies
Dimethylsulfoxid (DMSO)	41639	Sigma-Aldrich
Eau Bi-Distillee	40503012	Galen İlaç Sanayii
Ethanol	32205	Sigma-Aldrich
Ethylenediamine tetraacetic acid (EDTA)	E5134	Sigma-Aldrich
Glycerol	G5516	Sigma-Aldrich
Glycine	A1377	AppliChem
Hydrochloric acid	A2427	AppliChem
	100314	Merck
Igepal CA-630	I3021	Sigma-Aldrich
Methanol	32213	Sigma-Aldrich
Milk powder	-	Sucofin
RNaseZap	R2020	Sigma-Aldrich
Sodium chloride	31434	Sigma-Aldrich
Sodium deoxycholate	D5670	Sigma-Aldrich
Sodium dodecyl sulfate	L5750	Sigma-Aldrich
Tris (Trizma base)	T1503	Sigma-Aldrich
Tween 20	P1379	Sigma-Aldrich

Table 3.23. Commercially available kits used in various experiments.

Kit	Catalog No.	Company
DNaseI Amplification Grade	18068-015	Invitrogen
FastStart Taq DNA Polymerase, dNTPack	4738357001	Roche Diagnostics GmbH
FastStart Universal Probe Master (Rox)	4914058001	Roche Diagnostics GmbH
MagNA Pure Compact Nucleic Acid Isolation Kit I	3730964001	Roche Diagnostics GmbH
Oligo(dT)20 Primer	18418-020	Invitrogen
PAXgene Blood RNA Kit v2	762174	PreAnalytiX, Qiagen BD
PAXgene Blood RNA Tubes	762165	PreAnalytiX, Qiagen BD
QIAquick Gel Extraction Kit	28704	Qiagen
QIAshredder	79656	Qiagen
Random Primers	48190-011	Invitrogen
RNeasy Mini Kit	74106	Qiagen
SuperScript III Reverse Transcriptase	18080-044	Invitrogen

4. METHODS

The sequential order of the different methods performed in connection with various samples is summarized in Figure 4.1.

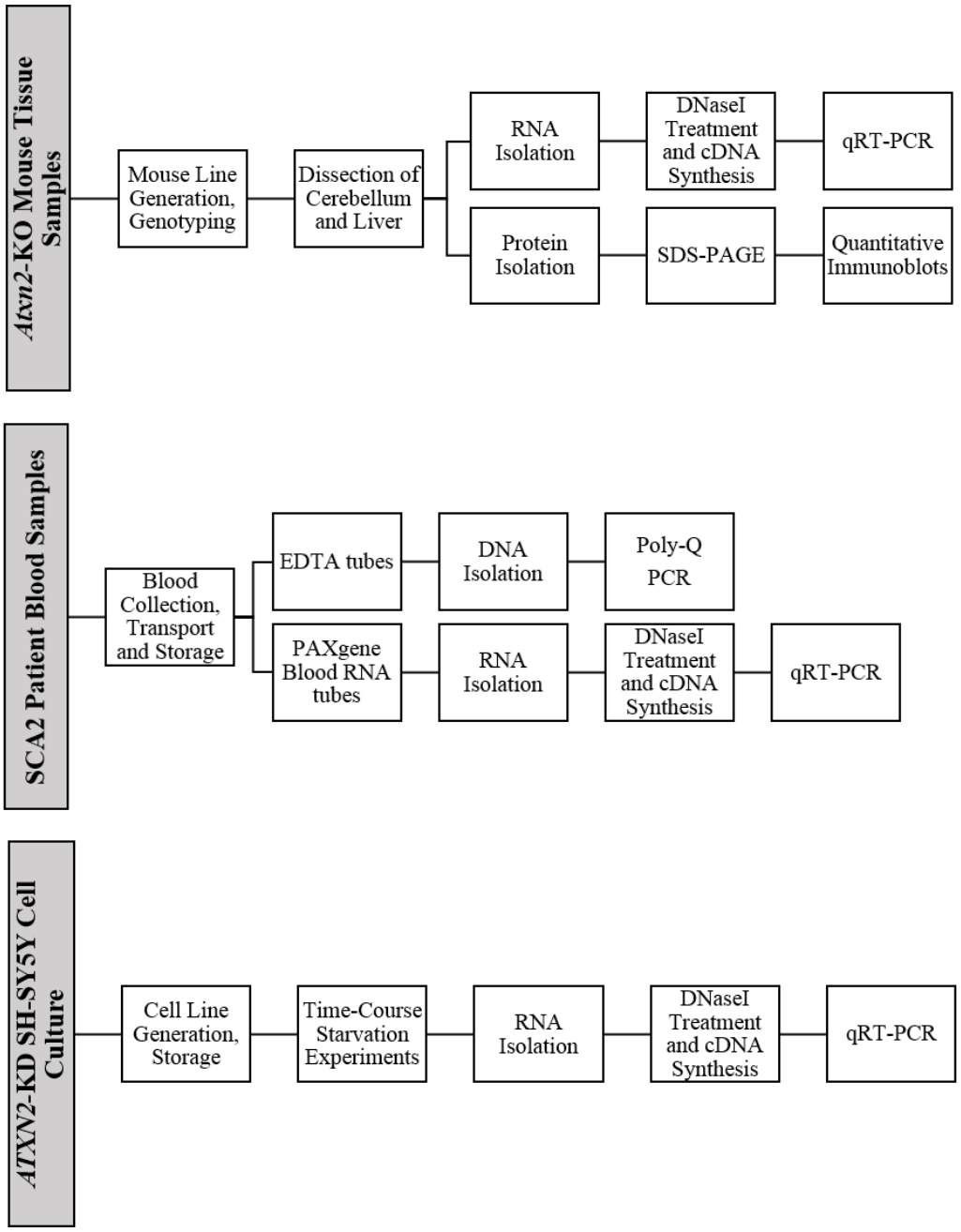

Figure 4.1. Flow chart summarizing the methods performed with *Atxn2*-KO mouse tissues, SCA2 patient blood samples and *ATXN2*-KD SH-SY5Y cells.

4.1. SCA2 Patient Peripheral Blood Samples

Several SCA2 patients from a large Turkish pedigree living in Burhaniye, Balıkesir were referred to NDAL for routine diagnostics. With the intention of further investigating ataxin-2 mechanism and pathology, we contacted the family for a planned sample collection.

4.1.1. Blood Collection, Transport and Storage

Peripheral blood samples were collected from five disease-manifesting and eight non-symptomatic family members in the same day, with informed written consent and approval of the Ethics Commission of Boğaziçi University. At the time of sample collection, all the individuals had fasted overnight. Blood samples into three EDTA and three PAXgene Blood RNA tubes were taken from every individual. PAXgene Blood RNA tubes were kept at room temperature for three hours as stated in the manufacturer's guide. Then, they were frozen in styrofoam boxes filled with dry ice. EDTA tubes were also placed in styrofoam boxes without dry ice. On the same day, all tubes were transported to Istanbul via air way, and PAXgene Blood RNA tubes were stored in -80 ^{o}C deep freezer immediately. EDTA tubes were stored at 4 ^{o}C refrigerator.

4.1.2. DNA Isolation and *ATXN2* Poly-Q Repeat Size Determination

Genomic DNA was extracted from 1000 µl of the peripheral blood samples collected into EDTA tubes via MagNA Pure Compact Instrument, according to the instructions stated in the MagNA Pure Compact Nucleic Acid Isolation Kit I manual. Amount and quality of the extracted DNA were measured with NanoDrop 2000c UV-Vis Spectrophotometer. 30-40 ng of genomic DNA was further used in the amplification of *ATXN2* CAG repeat tract with conventional PCR method. Content of the PCR mix for one

sample and cycling conditions are shown in Tables 4.1 and 4.2, respectively. The volume of each PCR reaction is adjusted to 25 µl with distilled H_2O after all reagents are mixed.

Table 4.1. Content of the *ATXN2* CAG repeat amplification PCR mix.

Reagent	**[Stock]**	**Volume (µl)**	**[Final]**
Buffer ($MgCl_2$ Positive)	10X	2.5	1X
$MgCl_2$	25 mM	1.5	3,5 mM
GC Rich	5X	5	1X
dNTP	5 mM	1	0,8 mM
Fwd Primer	12,5 pmole/µl	1	0,5 mM
Rev Primer (A or B)	12,5 pmole/µl	1	0,5 mM
FastStart Taq Polymerase	5 U/µl	0.2	1 U/µl

Table 4.2. PCR conditions for *ATXN2* CAG repeat amplification.

Initial Denaturation	94 ºC	5 min	
Denaturation	95 ºC	60 sec	30 cycles
Annealing	55.7 ºC	60 sec	
Extension	72 ºC	90 sec	
Final Extension	72 ºC	5 min	

For the determination of CAG repeat sizes via fragment length analysis, FAM labelled reverse primers (Reverse Primer B, Table 3.7) were utilized. *ATXN2* CAG expansion-negative and -positive samples, used in our laboratory for common diagnostics, were used as controls. Fragment length analysis was performed by RefGen, Ankara. Results were evaluated with Peak Scanner Software using 500LIZ size standards.

PCR products destined for Sanger sequencing were acquired using ‘Reverse Primer A’ set (Table 3.7) in the reaction mix. Gel electrophoresis with 2% agarose gels containing 30% GelRed was performed at 120 V for 40 minutes to assess the quality of the fragments. For individuals with a pathogenic expansion, two alleles were extracted separately from the agarose gel with QIAquick Gel Extraction Kit according to the manufacturer’s instructions. Sanger sequencing was performed by Macrogen Europe. Results were evaluated by CLC Main Workbench Software.

4.2. *Atxn2* Knock-Out Mouse Tissue Samples

Generation of *Atxn2*-KO mouse line and genotyping were performed by the current and former members of Prof. Georg Auburger's laboratory at Goethe University Hospital, Experimental Neurology Department (Lastres-Becker *et al.*, 2008a). Cerebellum and liver samples that were previously dissected, frozen in liquid N_2 and kept at -80 ^{o}C were kindly provided by Dr. Suzana Gispert for this study in January 2013.

4.3. *ATXN2* Knock-Down SH-SY5Y Cell Culture

Methodology regarding the generation of non-target (NT) and *ATXN2*-KD SH-SY5Y cell line, standard culturing conditions and time-course starvation experiments are explained in the following sections.

4.3.1. Generation of *ATXN2* Knock-Down Cell Line

Stable knock-down of the naïve SH-SY5Y cells with lentiviral delivery of non-target (NT) and *ATXN2* shRNAs, both of which contain a puromycin resistance cassette, and frequent testing of the knock-down status were performed in the context of the PhD theses of Michael Klinkenberg and Jessica Drost in Prof. Georg Auburger's laboratory at Goethe University Hospital, Experimental Neurology Department.

4.3.2. General Culture Conditions, Freezing and Thawing

Contents of the different media utilized in the culturing of *ATXN2*-KD SH-SY5Y cells are shown in Table 4.3. All the media and other solutions used in cell culture are pre-warmed at 37 ^{o}C water bath before use.

Table 4.3. Contents of the different media used in *ATXN2*-KD SH-SY5Y culture experiments.

Culture Medium	RPMI + 10% FCS + 1% L-glutamine + 0.01% Puromycin
Starvation Medium	HBSS + 0.01% Puromycin
Freezing Medium	40% Culture Medium 50% FCS 10% DMSO

NT and *ATXN2*-KD SH-SY5Y cells were previously prepared and kept frozen in liquid N_2 by the members of Auburger lab. Before thawing a vial of each cell type, 25 cm^2 cell culture flasks were coated with one milliliter FCS for at least 30 minutes in the 37 ^oC incubator with 5% CO_2. Excess FCS is aspirated afterwards. Frozen cryogenic vials are slowly warmed up in the 37 ^oC water bath. Thawed cells are added into 10 ml culture medium and centrifuged at 500xg for three minutes to get rid of the DMSO-containing freezing medium. Cell pellet is resuspended in three milliliters of culture medium and seeded into coated 25 cm^2 flasks. The next day, culture medium was replaced with fresh medium; old medium was aspirated, cells were washed with one milliliter PBS which was aspirated afterwards, and 3 milliliters fresh media was added. This procedure of medium replacement was applied until the cells reach full confluence.

As the cells reached 100% fluency, old medium was aspirated, cells were washed with PBS, one milliliter Trypsin-EDTA was added and the flasks were incubated at 37 ^oC for two minutes. When the cells lost adhesion and started to float in the solution, Trypsin was deactivated by the addition of culture medium. Since splitting was going to be performed in 1:3 ratio, eight milliliters of culture media was directly added onto Trypsin-EDTA and the cells were resuspended. The cell suspension was divided and seeded into three new flasks, which were incubated at 37 ^oC.

In order to replace the used stock, one vial of each cell type was frozen and stored in the liquid N_2 tank. Fully confluent cells in a 25 cm^2 flask were washed with PBS (1 ml) and trypsinized (1 ml, 2 min at 37 ^oC). Culture medium was added to deactivate Trypsin and the solution was centrifuged at 500xg for three minutes. The cell pellet was dissolved in freezing medium (1 ml) and was immediately taken into cryogenic vials that are stored first at -80 ^oC fridge and then at liquid N_2.

To reach a larger amount of cells for the future experiments, cells grown in two 25 cm^2 flasks were washed with PBS (1 ml), trypsinized (1 ml, 2 min at 37 ^oC) and seeded into a 75 cm^2 flask. The general culturing conditions and 1:3 splitting protocol were applied in the same way as 25 cm^2 flasks (using 15 ml of final culture medium volume and 5 ml Trypsin-EDTA).

4.3.3. Time-Course Starvation Experiments

Twenty four hours before the start of the time-course starvations, NT and *ATXN2*-KD SH-SY5Y cells grown in 75 cm^2 flasks were trypsinized (5 ml, 2 min at 37 ^oC) and diluted in fresh culture medium (10 ml). 10 µl of the cell suspension was loaded into the counting chamber and the average of cell count in four corner squares was taken (Figure 4.2). If the average number of cells in A, B, C and D was N; then it was assumed that the cellular concentration of the suspension was N x 10^4 cell / ml.

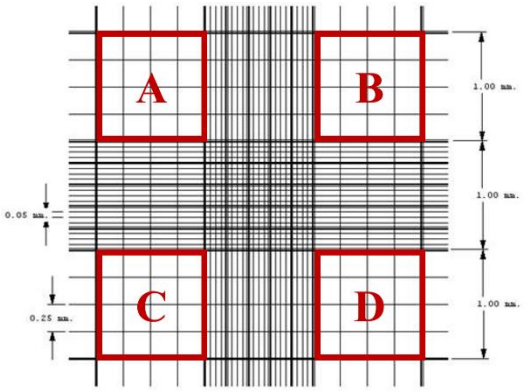

Figure 4.2. A schematic view of the counting chamber. The average of A, B, C and D regions assess the cellular concentration of the suspension (adapted from Petroff-Hausser Counting Chamber, EMS Catalog #60512-20).

After determination of the cell number present in a milliliter, $5x10^5$ cells were seeded per well in 6-well culture plates in quadruplicates and were supplemented with two milliliters of normal culture medium for a day in a 37 ^oC incubator. At the starting point of the time-course starvation experiment, media in all the wells were aspirated, cells were washed with one milliliter PBS, and two milliliters of fresh media was added; only one well of each cell type was supplemented with normal RPMI culture medium, whereas all the other wells were supplemented with the HBSS starvation medium. Cells in different wells were collected two, four, eight, 12, 24 and 48 hours after the starvation initiation. Cell collection was carried out by the aspiration of medium, addition of 300 µl PBS and scrapping the cells from the plate surface. The cell suspensions are taken into microcentrifuge tubes and frozen at -80 ^oC until all the samples from all time-points are collected. RPMI supplemented cells were collected at two hours as the control for this experiment (Figure 4.3).

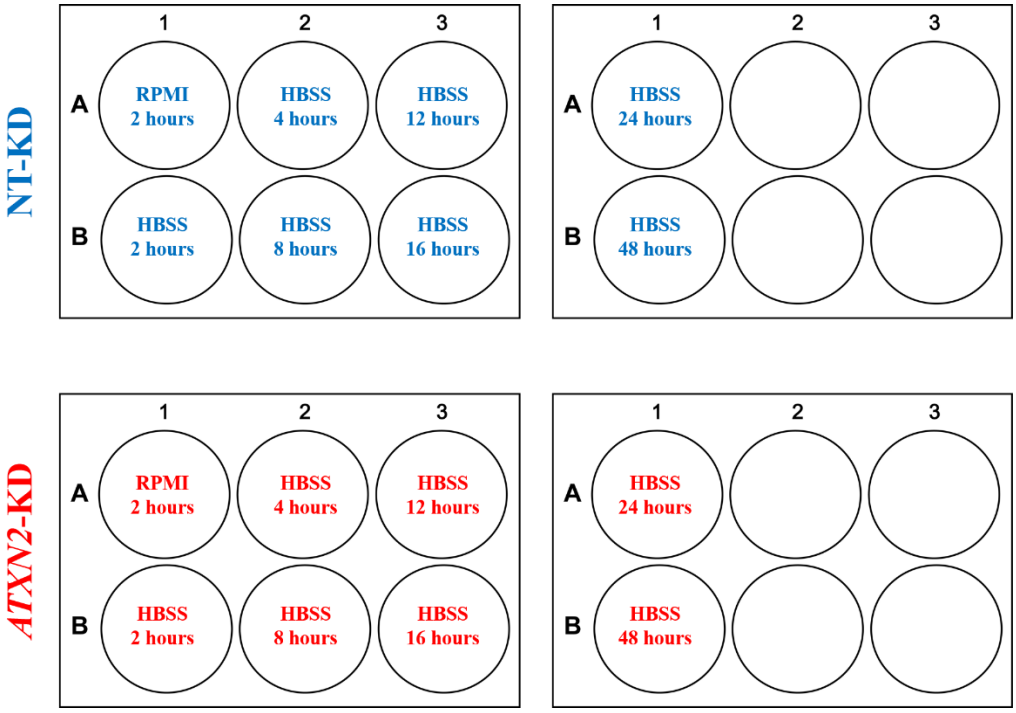

Figure 4.3. Layout of the 6-well plates designed for the time-course starvation experiments of NT and *ATXN2*-KD SH-SY5Y cells (adapted from Cell Signaling Networks Website, 6-well PlateTemplate).

4.4. RNA Isolation

Prior to total RNA isolation from any kind of sample, RNaseZAP was used for the inhibition of RNase molecules on bench surfaces, all laboratory equipment and gloves worn.

Total RNA samples extracted with Trizol Reagent from half of the cerebellum and liver tissues of six months-old wild-type (WT) and *Atxn2*-KO mice were kindly provided by Melanie Halbach and Mekhman Azizov in Prof. Georg Auburger's laboratory at Goethe University Hospital, Experimental Neurology Department.

For the isolation of total RNA from peripheral blood samples of SCA2 patients and controls, frozen PAXgene Blood RNA tubes were taken out from the -80 ºC deep freezer a day before and were incubated at room temperature overnight. Total RNA was isolated with PAXgene Blood RNA Kit v2 according to the manufacturer's instructions with one exception: the captured RNA within the column was eluted with 30 µl (15 µl + 15 µl) pre-warmed BR5 buffer instead of 80 µl (40 µl + 40 µl) as stated in the user's guide. Quality and the concentration of the isolated RNA from blood samples were measured with NanoDrop 2000c UV-Vis Spectrophotometer. Isolated RNA samples were stored at -80 ºC.

Isolation of total RNA from NT and *ATXN2*-KD SH-SY5Y cells was performed for each set separately. A set contains the cells from each type collected at all time-points between 2-48 hours (layout depicted in Figure 4.3). QIAshredder and RNeasy Mini Kits were used for total RNA isolation from cultured NT and *ATXN2*-KD SH-SY5Y cells according to the manufacturer's instructions. Elution of the captured RNA within the column was done with 30 µl pre-warmed RNase-free H_2O. The optional 2-mercaptoethanol addition to the RLT lysis buffer was performed immediately before cell lysis. Quantification and quality control of the isolated RNA from cultured cells were done using BioPhotometer device evaluating the absorbance value at 260 nm, $OD_{260/280}$ and $OD_{260/230}$. Isolated RNA samples were stored at -80 ºC.

4.5. DNaseI Treatment and cDNA Synthesis

One microgram of the total RNA isolated from mouse tissues, peripheral blood samples or cultured cells was treated with DNaseI prior to cDNA synthesis to digest DNA molecules that may not have been eliminated in the previous steps. One microliter DNase Amplification Grade and one microliter DNaseI Reaction Buffer were mixed with one microgram of total RNA, and the total volume was adjusted to 10 µl with RNase-free H_2O. After the 15 minute incubation at room temperature, one microliter EDTA was added and the samples were incubated at 65 ºC for 10 minutes to inactivate DNaseI. One microliter of each oligo$(dT)_{20}$ primer, random primer and dNTP solution were added and the samples

were incubated for five minutes at 65 ºC and one minute on ice. Reverse transcription of the RNA molecules into cDNA was achieved by the addition of four microliters of First Strand Buffer and one microliter of each DTT and SuperScript III Reverse Transcriptase enzyme into the samples and by subsequent incubations of five minutes at room temperature, an hour at 50 ºC and 15 minutes at 70 ºC. The final amount of the cDNA is assumed to be one microgram in 20 µl volume, hence the concentration is 50 ng/µl. cDNA samples are diluted to 5 ng/µl concentration with the addition of 180 µl dH_2O and stored at -20 ºC.

4.6. Expression Analyses with Quantitative Real Time-PCR

Expression analyses of various genes in mouse tissues, SCA2 patient blood samples and cultured cells were performed in 96-well MicroAmp plates using the StepOnePlus Real-Time PCR System Thermal Cycling Block. Taqman probes were utilized for the detection of amplification in a real-time manner. The content of the reaction mix for one well of the plate is shown in Table 4.4. The expression analyses of every gene, including the housekeeping genes *TBP* and *HPRT1*, were performed in duplicates for each cDNA sample. The conditions of the quantitative real-time PCR analysis with Taqman probes are shown in Table 4.5.

Table 4.4. Content of the reaction mix for qRT-PCR with Taqman probes.

Reagent	**[Stock]**	**Volume (µl)**	**[Final]**
cDNA	5 ng/µl	5	25 ng
Taqman Probes	20X	1	1X
FastStart Universal Probe Master	2X	10	1X
dH_2O		4	

Table 4.5. Cycling conditions of the qRT-PCR with Taqman probes.

Hold Stage	50 ºC	2 min
	95 ºC	10 min
Cycling Stage (40 cycles)	95 ºC	15 sec
	60 ºC	1 min

The expression data produced by the real-time detection of cDNA amplification via Taqman probes was analyzed using 2^-ΔΔCt method (Livak and Schmittgen, 2001). The 'cycle threshold' (Ct) values obtained from the qRT-PCR analysis express the number of cycles every sample went through in reaching to a threshold signal produced by the Taqman probes as amplification occurs. In the 2^-ΔΔCt method, the Ct value of the housekeeping gene (*TBP* or *HPRT1*) was subtracted from the Ct value of the target gene for every sample. The result of this calculation is termed ΔCt. Then, the average ΔCt value of controls (WT mice, healthy controls and RPMI supplemented cells collected at 2 hours) was subtracted from the ΔCt values of all samples, conceiving ΔΔCt values. 2^-ΔΔCt values were calculated for every sample and used in the assessment of expression differences between cases and controls. Further normalization was performed in mouse and patient data via dividing all 2^-ΔΔCt values by the average 2^-ΔΔCt of controls (WT mice and healthy individuals). Hence, the average of the normalized data from controls were adjusted to one, and the fold-change difference of expression in the case group (*Atxn2*-KO mice and SCA2 patients) could be assessed with respect to the controls.

4.7. Protein Isolation and Quantitation

Protein isolation from half of the mouse cerebellum and liver tissues was carried out in two steps; isolation of the soluble proteins (RIPA fraction) and isolation of the insoluble proteins (SDS fraction). Frozen WT and *Atxn2*-KO mice cerebella and livers were first weighed with an analytical balance. One hundred microliters of RIPA lysis buffer containing protease inhibitor cocktail was used per milligram of tissue sample. Murine tissues were homogenized with polypropylene pestles and pestle motor, then were rotated for 30 minutes at 4 ^{o}C. Lysates were sonicated due to high viscosity caused by DNA emergence and centrifuged at 14.000xg for 15 minutes at 4 ^{o}C. The supernatant, which is comprised of the soluble proteins, was taken into a fresh microcentrifuge tube (RIPA fraction). SDS lysis buffer in half the volume of previously added RIPA lysis buffer was applied to the pellet. The pellet was resuspended by pipetting and vortexing. The suspension was sonicated with three cycles of 10x1 second bursts. The lysate was

centrifuged at 16.000xg for 10 minutes at 4 ^{o}C. The supernatant, which contains the insoluble proteins, was taken into a fresh tube (SDS fraction).

Quantitation of the isolated proteins was performed with the Bradford assay and the BSA standard curve. In order to generate a standard curve, BSA dilutions ranging between 10-50 µg/µl for RIPA lysates and between 5-25 µg/µl for SDS lysates were prepared. Two microliters of the BSA standard dilutions or unknown mouse samples were mixed with 100 µl dH_2O and five milliliters of 1X Bradford solution. One milliliter of this solution for every standard and unknown sample were transferred into cuvettes and measured with BioPhotometer using readily defined Bradford Assay settings of the device. The BSA standard curve was plotted, and the protein concentrations of the unknown samples were assessed by incorporating their OD values into the best line equation of the standard curve.

4.8. SDS-PAGE and Quantitative Immunoblot Analyses

Sodium dodecyl sulfate-polyacrylamide gel electrophoresis (SDS-PAGE) was performed to separate the isolated proteins according to their molecular weight. Twenty microgram total protein was mixed with the adequate amount of dH_2O and 2X loading dye in the final volume of 10 µl. then, the samples were heated to 95 °C for five minutes to dissociate protein complexes and denature the proteins into primary structure. Discontinuous acrylamide gels were utilized in the electrophoresis; they consisted of an upper stacking part and lower resolving or separating part. The concentration of the stacking gel was the same for all runs, while the concentration of the resolving gel was determined according to the molecular weight of the target protein to be detected. Contents of the stacking and resolving gels and concentrations that were utilized for different molecular weight intervals are shown in Table 4.6. Electrophoresis was performed at 100V for 20 minutes while the proteins were in the stacking gel and at 120V for three to four hours as proteins get separated in the resolving gel. As the samples were loaded into the acrylamide gel and the electrophoresis was initiated, 1X transfer buffer was freshly prepared for every run as follows: 70% dH_2O, 20% methanol, and 10% 10X transfer buffer stock.

Table 4.6. Contents of the resolving and stacking gels casted in SDS-PAGE analysis.

Reagents	**Resolving Gel**				**Stacking Gel**
	8% (80-150kD)	**10% (40-80kD)**	**12% (20-40kD)**	**15% (<20kD)**	
dH_2O	7.05 ml	6.05 ml	5.05 ml	3.75 ml	3.05 ml
AA/BA	4.00 ml	5.00 ml	6.00 ml	7.50 ml	650 µl
Tris/HCl 1.5 M pH:8.9	3.75 ml	3.75 ml	3.75 ml	3.75 ml	---------
Tris/HCl 0.5 M pH:6.9	---------	---------	---------	---------	1.25 ml
SDS (10%)	150 µl	150 µl	150 µl	150 µl	50 µl
APS (10%)	50 µl	50 µl	50 µl	50 µl	25 µl
TEMED	10 µl	10 µl	10 µl	10 µl	5 µl

The separated proteins on the acrylamide gel were transferred to nitrocellulose or PVDF membranes. PVDF membranes were specifically activated by incubating in methanol for 5-10 minutes and washed with dH_2O for one minute. Membranes, filter papers and sponges were equilibrated in 1X transfer buffer for 5-10 minutes beforehand. The transfer cassette was constructed with sponges at the outer-most layers, followed by two pieces of filter paper on each side, the membranes and the resolving part of the acrylamide gel in the middle. The orientation of the cassette within the transfer tank was adjusted such that the membrane would be on the positive side and the applied current would carry the negatively charged proteins out from the gel towards the membrane. Blotting of the membranes was performed at 50V for 90 minutes, after which they were blocked with either 5% milk or BSA in TBS-T for an hour at room temperature on a shaker. TBS-T was prepared as follows: 89.5% dH_2O, 10% 10X TBS stock and 5% Tween (20%).

After blocking, the membranes were incubated in primary antibodies diluted in TBS-T overnight at 4°C on a rotator. Then, they were washed with TBS-T three times for 10 minutes at room temperature on a shaker. Secondary antibodies diluted in TBS-T were applied to the membranes for an hour at room temperature on a rotator. Light-proof brown tubes were utilized if the secondary antibody being used was fluorescent labeled. Then, the membranes were washed with TBS-T three times for 10 minutes in a dark box on a shaker.

Signal detection was done immediately with Li-Cor Odyssey Classic instrument if the secondary antibody was fluorescently labeled. Quantification was performed by image analysis using ImageStudio software provided by Li-Cor instrument. In the case of HRP-conjugated secondary antibodies, SuperSignal West Pico Chemiluminescent Substrates were used. Blotted membranes were incubated for five minutes in four milliliters of the 1:1 mixture of Lumino/Enhancer and Stable Peroxidase solutions. Excess ECL solution remaining on the blots was soaked by a tissue paper and the blots were placed in an exposure cassette with X-ray films in the dark room. Exposure was performed in variable time intervals for each antibody utilized. The X-ray films were soaked into developer and fixer solutions after which they were washed and dried. Quantification of the signals was done by scanning the films and analyzing the image with ImageJ software.

The signal values of the target proteins obtained from ImageStudio or ImageJ software were first normalized to the signal of the housekeeping gene for every sample. Then, the ratios of all samples were further normalized to the average signal of WT samples. Therefore, the average of WT samples was adjusted to one, and the exact fold change difference of the target protein in *Atxn2*-KO mice could be assessed compared to the WT mice.

4.9. High-Throughput Transcriptome Analyses

High-throughput transcriptome analyses performed with the WT and *Atxn2*-KO mice and with SCA2 patients and matching healthy controls are explained in the following sections.

4.9.1. Microarray Analysis of *Atxn2*-KO Mice

Transcriptome analysis using Affymetrix GeneChip HT Mouse Genome 430 2.0 Array Plates was performed with the RNA samples obtained from the cerebella and livers

of four WT and four *Atxn2*-KO mice (six, 12 and 24 weeks-old) at Microarray GeneChip Facility in Tübingen, Germany. Further information regarding hybridization, bioinformatics methodology and public access number to the raw data is published (Fittschen *et al.*, 2015).

4.9.2. Deep RNA-Sequencing Analysis of SCA2 Patients

Whole transcriptome analysis with the global blood RNA samples from three SCA2 patients and three age- and sex-matched healthy controls from the same family was performed at Alacris Theranostics GmbH, Berlin, Germany. After library preparation from 500 ng total RNA and mRNA selection, sequencing of the 2x50 bp paired-ends was performed with Illumina HiSeq2500 system. Processing of the raw data and all other bioinformatic analyses were performed by Alacris Theranostics; sequencing reads were mapped to GRCh37/hg19 human genome reference, hemoglobin gene reads were eliminated prior to the calculation of the expression values which was performed with 'reads per kilobase per million mapped reads' (RPKM) normalization. Differential expression between patients and controls was calculated with edgeR package in R Bioconductor and corrected for multiple testing. Significance of the differences were assessed using an exact test for overdispersed data.

4.10. Gene Set Enrichment Analysis

Gene Set Enrichment Analysis (GSEA) was performed with the deep RNA-sequencing results of three SCA2 patients and three controls from the same family utilizing the Java-based version GSEA-P of the software at the Broad Institute server. The ranked gene list contained all genes examined by the transcriptome analysis and was sorted out with respect to the base two logarithm of the fold change for every particular gene. During the enrichment analysis, c2, c5 and cc gene sets of the MSigDB v4.0 were used.

4.11. Statistical Analyses

Statistical tests to assess the significance of the observed effects were performed with the GraphPad Prism Software. Unpaired student's t-test was performed in comparing two groups of samples, and paired t-test was performed to compare specific age- and sex-matched patient-control combinations. Two-way ANOVA was used in cell culture experiments when comparing multiple groups of samples, and at the same time variation within a sample group. Results were displayed as bar graphs, showing mean values of each sample group and standard error of the mean (SEM). Significant differences were identified with asterisks (* $p < 0.05$; ** $p < 0.01$; *** $p < 0.001$, **** $p < 0.0001$). Samples showing a trend toward significance ($0.05 < p < 0.1$), were highlighted with T.

Outliers within each sample group were identified using the online GraphPad QuickCals Outlier Calculator tool which utilizes Grubbs' test.

5. RESULTS

A summary of the results obtained throughout this thesis from (i) the *Atxn2*-KO mouse and SCA2 patient biomarker investigations, and (ii) functional studies on the relationship between ataxin-2 and mitochondrial factors is shown in Figure 5.1.

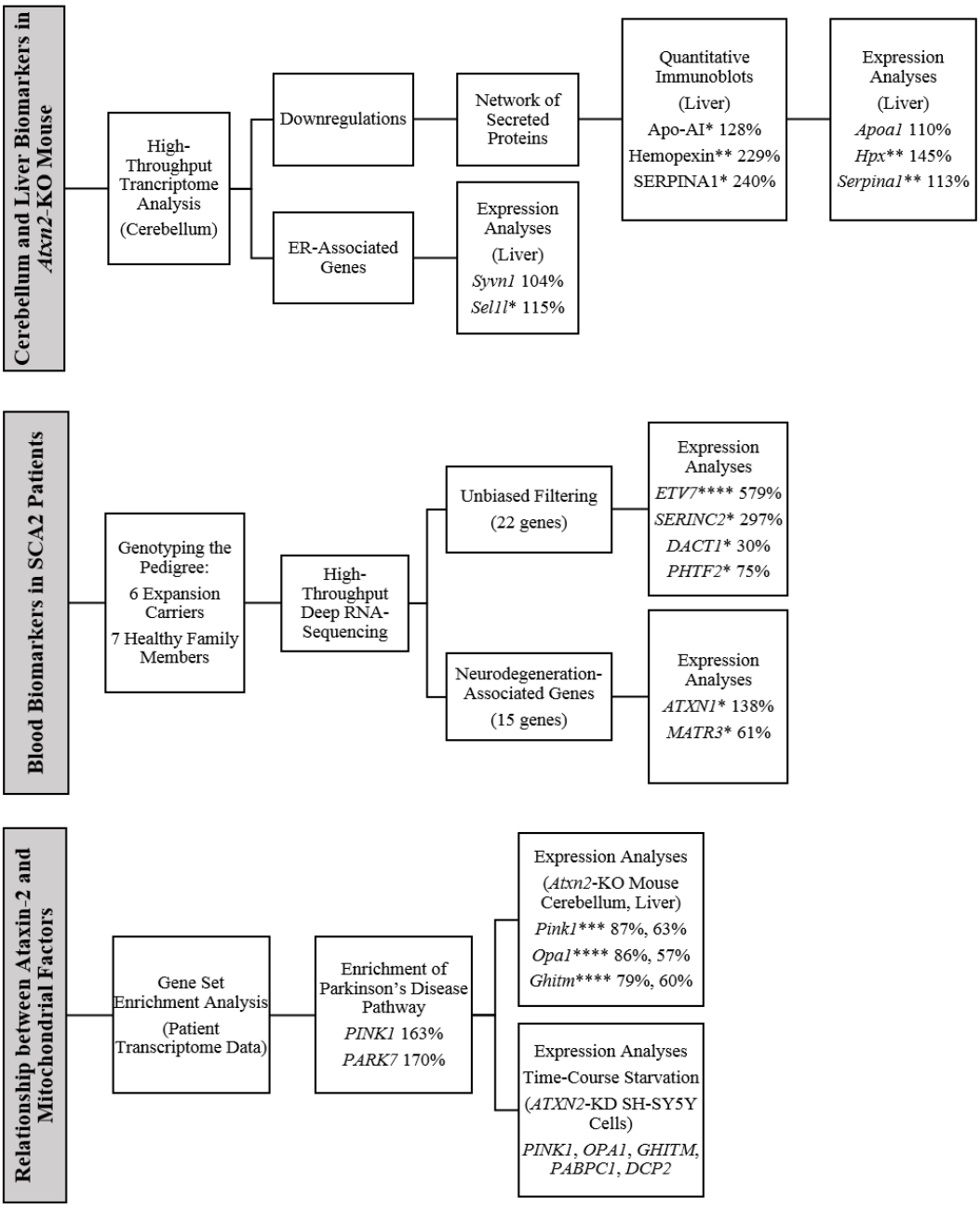

Figure 5.1. Summary of the results obtained throughout this thesis.

5.1. Identification of Cerebellum and Liver Biomarkers in *Atxn2*-KO Mice

5.1.1. High-Throughput Expression Analysis Results

The *Atxn2*-KO mouse model was generated in order to understand the function of normal ataxin-2, apart from the pathology it exerts when mutated. *Atxn2*-KO mice exhibit no signs of ataxia or neurological symptoms, but show reduced fertility with a distinct obesity phenotype that is associated with the insulin resistance resulting from reduced insulin receptor expression in both liver and cerebellum (Kiehl *et al.*, 2006; Lastres-Becker *et al.*, 2008a). In order to identify the differentially expressed genes that might explain the phenotype obtained in the absence of ataxin-2, high-throughput transcriptome analysis with Affymetrix GeneChip microarrays was performed utilizing the cerebellum and liver RNA samples of six, 12 and 24 weeks-old WT and *Atxn2*-KO mice (4 vs. 4) by the former and current members of Auburger Lab at Experimental Neurology Department, Goethe University Hospital. Increased levels of many transcripts that encode for ribosomal proteins, RNA metabolism factors (*Lsm12*, *Deadc1*, *Drbp1*/*Rbm45*), translation pathway components (*Paip1*, *Eif2s2*), and genes involved in lipid droplet biogenesis (*Plin3*) and apolipoprotein secretion (*Mttp*) had already been identified and studied (Fittschen *et al.*, 2015).

5.1.1.1. Network of Secreted Proteins among Differentially Downregulated Genes. The interaction network analysis of the 100 most differentially up- and downregulated genes in 24 weeks-old *Atxn2*-KO mice cerebellum was conducted utilizing the online STRING v10 software. Among the differential downregulations in the cerebellum data, a highly inter-connected network of proteins that are secreted to the extracellular fluids emerged (Figure 5.2). This network consisted of *Thy1* (thymus cell antigen 1), *Serpina1a* (serine/cysteine peptidase inhibitor, clade A, member 1A), *Serpina1b* (serine/cysteine peptidase inhibitor, clade A, member 1B), *Serpina1c* (serine/cysteine peptidase inhibitor, clade A, member 1C), *Serpina3k* (serine/cysteine peptidase inhibitor, clade A, member 3K), *Apoa1* (apolipoprotein A-I), *Apoa2* (apolipoprotein A-II), *Apoc1* (apolipoprotein C-I), *Alb* (serum albumin), *Fga* (fibrinogen alpha chain), *Hpx* (hemopexin) and *Ttr* (transthyretin) genes.

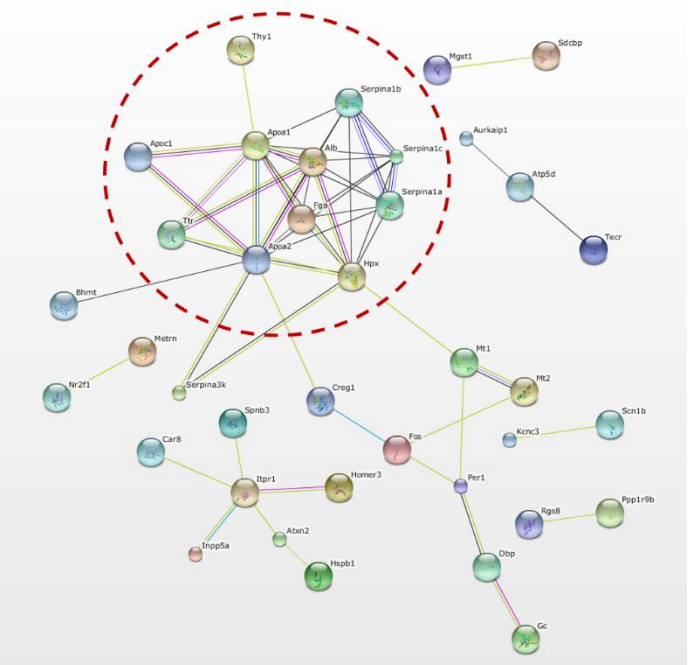

Figure 5.2. The interaction network among the 100 most downregulated genes in *Atxn2*-KO mice cerebellum. Red dashed circle indicates the sub-network of proteins secreted to extracellular fluids.

5.1.2. Secretion Network Protein Levels in *Atxn2*-KO Mice

The above-mentioned secretion network components that were found to be significantly downregulated in the cerebellar transcriptome data of the *Atxn2*-KO mice, together with several additional factors, inferred from the data as potential biomarker candidates, were further analyzed at the protein level via quantitative immunoblots in the cerebellum and liver tissues of 24 weeks-old mice. Both RIPA fractions, containing the soluble proteins, and SDS fragments, containing the insoluble membrane-bound or aggregated proteins, were analyzed for the factors that have commercially available specific antibodies. Due to the low levels of protein yield in the SDS fragments, no signals were detected for any of the tested antibodies. A total of nine antibodies detected a reliable signal with varying fold-change and significance in the RIPA fragments of cerebellum and liver protein extracts (Table 5.1). In the cerebellar extract, Apo-AI, Apo-AII, Apo-CI, Hemopexin, Serum Albumin, Transthyretin and VDBP proteins were detectable, however

without any significant change between WT and *Atxn2*-KO animals. Figure 5.3 shows the observed changes in the cerebella with the immunoblot band images that were quantified. In the RIPA fragments of liver lysates, Apo-AI, Hemopexin, LSM12, SERPINA1 and Serum Albumin proteins were detectable. Two different antibodies recognizing distinct domains of the LSM12 protein were utilized. Significant changes between WT and *Atxn2*-KO mice were obtained in Apo-AI (1.28-fold increase, p=0.0174 *), Hemopexin (2.29-fold increase, p=0.0024 **) and SERPINA1 (2.40-fold increase, p=0.0462 *) levels. Figure 5.4 shows the observed changes in the liver with the immunoblot band images that were quantified.

Table 5.1. Summary of the quantitative immunoblots analyses *Atxn2*-KO mice cerebellum and liver.

	Cerebellum		**Liver**	
	Fold Change	**p-Value**	**Fold Change**	**p-Value**
Apo-AI	0.76	0.1955	1.28	0.0174 *
Apo-AII	1.48	0.1293	-	-
Apo-CI	0.88	0.5594	-	-
Hemopexin	0.21	0.2086	2.29	0.0024 **
LSM12 C-terminus	-	-	1.14	0.4489
LSM12 Middle	-	-	0.96	0.8071
SERPINA1	-	-	2.40	0.0462 *
Serum Albumin	0.98	0.8895	1.16	0.3719
Transthyretin	1.04	0.6566	-	-
VDBP	0.83	0.7083	-	-

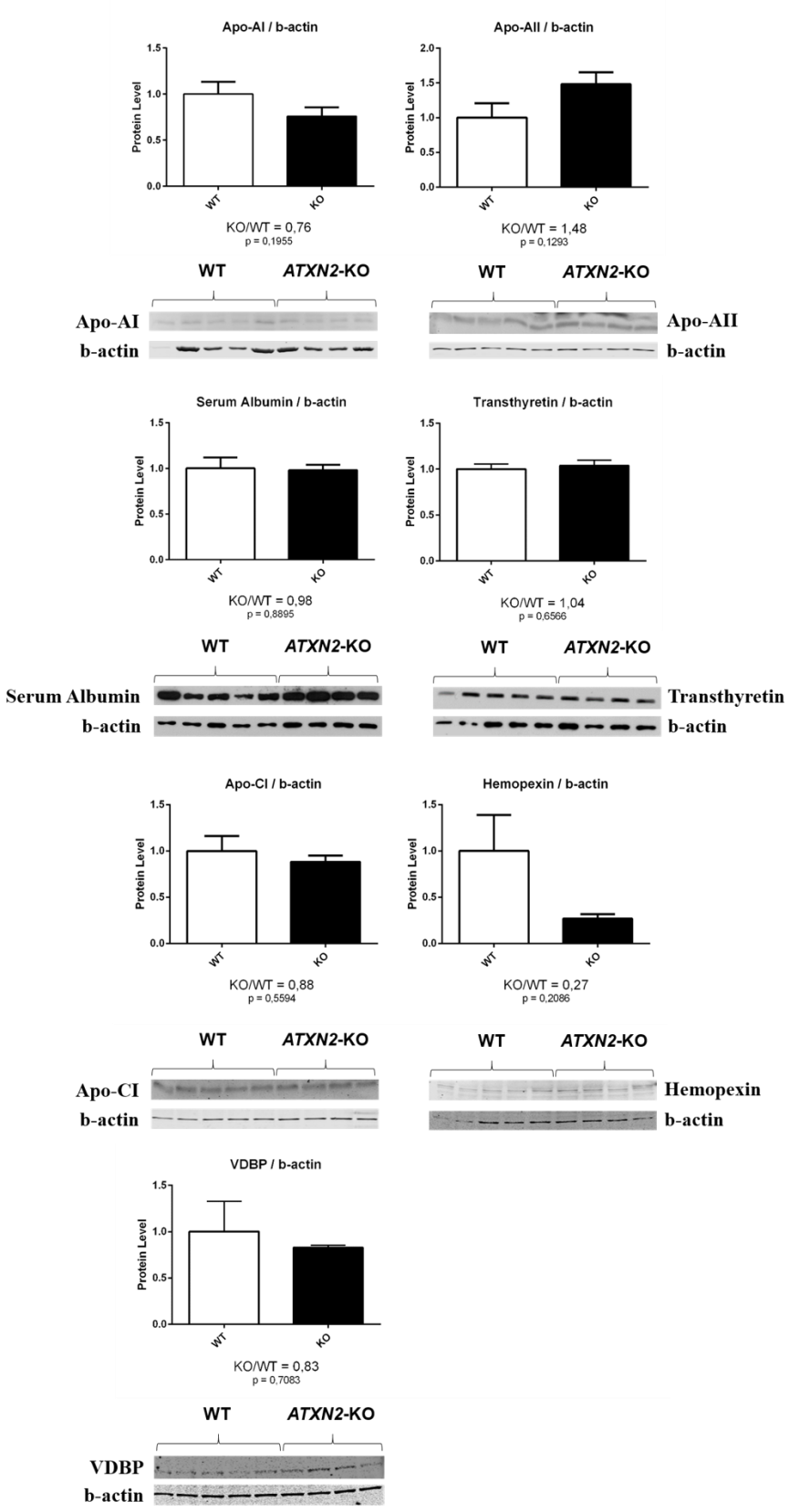

Figure 5.3. Fold-change differences of the biomarker candidates at the protein level in *Atxn2*-KO mice cerebellum.

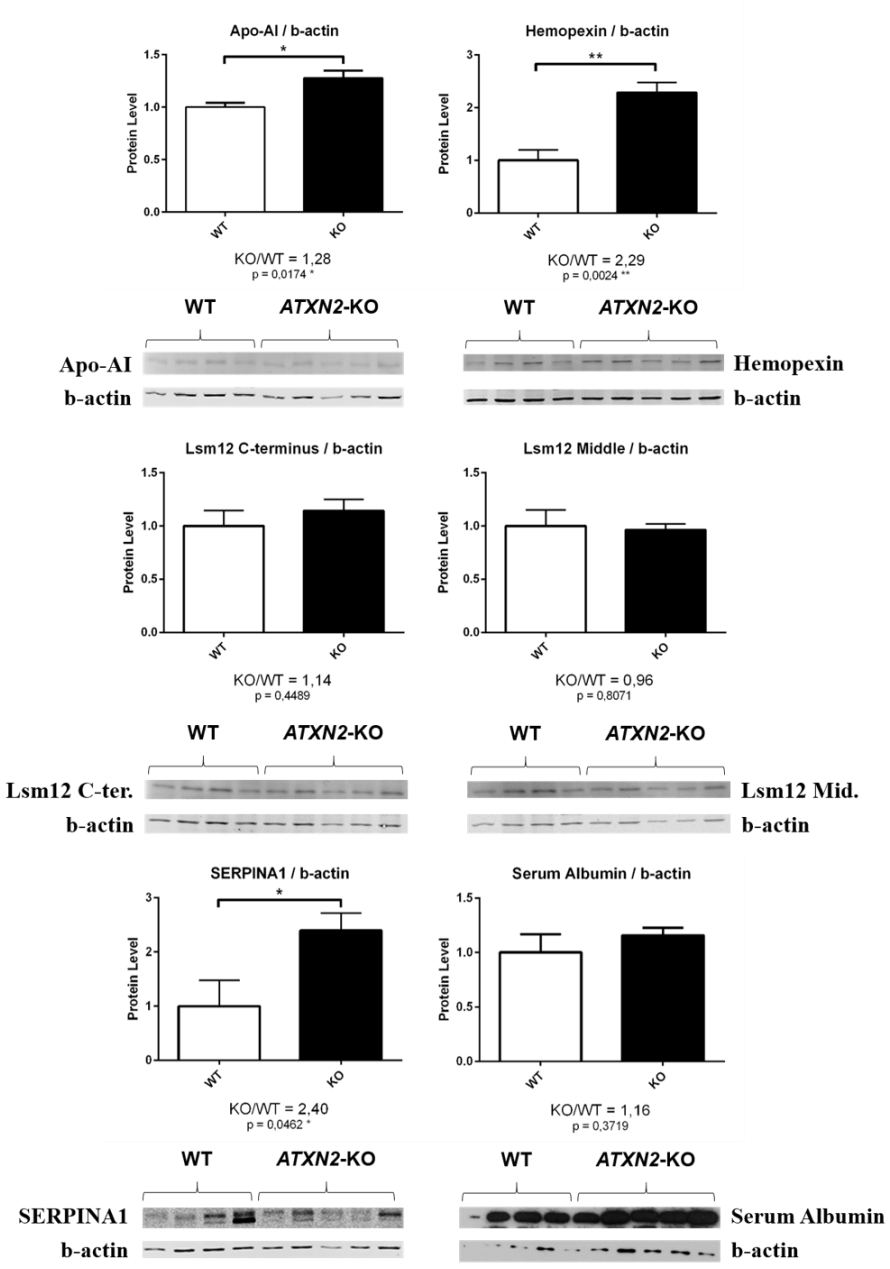

Figure 5.4. Fold-change differences of the biomarker candidates at the protein level in *Atxn2*-KO mice liver.

5.1.3. Expression Analysis of ER-Associated Genes in *Atxn2*-KO Mice

Several biomarker candidates had been chosen from the 100 most downregulated genes in the cerebellar transcriptome data of *Atxn2*-KO mice. Independent validations of these genes at the protein level with quantitative immunoblots revealed no significant change in the cerebellum, however three of these candidate proteins were upregulated to varying extents in the liver, although the initial transcriptome data suggested a severe downregulation. Since all three of these proteins are known to be secreted to the extracellular fluids under normal conditions, we hypothesized that a deficit in the ER-Golgi secretory pathway would increase the intracellular concentration of the normally secreted protein, the transcription of which would be shut off in response to this increase via a negative feedback mechanism. Re-examination of the *Atxn2*-KO mouse liver microarray data revealed significant dysregulations in two ER-associated genes, namely *Syvn1* (Synovial apoptosis inhibitor 1) and *Sel1l* (Suppressor of Lin12-like). *Sel1l* is a component of the retrotranslocation complex that carries the misfolded proteins accumulated in the ER lumen to cytosol, and *Syvn1* is a ubiquitin-ligase, activated by the unfolded protein response (UPR), that directs the misfolded proteins to proteosomal degradation (Kaneko *et al.*, 2002; Mueller *et al.*, 2008). Independent expression analysis of these genes was performed in the cerebellum and liver RNA extracts of 24 weeks-old WT and *Atxn2*-KO mice. Both in the cerebellum and liver samples, these two genes showed a similar expression profile (Figures 5.5 and 5.6). *Syvn1* was found to be 1.01- and 1.04-fold upregulated without significance in cerebellum and liver, respectively. *Sel1l* transcript was found to have a slight, yet significant, downregulation in the cerebellum (to 92%, p=0.0202 *), whereas in the liver *Sel1l* had a slight upregulation with significance (to 115%, p=0.0162 *).

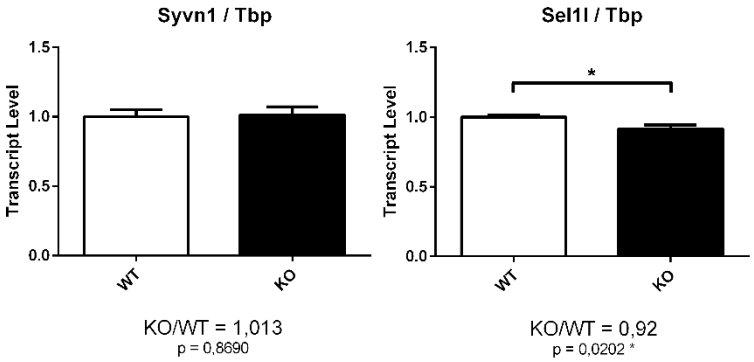

Figure 5.5. Expression levels of the ER-associated factors, *Syvn1* and *Sel1l*, in *Atxn2*-KO mice cerebellum.

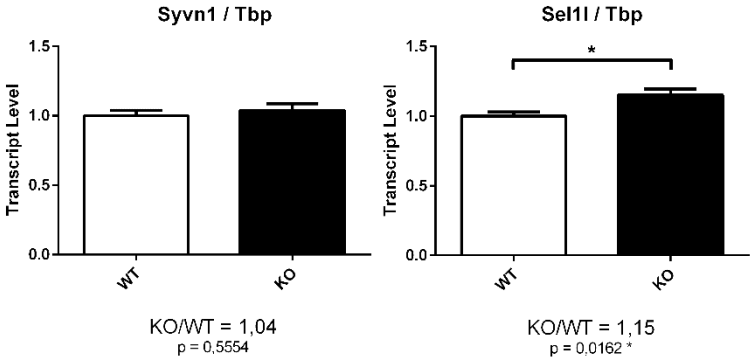

Figure 5.6. Expression levels of the ER-associated factors, *Syvn1* and *Sel1l*, in *Atxn2*-KO mice liver.

5.1.4. Expression Analysis of Secretion Network Genes in *Atxn2*-KO Mice

Significant alterations at the protein levels of Apo-AI, Hemopexin and SERPINA1 were observed in the liver tissues of 24 weeks-old *Atxn2*-KO mice. No major change of the two genes in the ER-Golgi secretory pathway, that were found dysregulated in the liver microarray data, was observed upon independent analyses with qRT-PCR. To assure the expression status of the candidate biomarkers, qRT-PCR analyses were performed in the

cerebellum and liver tissues of WT and *Atxn2*-KO mice with the relevant Taqman probes. Successful knock-out of *Atxn2* gene was assessed in both tissues (Figures 5.7 and 5.8). Curiously, *Hpx* levels were found significantly upregulated in both tissues (Cerebellum: 1.27-fold, p=0.0493 *, Liver: 1.45-fold, p=0.0013 **). *Apoa1* levels were also slightly upregulated in both tissues without significance (Cerebellum: 1.11-fold, p=0.6317, Liver: 1.10-fold, p=0.1359). There are six isoforms of *Serpina1* gene in mouse, among which *Serpina1a*, *Serpina1b* and *Serpina1c* were significantly dysregulated in the high-throughput transcriptome data. There was a commercially available Taqman probe designed to measure *Serpina1a* levels. However, two other available Taqman probes covered *Serpina1a* and *Serpina1c* together, and *Serpina1a*, *Serpina1b* and *Serpina1c* together. Expression analyses of the *Serpina1* genes were performed with all three Taqman probes in cerebellum and liver tissues (Figures 5.7 and 5.8). In the cerebellum, *Serpina1a* alone showed a 1.65-fold increase without significance, whereas the degree of the upregulation fell to 1.39-fold when *Serpina1a* and *Serpina1c* were quantified together. In the quantification of *Serpina1a*, *Serpina1b* and *Serpina1c* all together, a non-significant 1% downregulation was observed between the WT and *Atxn2*-KO mice cerebellum (Figure 5.7). On the contrary, while *Serpina1a* alone in the liver showed a 1% downregulation, quantification of *Serpina1a* and *Serpina1c* together presented a 1.06-fold upregulation without significance. The total transcript levels of all three isoforms in the liver interestingly showed a significant 1.13-fold upregulation as shown in Figure 5.8 (p=0.0085 **).

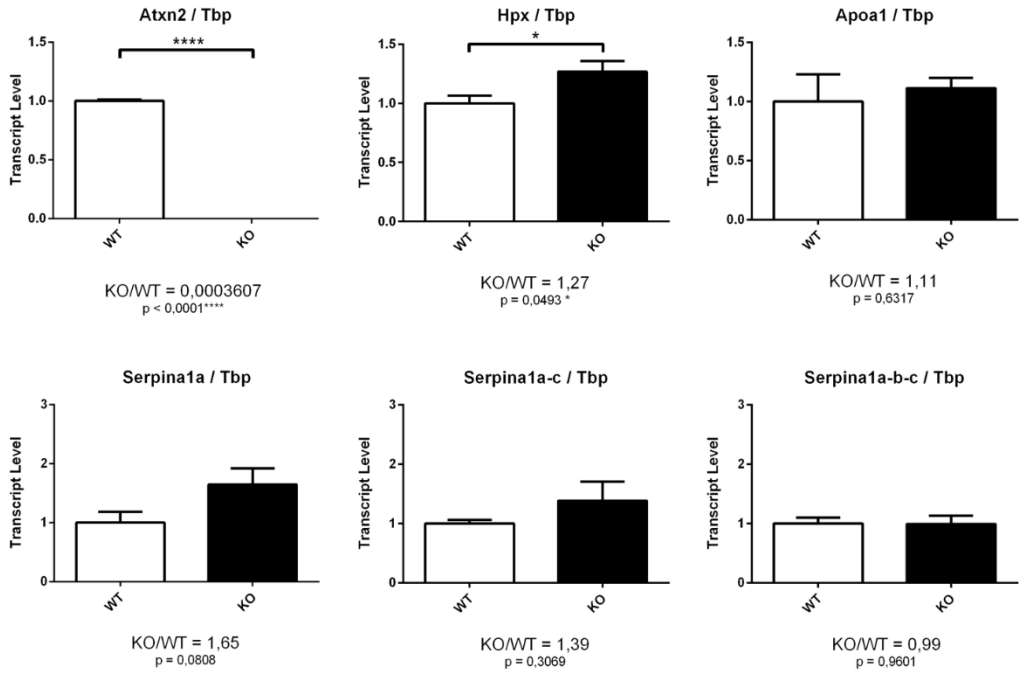

Figure 5.7. Expression levels of the candidate biomarker genes in *Atxn2*-KO mice cerebellum.

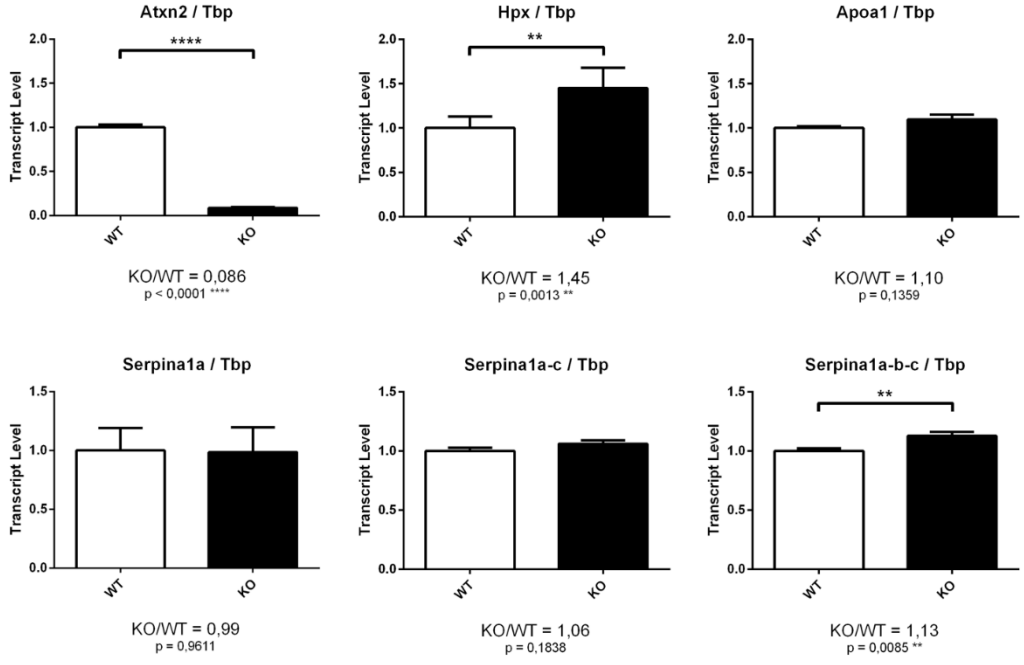

Figure 5.8. Expression levels of the candidate biomarker genes in *Atxn2*-KO mice liver.

5.2. Identification of Blood Biomarkers in SCA2 Patients

5.2.1. Genotypes of the SCA2 Pedigree

In order to determine the number of CAG repeats in the *ATXN2* gene of the blood donors from the large SCA2 pedigree living in Balıkesir, Turkey (Figure 5.9), also to assess the purity of the repeat regions (absence of CAA interruptions), fragment length analysis (RefGen, Ankara) and Sanger sequencing (Macrogen, Europe) were performed following the amplification of the repeat region by conventional PCR. Five individuals already presenting SCA2 symptoms at the time of sample collection were found to carry an expanded allele varying between 39-44 repeats (Table 5.2). Another individual in the family, with no disease manifestation yet, was found to carry a long-intermediate allele with 32 repeats. Rest of the non-symptomatic family members were found negative for an expanded *ATXN2* allele. All the normal-length alleles in the family were interrupted at least once with a CAA triplet. The expanded alleles, in contrast, consisted of pure CAG repeats, a characteristic feature exclusive to SCA2. Therefore, the individual with pure 32 CAG repeats in this family was grouped with ‘patients’ in the up-coming analyses, in line with the scope of this study, which investigates the basis of pathogenicity caused by *ATXN2* expansions.

Anticipation, which is another characteristic feature of SCA2, is also observed within this family. Individual #3, carrying an expanded allele with 40 repeats, transmitted this allele to his offspring with 44 repeats (individuals #6 and #7). The offspring show an earlier manifestation of the disease with a faster progression.

Table 5.2. Genotype information of the blood donors from the Turkish SCA2 pedigree.

No.	Birth	AO	Age at SC	CAG Repeat # and Pattern		RNA-Seq
#1	1964	---	49	22	$(CAG)_8$-(CAA)-$(CAG)_4$-(CAA)-$(CAG)_8$	
				32	$(CAG)_{32}$	
#3	1961	32	52	22	$(CAG)_{13}$-(CAA)-$(CAG)_8$	+
				40	$(CAG)_{40}$	
#6	1988	12	25	22	$(CAG)_{13}$-(CAA)-$(CAG)_8$	
				44	$(CAG)_{44}$	
#7	1994	<10	19	22	$(CAG)_{13}$-(CAA)-$(CAG)_8$	+
				44	$(CAG)_{44}$	
#9	1979	34	34	22	$(CAG)_8$-(CAA)-$(CAG)_4$-(CAA)-$(CAG)_8$	
				40	$(CAG)_{40}$	
#12	1947	53	66	22	$(CAG)_8$-(CAA)-$(CAG)_4$-(CAA)-$(CAG)_8$	+
				39	$(CAG)_{39}$	
#2	1967		46	22	$(CAG)_8$-(CAA)-$(CAG)_4$-(CAA)-$(CAG)_8$	
				22	$(CAG)_8$-(CAA)-$(CAG)_4$-(CAA)-$(CAG)_8$	
#4	1964		49	22	$(CAG)_8$-(CAA)-$(CAG)_4$-(CAA)-$(CAG)_8$	
				22	$(CAG)_{13}$-(CAA)-$(CAG)_8$	
#5	1986		27	22	$(CAG)_{13}$-(CAA)-$(CAG)_8$	+
				22	$(CAG)_{13}$-(CAA)-$(CAG)_8$	
#8	1965		48	22	$(CAG)_8$-(CAA)-$(CAG)_4$-(CAA)-$(CAG)_8$	
				22	$(CAG)_{13}$-(CAA)-$(CAG)_8$	
#10	1941		72	22	$(CAG)_8$-(CAA)-$(CAG)_4$-(CAA)-$(CAG)_8$	+
				22	$(CAG)_{13}$-(CAA)-$(CAG)_8$	
#11	1944		69	22	$(CAG)_8$-(CAA)-$(CAG)_4$-(CAA)-$(CAG)_8$	+
				22	$(CAG)_{13}$-(CAA)-$(CAG)_8$	
#13	1976		37	22	$(CAG)_8$-(CAA)-$(CAG)_4$-(CAA)-$(CAG)_8$	
				22	$(CAG)_8$-(CAA)-$(CAG)_4$-(CAA)-$(CAG)_8$	

5.2.2. High-Throughput Deep RNA-Sequencing Analysis Results

In addition to the transcriptome data obtained from the *Atxn2*-KO mouse that gives insights into the native function of normal ataxin-2, we have performed high-throughput deep RNA-sequencing with the total blood transcriptome of three SCA2 patients carrying an expanded allele and three age- and sex-matched healthy controls with Illumina HiSeq2500 system to assess the global expression changes dependent on ataxin-2 pathology (Table 5.2). After the processing of the raw data and subsequent bioinformatic

analyses, an excel file with the differential expression information of ~19.000 genes was obtained. Large expression changes with significance in the immunoglobulin and T-cell receptor genes were prominent. Many other significant up- and downregulations were obtained with changes greater than 2.0-fold.

5.2.2.1. Candidate Genes Acquired by Unbiased Filtering. The initial filtering was done by i) removing the genes that show zero expression in at least one of the individuals analyzed, ii) eliminating the genes that show unreliable expression values between patient and control groups, also among the individuals in a group, and iii) setting a significance threshold at < 0.05 for the unpaired t-test p value. Unbiased filtering had been applied until this point, and from the remaining ~2300 genes, biomarker candidates that might be relevant to the disease phenotype or the known ataxin-2 function were selected for further validations. Several genes that did not show a significant differential expression in the unpaired t-test, but known to be associated with ataxin-2 pathology, were also included in the validation list shown in Table 5.3.

Table 5.3. List of the differentially expressed candidate biomarker genes in SCA2 patients.

Ensembl ID	**Gene Name**	**Log_2FoldChange**	**p-Value (Unpaired t-test)**
ENSG00000173208	*ABCD2*	-2,129788925	0,00000038
ENSG00000148408	*CACNA1B*	2,711787925	0,00000000
ENSG00000165617	*DACT1*	-2,333179636	0,00000042
ENSG00000010030	*ETV7*	2,966483564	0,00000000
ENSG00000128683	*GAD1*	-5,366243024	0,00000000
ENSG00000178075	*GRAMD1C*	-2,025071198	0,00000150
ENSG00000178502	*KLHL11*	-2,610175233	0,00001181
ENSG00000174405	*LIG4*	-2,150080143	0,00000042
ENSG00000188906	*LRRK2*	-0,736416349	0,05900413
ENSG00000100985	*MMP9*	2,869522777	0,00000000
ENSG00000134323	*MYCN*	-2,402353442	0,00047082
ENSG00000006576	*PHTF2*	-2,02089208	0,00000082
ENSG00000141682	*PMAIP1*	-2,094740329	0,00000071
ENSG00000205155	*PSENEN*	1,448389209	0,00025320
ENSG00000176641	*RNF152*	-7,836455776	0,00000000

Table 5.3. List of the differentially expressed candidate biomarker genes in SCA2 patients (cont.).

Ensembl ID	Gene Name	Log_2FoldChange	p-Value (Unpaired t-test)
ENSG00000168528	*SERINC2*	2,371222543	0,00000002
ENSG00000180879	*SSR4*	1,146068475	0,00354446
ENSG00000174093	*TBC1D3*	-0,461907287	0,24557135
ENSG00000145850	*TIMD4*	-2,024242181	0,00056236
ENSG00000175073	*VCPIP1*	-0,92142705	0,01896343
ENSG00000180776	*ZDHHC20*	-2,513946096	0,00000001
ENSG00000196110	*ZNF699*	-2,073048123	0,00001618

Independent validations of the 22 differentially expressed genes acquired from the whole blood deep RNA-sequencing data, obtained with the above-mentioned strategy, were performed via Taqman assay-based qRT-PCR analyses. cDNA samples of six expansion carriers and six healthy controls from the same family, including the samples subjected to RNA-sequencing, were analyzed for the selected biomarker candidates. The expression changes obtained in 14 of these genes with qRT-PCR analyses did not show statistical significance: *ABCD2* 0.79-fold p=0.1594, *CACNA1B* 0.93-fold p=0.6671, *GAD1* 0.06-fold p=0.1431, *GRAMD1C* 1.01-fold p=0.9394, *LIG4* 0.81-fold p=0.3589, *LRRK2* 1.13-fold p=0.6394, *MYCN* 1.06-fold p=0.8097, *PMAIP1* 0.70-fold p=0.2337, *PSENEN* 1.44-fold p=0.1258, *RNF152* 1.51-fold p=0.5174, *SSR4* 1.02-fold p=0.8738, *TIMD4* 0.75-fold p=0.1708, *VCPIP1* 1.11-fold p=0.5653, and *ZDHHC20* 0.89-fold p=0.6148. Figure 5.9 shows the relative expression levels of the candidate genes that showed no significance in a collective bar graph.

An extreme 0.06-fold downregulation was obtained in *GAD1* levels after the normalization of the expression data was done with respect to the average of the healthy controls. Normalized expression values of *GAD1* were highly variable among the controls (ranging from 0.03 to 3.33), whereas less variation was present in the patients (ranging from 0.02 to 0.11). None of the control values was identified as an outlier with Grubbs' test, since they were evenly distributed within the 0.03-3.33 range. Hence, the seemingly 0.06-fold expression change in *GAD1* did not show statistical significance.

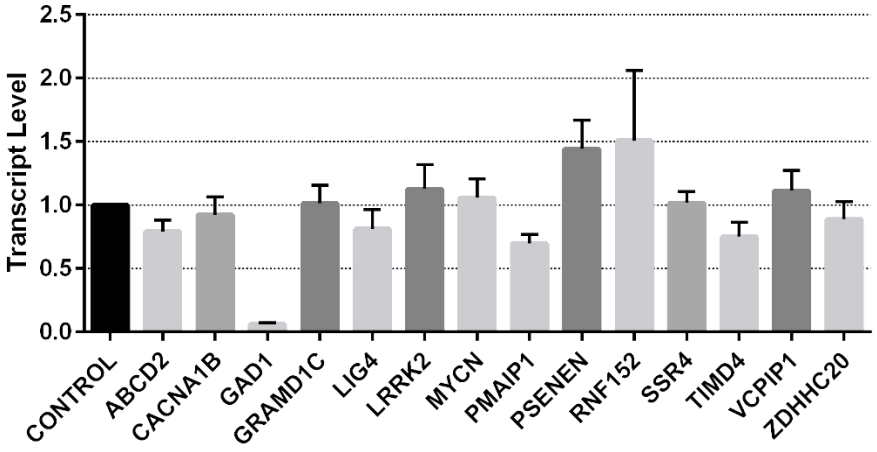

Figure 5.9. Expression levels of the candidate biomarker genes in SCA2 patients showing no statistical significance (p>0.05).

The expression change in four of the candidate genes showed a trend towards significance with the p-values between 0.05 and 0.10 (Figure 5.10). *MMP9* (4.79-fold p=0.0633) and *TBC1D3* (1.79-fold p=0.0623) genes showed upregulation, whereas *KLHL11* (0.91-fold p=0.0528) and *ZNF699* (0.68-fold p=0.0544) showed downregulated transcript levels. High variation was observed in the *MMP9* levels among the SCA2 patients; normalized expression values of the controls ranged between 0.59 and 1.26, whereas the relative expression range of the patients was between 1.21 and 12.29 with an even distribution.

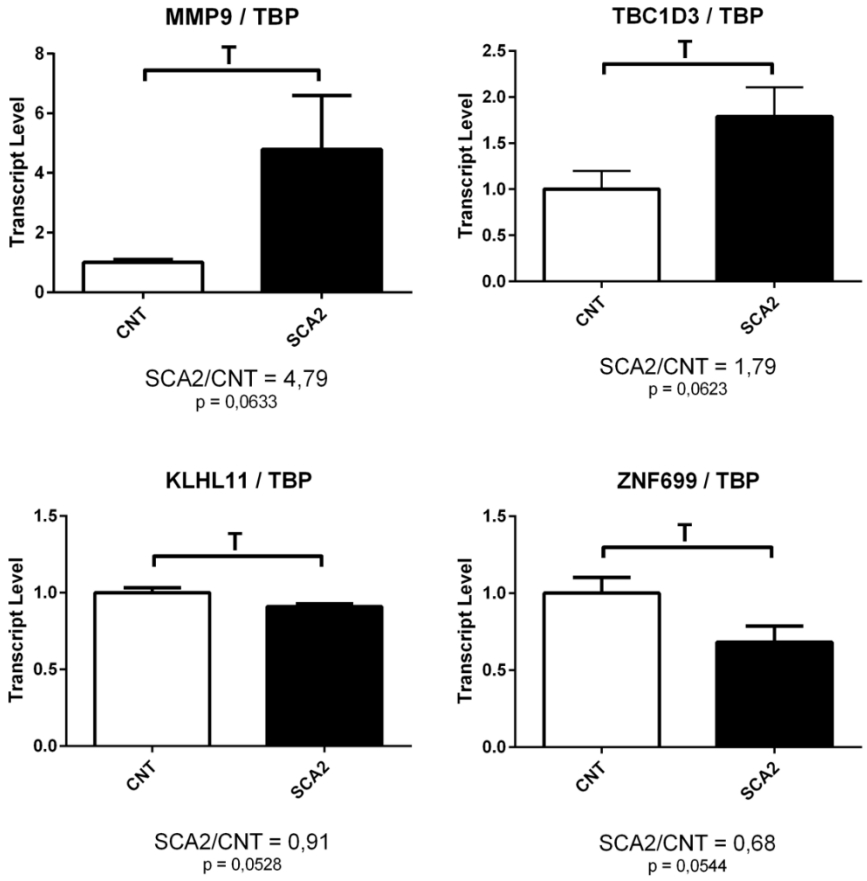

Figure 5.10. Expression levels of the candidate biomarker genes in SCA2 patients showing a trend towards significance (0.05<p<0.10).

Four of the analyzed candidate biomarker genes showed statistically significant dysregulations at the transcript level in the qRT-PCR analyses (Figure 5.11). *ETV7* (5.79-fold p < 0.0001 ****) and *SERINC2* (2.97-fold p=0.0139 *) levels were found to be upregulated, whereas *DACT1* (0.30-fold p=0.0171 *) and *PHTF2* (0.75-fold p=0.0133 *) levels showed a decrease in the SCA2 patients. The strongest effect was the 579% upregulation in *ETV7* gene, which is a member of the ETS family of transcription factors predominating in the hematopoietic tissues (Potter *et al.*, 2000), with very high significance and low variation among individuals in both sample groups. The second strongest effect with 297% upregulation was observed in *SERINC2*, which functions in the incorporation of serine into phosphatidylserine and sphingolipids (Inuzuka *et al.*, 2005), with a slight variation among patients. The 70% downregulation observed in *DACT1*, that modulates the transcriptional activation of Wnt/b-catenin pathway targets (Lagathu *et al.*,

2009), was followed by the modest 25% downregulation in *PHTF2*, whose function is not fully understood, however is pronounced in GWAS studies of childhood obesity, chronic kidney disease and blood lipid phenotypes (Comuzzie *et al.*, 2012; Kathiresan *et al.*, 2007; Köttgen *et al.*, 2010).

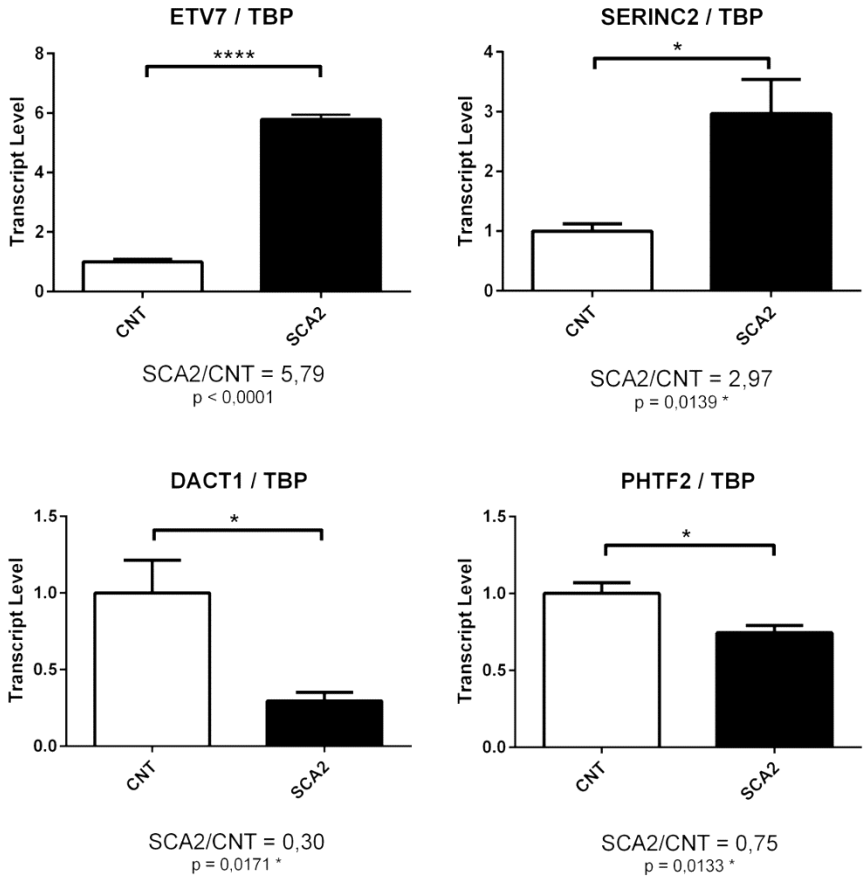

Figure 5.11. Expression levels of the candidate biomarker genes in SCA2 patients showing statistically significant dysregulations ($p<0.05$).

5.2.2.2. Neurodegeneration-Associated Genes as Candidates. In a parallel approach with the candidate gene selection after unbiased filtering of the transcriptome data, genes associated with other neurodegenerative diseases, such as ALS and other ataxias, were sorted out. A list of 33 genes associated with ALS was acquired from the ALSoD database, and 332 ataxia-associated genes included in the Ataxia Exome Panel of The University of Chicago, Genetic Services was also obtained. A total of 365 neurodegeneration-associated

genes were isolated from the transcriptome data and the significant dysregulations between each patient and the matched control were acquired (pairwise t-test p-value < 0.05). Figure 5.12 shows the result of the interaction network analysis of all the significantly dysregulated neurodegeneration-associated genes performed with the online STRING v10 software. A cluster of interaction is predicted between *ATXN1*, *ATXN2*, *ATXN3*, *ATXN7*, *UBE3A*, *UBQLN2*, *TARDBP* and *FUS*. Some ALS genes, such as *CHMP2B*, *C9orf72*, *SETX*, *ALS2*, *SPG11* and *SPAST* are also linked to this sub-network rather distantly.

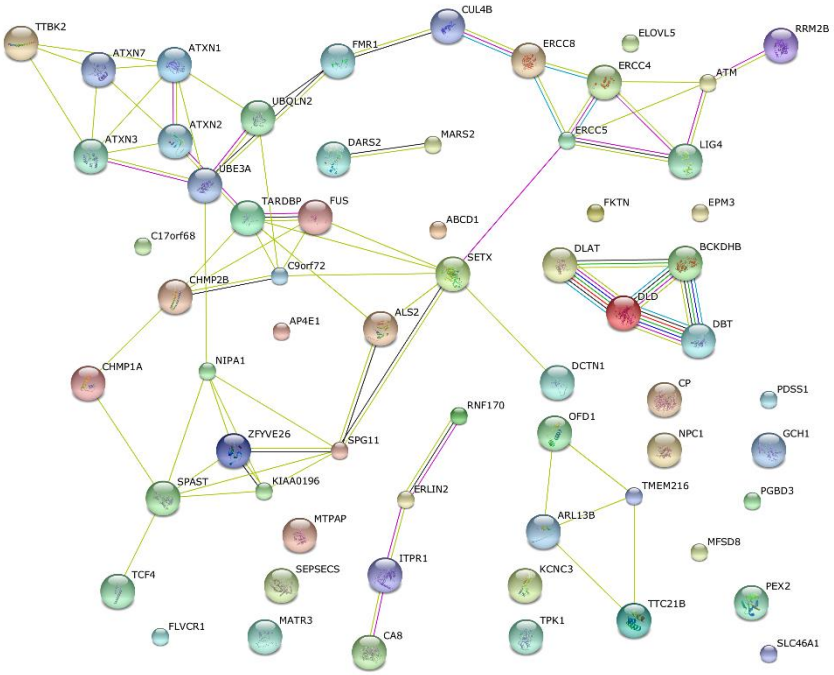

Figure 5.12. The interaction network of the significantly dysregulated ALS- and ataxia-associated genes in SCA2 patients.

A subset of significantly dysregulated genes, chosen with respect to the fold-change expression difference and functional relevance, was enrolled to further validations (Table 5.4). Only a small portion of the many ataxia-associated genes isolated from the whole transcriptome data showed significance, and even a smaller subset of these were chosen for further validations. From the 33 ALS-associated genes, 11 showed significant dysregulations with variable differential expressions, and all were enrolled to the validation step.

Table 5.4. List of the differentially expressed ALS and ataxia-associated genes in SCA2 patients.

Ensembl ID	Gene Name	Log_2FoldChange	p-Value (Paired t-test)	
ENSG00000003393	*ALS2*	-0,789346608	0,041372161	ALS
ENSG00000147894	*C9orf72*	-1,133852044	0,001501931	
ENSG00000083937	*CHMP2B*	-0,655969156	0,002109857	
ENSG00000204843	*DCTN1*	0,900790634	0,044650009	
ENSG00000089280	*FUS*	0,080844173	0,048053555	
ENSG00000015479	*MATR3*	-0,957756569	0,025050938	
ENSG00000107290	*SETX*	-0,340285166	0,037072306	
ENSG00000021574	*SPAST*	-0,92537921	0,007557285	
ENSG00000104133	*SPG11*	-0,594161255	0,017930157	
ENSG00000120948	*TARDBP*	-0,497581848	0,023442329	
ENSG00000188021	*UBQLN2*	-0,612383385	0,00676847	
ENSG00000149311	*ATM*	-1,274105292	0,010976427	Ataxia
ENSG00000124788	*ATXN1*	-0,29589134	0,039717241	
ENSG00000066427	*ATXN3*	-0,634235648	0,034851496	
ENSG00000150995	*ITPR1*	-1,036002288	0,019540225	

Independent validations of the differentially expressed ALS and ataxia genes obtained from the whole blood deep RNA-sequencing data were also performed via Taqman assay-based qRT-PCR analyses in six expansion carriers and six healthy controls. Ten of the 11 ALS genes and three of the four ataxia genes analyzed did not show a significant expression difference between SCA2 patients and healthy controls: *ALS2* 1.23-fold p=0.1311, *C9orf72* 1.05-fold p=0.8846, *CHMP2B* 1.10-fold p=0.59, *DCTN1* 1.13-fold p=0.1750, *FUS* 1.03-fold p=0.8447, *SETX* 1.42-fold p=0.1511, *SPAST* 1.14-fold p=0.5444, *SPG11* 1.08-fold p=0.6062, *TARDBP* 1.12-fold p=0.1375, *UBQLN2* 1.02-fold p=0.9293, *ATM* 1.11-fold p=0.5225, *ATXN3* 0.84-fold p=0.2078, and *ITPR1* 1.06-fold p=0.4545. Figure 5.13 shows the relative expression levels of the neurodegeneration-associated genes that showed no significance in the qRT-PCR analyses.

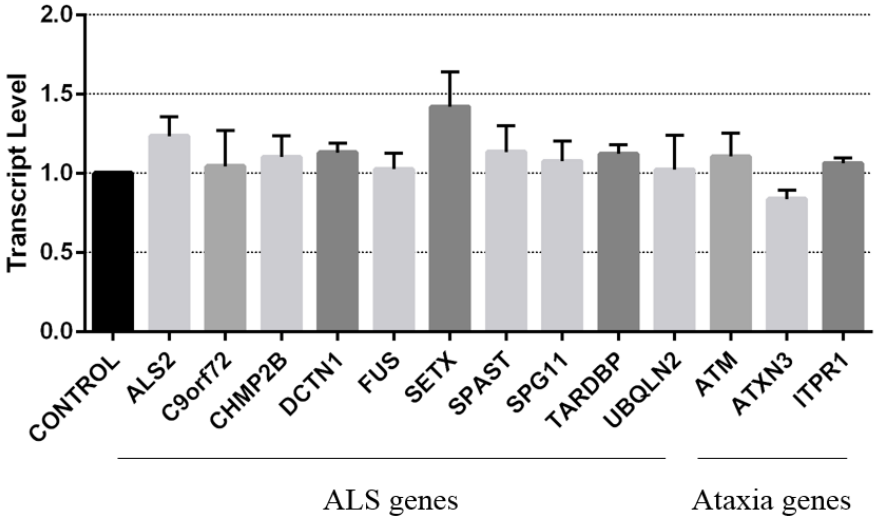

Figure 5.13. Expression levels of the ALS- and ataxia-associated genes in SCA2 patients showing no statistical significance ($p>0.05$).

One of the ALS- and one of the ataxia-associated genes showed statistical significance in the expression analysis with qRT-PCR (Figure 5.14). *MATR3*, an ALS gene that functions in mRNA stabilization and interacts with TDP-43 (Johnson *et al.*, 2014), was found to be downregulated to 61% ($p=0.0153$ *) in SCA2 patients. On the other hand, *ATXN1*, the first identified SCA gene that functions in transcriptional repression via chromatin binding and a known interactor of ataxin-2 (Lim *et al.*, 2006), was found to be upregulated to 138% ($p=0.00348$ *) at the transcript level.

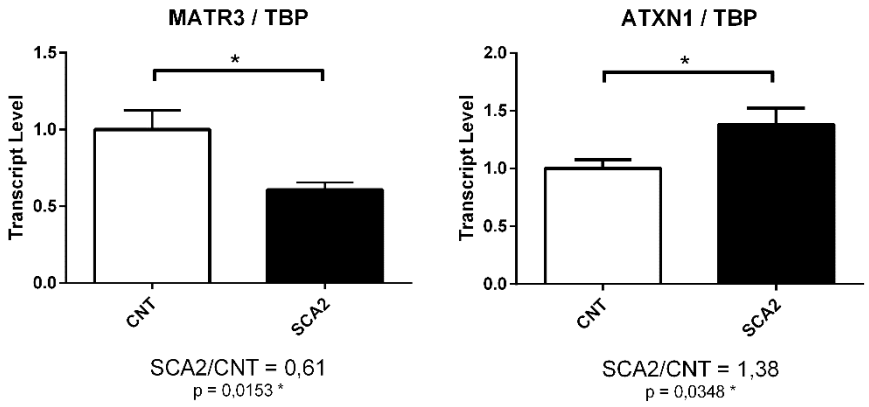

Figure 5.14. Expression levels of the *MATR3* and *ATXN1* genes in SCA2 patients showing significant dysregulations ($p<0.05$).

5.3. Characterization of the Interplay between Ataxin-2 and Mitochondrial Factors

5.3.1. Enrichment of the Parkinson's Disease Pathway Genes in SCA2 Patients

Gene Set Enrichment Analysis (GSEA), provided by Broad Institute server, was performed utilizing the whole blood transcriptome data of three SCA2 patients and three age- and sex-matched controls from the large Turkish pedigree. The ranked gene list, sorted with respect to the base two logarithm of each gene's fold change, was obtained by unbiased processing of the raw high-throughput expression data. Enrichment analysis revealed a number of pathways to be significantly upregulated at a maximal level with nominal p-value, false discovery rate (FDR) q-value, and family-wise error rate (FWER) p-value being equal to 0.0. Among the maximally significant enrichments, several pathways were related to mRNA metabolism (3'-UTR Mediated Translational Regulation, Metabolism of RNA, Regulation of mRNA Stability by Proteins that Bind to AU-Rich Elements, etc.), some were related to proteostasis and secretion (SRP-dependent Cotranslational Protein Targeting to Membrane, Lysosome Pathway, Extracellular Region Gene Set, etc.), whereas some were linked to mitochondrial function (Huntington's Disease Pathway, Parkinson's Disease Pathway, etc.) (Table A2). Among the significant

downregulations, pathways related to olfaction (Olfactory Signaling Pathway, Olfactory Transduction), transcription (Generic Transcription Pathway), proteostasis (Ubiquitin Mediated Proteolysis) and transport of variable molecules (SLC-Mediated Transmembrane Transport, Transport of Mature Transcript to Cytoplasm, Transport of Glucose and Other Sugars, Bile Salts, Organic Acids, Metal Ions and Amine Compounds) were observed (Table A3).

Taking the reported involvement of *ATXN2* long-intermediate expansions in PD manifestation and the shared brain pathology and clinical symptoms with SCA2 into consideration, the enrichment observed in the PD pathway entailed further investigation. The enrichment was maximally significant with nominal p-value, FDR q-value and FWER p-values equal to 0.0 and with a high normalized enrichment score (NES) of 4.31 (Figure 5.15). Every dash below the enrichment plot represents the contribution of an individual gene in the pathway. The addition of every new gene alters the enrichment status of the pathway to different extents. The expression data predicts that certain PD pathway genes cumulatively enhance the pathway until a point, whereas incorporation of some other genes in this pathway lowers the enrichment after the breaking point. In the case of the PD pathway enrichment plot in Figure 5.15, more genes are represented on the left side of the plot cumulatively contributing to the enrichment of pathway suggesting a trend towards upregulation. The other PD pathway genes incorporated into the enrichment analysis after the maximal point are those predicted to decrease the overall enriched status of the pathway. Among the genes contributing positively to the enrichment of the pathway, *PINK1* and *PARK7* mRNAs, both of which are known PD genes and take roles in mitochondrial function, were upregulated by 1.63- and 1.70-fold, respectively.

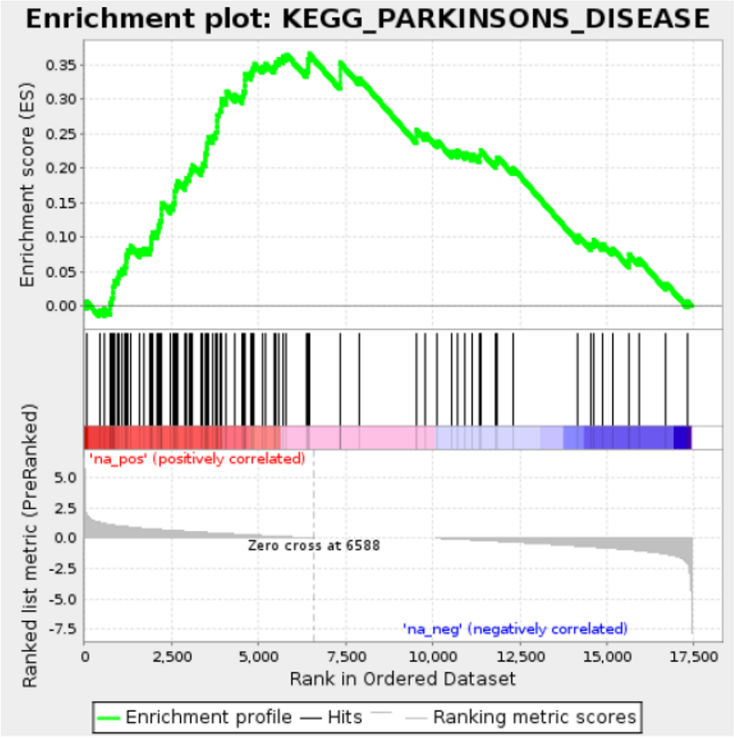

Upregulated in class	disease
GeneSet	KEGG_PARKINSONS_DISEASE
Enrichment Score (ES)	0.36538
Normalized Enrichment Score (NES)	4.311161
Nominal p-value	0.0
FDR q-value	0.0
FWER p-Value	0.0

Figure 5.15. Highly significant enrichment in the Parkinson's disease pathway. Majority of the genes in this pathway are positively correlated (red region), enhancing the upregulation.

5.3.2. Expression Analysis of the Mitochondrial Genes in *Atxn2*-KO Mice

In order to understand if these dysregulations in the mitochondria-associated factors were due to the gain of a novel function of the expanded ataxin-2, present in SCA2 patients, and also to see if the reverse effects will be observed in the loss of ataxin-2, the previously obtained cerebellum and liver transcriptome data of the *Atxn2*-KO mice was examined by Prof. Auburger. No significant change in *Park7* levels was observed, however *Pink1* mRNA levels were significantly downregulated, along with many other

mitochondria-associated genes, in both cerebellum and liver tissues. Independent validations of a set of these genes in the six months-old WT and *Atxn2*-KO mice cerebellum (15 WT vs. 10 KO) and liver (8 WT vs. 7 KO) via qRT-PCR analysis confirmed the downregulation of *Pink1* (to 87% in cerebellum with p<0.0001, to 63% in liver with p<0.0001), *Opa1* (to 86% in cerebellum with p<0.0001, to 57% in liver with p<0.0001) and *Ghitm* (to 79% in cerebellum with p<0.0001, to 60% in liver with p<0.0001) transcripts in both tissues (Figure 5.16) (performed by Bianca Scholz in Prof. Auburger's Lab in the Experimental Neurology Department of Goethe University Hospital).

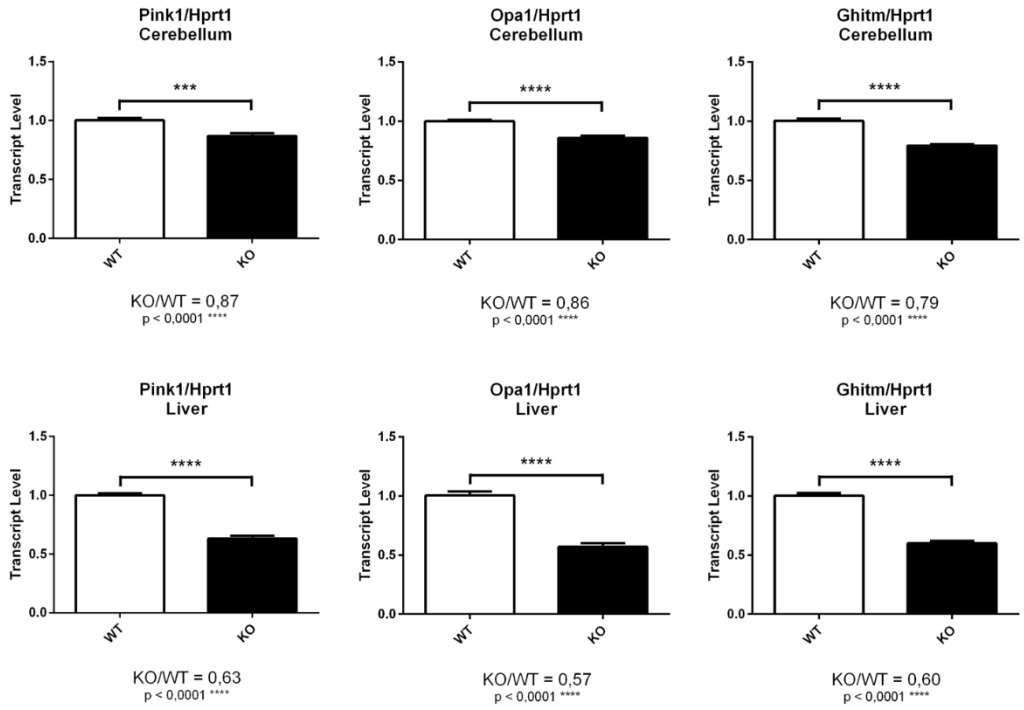

Figure 5.16. Significant downregulations of the mitochondrial genes in *Atxn2*-KO mice cerebellum and liver (provided by Auburger Lab).

5.3.3. Expression Analysis of the Mitochondria- and Ataxin-2-Associated Genes in *ATXN2*-KD SH-SY5Y Cells

The expression of *PINK1* has been reported to be enhanced in a time-course manner by nutrient deprivation *in vitro* (Klinkenberg *et al.*, 2012). Upon upregulation in response to starvation, *PINK1* induces the selective consumption of the dysfunctional mitochondria as a nutrient source (Jin and Youle, 2012). In order to elucidate the relationship between ataxin-2 and *PINK1*, and to see if the time-course change in *PINK1* levels upon starvation stress will be affected from the silencing of *ATXN2*, the expression status of *PINK1* and several other mitochondrial and ataxin-2-associated factors were investigated over time in the context of nutrient-deprived SH-SY5Y neuroblastoma cells stably transduced with *ATXN2* or non-target (NT) shRNAs.

Expression analyses were performed after two, four, eight, 12, 16, 24, and 48 hours of starvation using NT- and *ATXN2*-KD SH-SY5Y cells cultured in HBSS starvation medium without the supplement of any other nutrients. The expression value of each gene was normalized to *HPRT1* levels, and expression values at all the time-points were compared to the non-starved NT-KD cells cultured for two hours in RPMI+FCS general culture medium.

Maintenance of the *ATXN2* knock-down was confirmed with high significances at all time-points (n=8 replicates). In the NT-KD cells, an immediate 1.5-fold induction of *ATXN2* expression is observed starting at two hours, reaching to the maximum 3.5-fold change after 12 hours and clearing out gradually over the next 36 hours. A slight tendency towards upregulation is also present in *ATXN2*-KD cells over time, which is suppressed by the stably expressed shRNA constructs (Figure 5.17).

No significant change in the expression of *PINK1* was observed throughout 48-hour starvation between NT- and *ATXN2*-KD cells (n=8). Although no major dysregulation in the transcript level emerged, the induction pattern of *PINK1* greatly resembled that of

ATXN2; making a huge leap at eight hours, reaching the maximum 3.5-fold change at 12 hours and then gradually decreasing. Even though the change is not significant, a greater increase in the *PINK1* level is obvious in the *ATXN2*-KD cells compared to NT-KD cells at eight-hour (3.2-fold vs. 2.5-fold), 12-hour (3.5-fold vs. 3.2-fold), 16-hour (3.4-fold vs. 3.0-fold) and 24-hour (3.2-fold vs. 3.0-fold) time-points despite the initial transcript amounts were the same for both cell types, suggesting *PINK1* is induced more in response to nutrient starvation in the absence of ataxin-2 (Figure 5.17).

The expression data of *OPA1* acquired from NT- and *ATXN2*-KD cells (n=8) consisted high variation among replicates, therefore is not sufficient to make a conclusion. However, a general time-course induction and clearance with a similar pattern to that of *ATXN2* is observed. None of the changes at different time-points between two cells types were found significant (Figure 5.17).

The native expression pattern of *PABPC1* in NT-KD cells (n=4) showed a gradual increase over time until it reaches the maximum of 4.5-fold at 24 hours and slightly decreases at 48 hours to approximately 3.5-fold. Expression in *ATXN2*-KD cells (n=6), on the other hand, started with the same levels of *PABPC1* transcript, but showed less induction especially after eight hours. The difference between NT- and *ATXN2*-KD cells reaching to a maximum at 24-hour and 48-hour time-points were found significant with 2-way ANOVA test. The induction in the expression of *PABPC1* upon time-course starvation seems to be impaired in the absence of ataxin-2 starting from 8 hours, and transcript levels remain low for the following 40 hours (Figure 5.17).

The normal expression pattern of *GHITM* transcript in NT-KD cells (n=6) shows a small increase in response to starvation after two hours, after a slight decrease at 4 hours, got into an induction trend and reached the maximum of 2.0-fold at 16 hours. A phasic decrease was observed afterwards. No major effect of *ATXN2* depletion was present in the expression pattern of *GHITM*, except for the initial increase of the transcript in nutrient supplemented cells at two hours, which showed high variation among replicates and may

be specific to this experiment. *GHITM* expression seemed to be stalled at the very beginning in response to starvation when ataxin-2 was absent, but was slightly induced afterwards in a time-dependent manner. The maximum induction of *GHITM* in *ATXN2*-KD cells (n=6) occurred with approximately 1.4-fold change at 16-hour time-point. Although they follow a similar pattern of induction, a decrease of the *GHITM* transcript level in *ATXN2*-KD cells was obvious, however not significant, compared to NT-KD cells at all time-points analyzed, except for the non-starving cells at two hours (Figure 5.17). Hence, the induction of *GHITM* to greater extents under cellular stress via starvation seems to be dependent on the presence of ataxin-2.

The expression pattern of *DCP2* transcript in NT-KD cells (n=6) upon nutrient deprivation seemed to be constant at the very beginning, experiencing a big leap of induction at eight hours, remaining high until 24 hours with a maximum change of 2.0-fold upregulation. *DCP2* levels drastically fell between 24 and 48 hours. Exactly the same expression profile was observed for DCP2 in *ATXN2*-KD cells (n=7) with a steady level in the beginning, a sudden increase at eight hours, remaining relatively constant until 24 hours with approximately 1.5-fold upregulation and a marked decrease at 48 hours (Figure 5.17). However, lower levels of *DCP2* in *ATXN2*-KD cells was obtained from the very beginning even in the nutrient supplemented cells, suggesting that not only the induction of *DCP2* in response to starvation, but also the general transcript level is dependent on the ataxin-2 function.

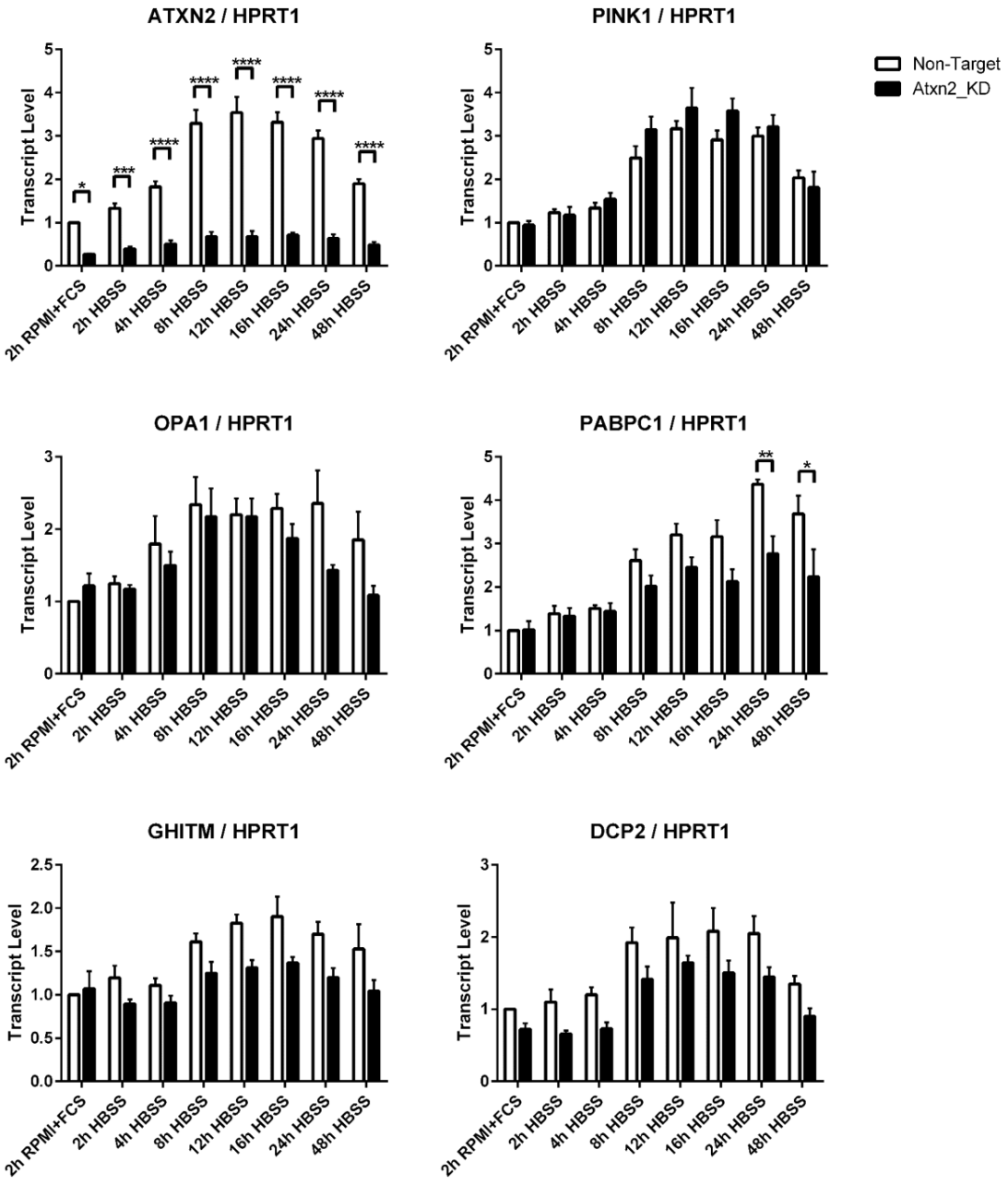

Figure 5.17. Expression analysis results of the mitochondria- and ataxin-2-associated genes after time-course starvation of NT- and *ATXN2*-KD SH-SY5Y cells.

6. DISCUSSION

Spinocerebellar Ataxia Type 2 is a progressive neurodegenerative disorder caused by the neuronal loss mainly in the cerebellum, and also in the midbrain, spinal cord and brain cortex. Degeneration of the Purkinje neurons in the cerebellum, the dopaminergic neurons in the substantia nigra, and the motor neurons in the spinal cord and brain cortex underlies the incoordination, postural rigidity, velocity saccade loss, dysarthria and distal amyotrophy present in SCA2 patients (Lastres-Becker *et al.*, 2008b). These symptoms, with the addition of cognitive deficiencies and loss of autonomic tasks, severely increase throughout the disease progression, cumulatively contributing to the eventual decease of the patient in approximately 10 years. As the disease is autosomal dominantly inherited, even *de novo* occurrence of the expansion in a generation easily turns into a familial case potentially affecting many individuals, unfortunately without the possibility of a preventive treatment.

Although not as frequent as in Cuba, SCA2 is the most common type of autosomal dominant cerebellar ataxia in Turkey (Statistical data obtained from NDAL patient cohort). Turkey is a pool of not only dominant, but also recessive genetic disorders primarily due to the high rate of consanguinity, early marriages and conceiving large number of offspring prior to disease manifestation. Therefore, there are many families present in Turkey, similar to the one examined in the context of this thesis, several members of which are suffering from SCA2 and awaiting a potent cure.

The development of therapies that not only alleviate the symptoms, as the current treatments do, but directly target the disease is dependent on the thorough comprehension of the causative pathogenesis, that is poly-Q expansions in the *ATXN2* gene. To this day, expansion-induced pathogenesis underlying poly-Q disorders has been defined to possess both gain- and loss-of-function characteristics (Lim *et al.*, 2008). The intracellular protein aggregates and the RNA foci induced by the expansion in distinct brain regions have been hypothesized to cause toxicity that leads to the dysfunction and death of the neurons (Li and Li, 2004; Orr and Zoghbi, 2007). The loss-of-function theory, on the other hand, suggests that the expansion leads to the clearance of the protein from its native habitat as a

result of aggregations, and also to a decrease in its normal interaction capability with other proteins due to alterations in the 3-D conformation and disruption of the functional domains. The knock-out models of several poly-Q disorders, although share similarities regarding the dysregulated expression levels of some transcripts with the knock-in model, do not show neurological symptoms that mimic the normal disease phenotype (Crespo-Barreto *et al.*, 2010; Kiehl *et al.*, 2006; Lastres-Becker *et al.*, 2008a; Zeitlin *et al.*, 1995).

Having the *Atxn2*-KO mouse model on one hand, and the large Turkish SCA2 pedigree on the other, we believe to have gathered a strong sample set and a great advantage in dissecting the loss-/gain-of-function phenomenon of *ATXN2* expansions. Examination of the pathogenesis-induced downstream transcriptional changes in the SCA2 patients especially, rather than a disease model, also holds benefit towards making more accurate and insightful inferences. In this sense, the family investigated in this thesis to elucidate the downstream effects of ataxin-2 pathology, and maybe even to look deeper at the different stages of the disease, is exceptionally important due to the reduced genetic background shared among family members and minimal epigenetic differences, as they all live in the same region with similar life-style preferences and subjected to the same environmental cues. In addition to the genetic and epigenetic suitability for functional studies, the best possible conditions for the high-throughput transcriptome analysis of this family were provided, since the blood transcriptome profile may easily be affected from the simplest stimulants. All individuals had fasted over-night prior to sample collection and peripheral blood samples were collected simultaneously from all donors into PAXgene Blood RNA tubes. Within the three hour incubation of the tubes at the room temperature, the total blood RNA was fixed by the solution provided in the PAXgene tube, after which samples were frozen and transported to Istanbul all together in the same day. The subsequent processing of the blood samples, such as RNA isolation, DNaseI treatment and cDNA synthesis, were all performed in parallel to prevent any disturbance. Hence, we are confident that the global transcriptome profile of the SCA2 pedigree is as accurate as possible for a patient-based study.

Even though our general aim is to elucidate ataxin-2 mechanism and the basis of pathogenicity, understanding the progressive changes in both loss- and toxic gain-of-function scenarios are of equal importance. Most of the NDs show similar phases of

pathogenesis; starting with the induction in a single or several cells, followed by a latent period where minute molecular and cellular alterations occur locally and accumulate without an obvious manifestation. After a certain threshold the first symptoms appear, and depending on the strength of the primary cause, symptoms worsen progressively and the pathology spreads to other regions of the CNS leading to additional secondary symptoms. Therefore, the phasic progression seen in SCA2 might be due to the dynamic nature of ataxin-2 pathology imposed by the collective changes in 3-D conformation, interaction partners and aggregation rate to different levels throughout the disease course. Hence, different cellular mechanisms are altered at different stages of the disease. The progressive pathology asserted by ataxin-2 also correlates well with the fact that intermediate and short-pathogenic expansions occasionally present distinct phenotypes and are associated with various NDs. The genetic background of the individual bearing the expansion, together with the environmental factors, jointly contribute to manifestation of the *ATXN2* expansion-induced pathogenesis with a range of symptoms belonging to a spectrum of disorders.

6.1. Cerebellum and Liver Biomarkers in *Atxn2*-KO Mouse

Examining the global transcriptome profiles of *Atxn2*-KO mice and SCA2 patients in parallel holds great potential to unravel the native function of ataxin-2 and the expansion-induced pathology, also to identify disease biomarkers. The microarray data of *Atxn2*-KO mice was examined to see if a global dysregulation in transcription and translation machineries was present considering the roles of ataxin-2 in RNA-binding, translation and stress granule formation. Among the upregulated factors, ribosomal proteins were the predominant observation, accompanied by RNA processing factors (several *DCP* genes, *Lsm12*), and regulators of lipid droplet biogenesis (*Plin3*) and apolipoprotein secretion (*Mttp*) (Fittschen *et al.,* 2015). For the investigation of the downregulated factors in the mouse microarray data, an interaction network was generated taking the 100 most significant changes, and a closely connected sub-network of factors secreted to extracellular fluids was observed. The validation of these dysregulations was conducted using the cerebellum and liver tissues of *Atxn2*-KO mice at the protein level to identify biomarker candidates for future analysis in SCA2 patients. None of the detected

factors showed significant changes in cerebellum, whereas three factors, Apo-AI (+1.3-fold), Hemopexin (+2.3-fold) and SERPINA1 (+2.4-fold), were all found significantly upregulated in *Atxn2*-KO mouse liver. Apo-AI is the major protein component of high density lipoproteins, and mediates the cholesterol efflux from the cells (Phillips, 2014). Hemopexin is a glycoprotein found in the plasma that strongly binds and transports the heme groups to the liver for breakdown and iron recovery, in the meantime protecting cells from oxidative stress. Loss of Hemopexin in mice show increased iron staining in the brain slices at basal ganglia level (Tolosano *et al.*, 2010). SERPINA1 is a serine protease inhibitor found in the serum, whose main substrate is the Elastase enzyme that breaks down elastic fiber proteins of the connective tissue in the alveolar walls and a series of other tissues (Gettins, 2002).

6.1.1. Potential Dysregulation of the ER-Golgi Secretory Pathway

Interestingly, a relationship between ataxin-2 and the secreted lipid-traffic factors was previously shown in a study examining the blood proteome of SCA2 patients. Significant dysregulations of Apo-AI (-3-fold), Apo-CII (-2-fold), Apo-CIII (-4-fold) and Apo-E (+4-fold) were reported at the protein level. Also, transthyretin and albumin protein levels, members of our secretion sub-network that showed no significant change in validations, have been found significantly dysregulated in patient blood (3-fold down and 4-fold up, respectively) (Swarup *et al.*, 2013). The observed increase in the intracellular protein levels of the secreted factors, although their mRNAs were initially found downregulated in the transcriptome data, brought up the hypothesis that a deficit might have been present in the ER-Golgi secretory pathway. The accumulation of the proteins, which were supposed to be secreted to the extracellular fluids, due to a problem in this pathway might be activating a negative feedback response that halts the transcription of the relevant genes. Examination of the mouse transcriptome data again revealed significant dysregulations of *Sel1l*, taking role in the retrotranslocation of the misfolded proteins back to the cytosol, and *Syvn1*, a ubiquitin-ligase activated upon ER-stress and mediates the degradation of accumulated proteins (Kaneko *et al.*, 2002; Mueller *et al.*, 2008).

Independent validations with qRT-PCR, however, showed no major change in the expression of these genes both in the cerebellum and liver of the *Atxn2*-KO mice.

The expression analyses of *Apoa1*, *Hpx* and *Serpina1a/b/c* transcripts in both tissues also showed controversy compared to the transcriptome data acquired from *Atxn2*-KO mouse cerebellum. Validations with independent methods, such as qRT-PCR, are preferred for the currently improving high-throughput analyses. Taking these results into consideration, we would have to say that no major change is actually present in the transcript levels of *Apoa1* and *Serpina1a/b/c* in both cerebellum and liver, although the transcriptome data suggested otherwise. However, their protein levels are still significantly upregulated in the liver by 1.3- and 2.4-fold, respectively. *Hpx* transcript, on the other hand, is significantly upregulated by 1.3- and 1.5-fold in the cerebellum and liver, respectively, also showing an induction of the protein in the liver by 2.3-fold. The disproved downregulations in the transcript levels of *Apoa1*, *Hpx* and *Serpina1a/b/c* might also refute the "ER-Golgi secretory pathway deficiency" hypothesis and steady levels of ER-associated factors *Syvn1* and *Sel1l* would be explained. Yet, the accumulation of apolipoproteins within the liver cells, their decrease in the patient blood plasma, and the increase in the apolipoprotein secretion mediator, *Mttp*, all suggest a problem in the secretion machinery and an effort to mitigate intracellular apolipoprotein accumulation. There may have been other factors in the mouse transcriptome data that we have overlooked, maybe more relevant to the Golgi apparatus and the secretion part of the pathway rather than ER-associated degradation.

Combining the global findings provided by the high-throughput transcriptome studies in *Atxn2*-KO mouse, one might conclude that ataxin-2 is indeed involved in the processing and the translation of the mRNAs, also regulating the biogenesis and transport of the lipids and other nutrient carriers. The expansion-induced pathogenesis, therefore, might be due to the alterations in the global protein synthesis occurring at the rER, where ataxin-2 localizes and interacts with polysomes. Cerebellar Purkinje cells, spinal and cortical motor neurons and dopaminergic neurons of the substantia nigra, the most affected neurons in SCA2, are among the most vulnerable cell types against the alterations in

proteostasis due to high numbers of large rER structures, complex dendritic spine networks and massive metabolic activities. Thus, the selective vulnerability of these magnocellular neurons in SCA2 pathogenesis might be explained to some level with the global impairment of proteostasis and induction of the cellular stress. Regulation of the energy and nutrient consumption is among the primary stress responses of a cell. Taking the involvement of ataxin-2 in lipid storage, secretion and transport into consideration, the cellular stress induced by the malfunctioning of the translation machinery due to *ATXN2* expansions, may not be handled properly. Therefore, the expansions in *ATXN2* not only alter the global mRNA metabolism and protein synthesis, but may also impair the response given to the intracellular stress induced by these alterations.

6.2. Blood Biomarkers in SCA2 Patients

The investigation of SCA2 blood biomarkers initially started with the attempt of validating the secretion network components, acquired from the *Atxn2*-KO mouse data, at the protein level in SCA2 blood samples, and to assess if the opposite effects will be observed when the loss- and the toxic gain-of-function models are compared. Unfortunately, quantitative immunoblots performed with the whole proteins isolated from SCA2 patient blood showed no success due to the dominating amount of hemoglobin in the serum. Although depletion was performed prior to the immunoblot analyses with hemoglobin-binding beads, even many more times than suggested by the manufacturer, the remaining hemoglobin was still enough to interfere with the quantitation of the total isolated proteins. The protein sample loaded to the SDS gel mostly consisted of hemoglobin, rendering other proteins in such a minute amount that could not be detected by the same antibodies previously used in mouse experiments. Hence, no comparison of the Apo-AI, Hemopexin and SERPINA1 protein levels was possible between *Atxn2*-KO mouse liver and the patient blood samples.

In the meantime, high-throughput RNA-sequencing results of three patients and three healthy individuals from the same family were compared in order to identify RNA biomarkers of SCA2 that would represent the ataxin-2 pathology and possibly the

progression of the disease. Significant dysregulations greater than 2-fold were observed in many transcripts, and two different filtering approaches were utilized. First, all the transcripts were sorted out with respect to the fold-change difference and the significance of this change. In the second approach, known ALS- and ataxia-associated genes gathered from online databases were filtered out from the whole transcriptome data and eliminated again with respect to the fold change and significance. The first approach has advantages in finding novel transcripts affected by the expansion, and might unravel a previously unknown aspect of ataxin-2 pathology. Selection of dysregulated ND-associated genes, on the other hand, might help in clarifying the commonality of several molecular mechanisms or phenotypes prominent in diverse NDs. Examining the ND-associated genes in the transcriptome of SCA2 patients, where ataxin-2 can fully exert its pathologic effect, may raise novel explanations of wide ataxin-2 involvement in many disorders.

Among the candidate biomarker genes chosen by the first approach, *ETV7*, *SERINC2*, *DACT1* and *PHTF2* were validated as significant changes. The greatest effect was observed in the blood variant of ETS-family transcription factors, *ETV7*. Another member of this family, ETS1, is the only identified transcription factor regulating *ATXN2* expression (Scoles *et al.*, 2012). Therefore, the 579% increase of the *ETV7* transcript level in patient blood is in excellent agreement with the previous findings and paves the way of new inquiries regarding the regulation of *ATXN2*. Two other large effects were observed in *SERINC2* with 279% increase, and *DACT1* with 70% decrease of the transcript levels in patient blood. The expression of *SERINC2*, which normally functions in the incorporation of serine amino acid into phosphatidylserine and sphingolipids, has been found upregulated in the rat hippocampus and the cerebellar Purkinje layer. The expression increased even more in the hippocampus upon seizures induced by kainite, a neuroexcitatory amino acid that activates glutamatergic receptors (Inuzuka *et al.*, 2005). Therefore, the upregulation of the *SERINC2* transcript we observed in the SCA2 patient blood samples might be relevant to the neurological syndrome and represent the ongoing pathology in the brain. The decrease observed in plasma *DACT1* levels might also be relevant to the pathology due to its involvement in the morphogenesis of the notochord and establishment of the excitatory synapses during development. DACT1 normally antagonizes the transcription of the Wnt/beta-catenin pathway target genes by regulating the membrane localization or

degradation of beta-catenin and recruiting HDAC1, which enhances heterochromatin formation, to the target gene promoters (Lagathu *et al.*, 2009). *Dact1* null mice show severe posterior malformations due to the problems in primitive streak morphogenesis and depletion of the mRNA in Xenopus results in the loss of notochord and head structures (Suriben *et al.*, 2009). Further investigation of these huge downstream effects of *ATXN2* expansion on *SERINC2* and *DACT1* might reveal novel aspects of the pathology or explain at least some of the previously unsolved mechanistic impairments. Although there is scarce information on the function of *PHTF2* in the literature, several GWAS studies show its association with chronic kidney disease, childhood obesity and blood lipid phenotype. The 25% decrease seen in *PHTF2* might be relevant to ataxin-2 pathology, considering the obesity phenotype of the *Atxn2*-KO mouse and the impairments of apolipoprotein levels both in *Atxn2*-KO mouse tissues and patient blood plasma, previously discussed in this chapter.

Two genes previously associated with neurodegenerative disorders, *MATR3* and *ATXN1*, showed significant changes in SCA2 patient blood. *MATR3* is an ALS-associated gene involved in mRNA stabilization, normally located in the nuclei of motor neurons and the surrounding glia of the spinal cord. However, a diffuse distribution of MATR3 in the cytoplasm is observed along with intense nuclear localization in the spinal cord sections of ALS patients. MATR3 interacts with TDP-43, another ALS-associated protein involved in mRNA metabolism in the nucleus, but shuttles to the cytoplasm to form stress granules (Johnson *et al.*, 2014). The 40% decrease seen in *MATR3* level is quite interesting and emphasizes the *ATXN2* involvement in ALS and the similarities between the pathogenesis of both disorders that are aberrant RNA metabolism and possibly alterations in stress granule dynamics. The 138% increase observed in *ATXN1* levels is also anticipated and strengthens the previous reports suggesting its direct and strong interaction with ataxin-2, and the regulation of ataxin-1 toxicity by the sequestration of ataxin-2 into intranuclear aggregates (Al-Ramahi *et al.*, 2007; Lim *et al.*, 2006). In the same sense, the observed increase of *ATXN1* in patient blood may be contributing to the expanded ataxin-2 toxicity.

The emergence of two genes, that are especially involved in the most pronounced pathogenic mechanism and are established interactors of ataxin-2, among many ND-associated genes examined, provides a proof of principle for the targeted filtration approach we employed. Also, the presence of great expression changes in previously unrelated factors to ataxin-2 evokes the discovery of completely novel mechanisms affected by or contributing to the pathology exerted by *ATXN2* expansions.

6.3. Gene Set Enrichment Analysis

The enrichment analysis revealed dysregulations in many pathways and gene sets to be maximally significant with nominal p-value, FDR q-value, and FWER p-values equal to zero. Upregulations of several mRNA metabolism, lysosomal degradation and secretion pathways, with mitochondrial dysfunction-associated disease gene sets were observed (Table A2). Specifically, upregulations in '3'-UTR Mediated Translational Regulation' and 'Regulation of mRNA Stability by Proteins that Bind to AU-Rich Elements' pathways are in good agreement with the previously reported binding of ataxin-2 to AU-rich elements in the 3'-UTRs of mRNA molecules, which promotes the stability of the translation machinery and enhances translation (Yokoshi *et al.*, 2014). Moreover, two members of the enriched 'Extracellular Region Gene Set', namely *APOA1* and *APOE*, have been previously found dysregulated at the protein level in SCA2 patient serum. However, the mode of dysregulations in our blood transcriptome and the reported blood proteome data show opposition; *APOA1* is increased at the mRNA level (+2.1-fold) and decreased at the protein level (-2.9-fold), whereas *APOE* has a decreased mRNA (-0.69-fold) and an increased protein level (+4.4-fold) in the serum of SCA2 patients (Swarup *et al.*, 2013).

It is also interesting to note that the maximally enriched transcript in the 'Extracellular Region Gene Set' is *MMP9*, which was among the validated genes acquired by unbiased selection in SCA2 blood RNA biomarker investigation, showing a trend towards significance ($0.05 < p < 0.1$) (Figure 5.10). MMP9 is a zinc-dependent endopeptidase involved in the degradation of extra-cellular matrix components, such as

type IV and V collagens. High levels of MMP9 protein is detected in the cerebrospinal fluids of multiple sclerosis and tuberculosis meningitis patients (Gijbels *et al.*, 1992; Price *et al.*, 2001), and the release of MMP9 is believed to induce hematopoietic progenitor cell mobilization in the bone marrow by the cleavage of the surrounding ECM molecules (Pruijt *et al.*, 1999). Moreover, MMP9 has been reported as a determinant of neuronal death in ALS mouse models, showing >10-fold increase in the selectively vulnerable fast motor neurons (Kaplan *et al.*, 2014). Its co-distribution with ETV5, an ETS-family transcription factor variant highly expressed in brain, in various carcinomas, also makes a contribution to its relevance with ataxin-2 pathology considering the reported regulation of *ATXN2* expression by ETS1, and the significant 579% increase of the *ETV7* transcript in the serum of SCA2 patients reported in this thesis (Planagumà *et al.*, 2011; Scoles *et al.*, 2012).

Altogether, GSEA revealed several dysregulated pathways that ataxin-2 was already known to be involved in, such as mRNA and translation stabilization and strengthened their association with the pathology. However, investigating the contributory transcripts to these known pathways, as well as examining the rather rarely pronounced pathways, led to the identification of novel players, such as apolipoproteins and *MMP9*, that may clarify a part of the complex ataxin-2 network.

6.4. The Relationship between Ataxin-2 and the Mitochondrial Factors

Enrichment of two pathways, Parkinson's disease and Huntington's disease, was especially interesting, since both disorders share mitochondrial dysfunction features underlying the disease pathogenesis, and alterations in the expression of mitochondrial genes in SCA2 patient samples is a novel finding. The common brain pathology, shared clinical symptoms and the involvement of intermediate *ATXN2* expansion in the disease manifestation, provoked further investigation of the Parkinson's disease pathway. Two genes pronounced in autosomal recessive juvenile PD, *PINK1* and *PARK7*, both of which function in the mitochondrial mechanisms, were found upregulated by 1.63- and 1.70-fold, respectively. The expression analyses of several mitochondria-associated genes were

conducted in *Atxn2*-KO mouse in order to see if the reverse effect would be observed. Indeed, the transcript levels of *Pink1, Opa1* and *Ghitm* were found downregulated in *Atxn2*-KO mouse cerebellum and liver with maximal significances, strengthening the association between ataxin-2 and mitochondrial genes (Figure 5.16).

The transcription of *PINK1* can be induced by nutrient starvation which leads to the degradation of dysfunctional mitochondria by a selective autophagy process called 'mitophagy' (Jin and Youle, 2012; Klinkenberg *et al.*, 2012). The PTEN-dependent activation of PINK1 is regulated by the upstream PI3K signaling cascade that maintains lipid and carbohydrate metabolisms in balance depending on the availability of these nutrients. PI3K signaling is tightly interconnected with the mTOR pathway that detects amino acid availability and eventually regulates growth and cell proliferation. The yeast homolog of ataxin-2 has been shown to sequester the TORC1 subunit of mTOR into stress granules during heat stress and low energy input, interfering with native mTOR function and leading to the transient cellular arrest (DeMille *et al.*, 2014; Takahara and Maeda, 2012). Therefore, ataxin-2 is a more general factor responding to the starvation stress by halting cell growth, whereas PINK1 is particularly employed in the degradation of dysfunctional mitochondria to recycle lipids and amino acids as food source. The obesity phenotype and the reduced level of *Pink1* transcript in *Atxn2*-KO mouse are consistent with this mechanism, since the lack of ataxin-2 exterminates the control over growth and proliferation of the fat cells and the excess energy provided by *ad libitum* feeding is stored in this tissue, without the need of mitophagy as long as the mice are under no starvation stress. In contrast, *PINK1* levels are upregulated in the SCA2 patient blood, representing a stress condition probably caused by the induction of autophagy in the degenerating tissues.

A time-course starvation experiment with *ATXN2*-KD SH-SY5Y cells was designed to investigate the relationship between ataxin-2 and the mitochondria-associated genes, also to assess if the time-course induction pattern of *PINK1* will be affected from *ATXN2* silencing. The pattern of *PINK1* expression in *ATXN2* depleted and normal cells are similar, but a greater *PINK1* induction is observed in the absence of *ATXN2* possibly representing a compensatory effort to overcome the starvation stress, especially after eight hours of starvation. The expression of *ATXN2* immediately increases in the first two hours of starvation in normal cells, hence the initial delay observed in *PINK1* induction in

ATXN2-KD cells suggests that ataxin-2 might be in the upstream of PINK1 as a stress sensor, in the absence of which *PINK1* gets to be induced by an alternative mechanism with a slight delay.

Drawing a meaningful conclusion for the expression status of *OPA1*, another mitochondrial factor associated with autosomal dominant optic atrophy, in starved *ATXN2*-KD cells is impossible due to the high variation between replicate sets at every time point. In contrast to *PINK1*, the expression levels of *GHITM*, which is involved in mitochondrial morphology and the release of apoptotic cytochrome c from mitochondria, shows a slight reduction in *ATXN2* depleted cells at the beginning of starvation, in line with the decrease observed in *Atxn2*-KO mouse tissues. The downregulation of *GHITM* is reported to cause mitochondrial fragmentation and the release of proapoptotic proteins (Oka *et al.*, 2008). The anti-apoptotic control over *GHITM* expression under stress conditions, potentially exerted by ataxin-2, is initially diminished in *ATXN2*-KD cells, comprising the risk of mitochondrial fragmentation and apoptosis. *GHITM* levels increase in the *ATXN2*-KD cells to a smaller extent compared to normal cells, probably under the control of an alternative mechanism starting from eight hours of starvation (Figure 5.17).

The expression patterns of two genes related to ataxin-2 function, *DCP2* and *PABPC1*, were investigated in the time-course starved *ATXN2*-KD cells along with mitochondrial factors. In a previous study, the increase in *ATXN2* levels was shown to interfere with the p-body formation leading to a reduction in their number, whereas the decrease of *ATXN2* altered stress granule assembly and increased intracellular PABP levels (Nonhoff *et al.*, 2007). The expression of *DCP2*, which is a key component of the mRNA de-capping machinery and found in p-bodies, is reduced in *ATXN2*-KD cells from the beginning of starvation compared to the normal cells. The initially constant expression and the rise after eight hours are similar in both cell types suggesting *ATXN2* involvement not in the timing, but in the degree of *DCP2* induction. In the case of *PABPC1*, which is a stress granule component liberating to the cytoplasm in the depletion of *ATXN2*, a gap in the transcript levels emerge between the *ATXN2*-KD and normal cells only after eight hours, showing the same expression rate until this point. The only statistically significant

results in the time-course starvation experiments were obtained at the 24- and 48-hour time point expression level differences of *PABPC1*. However, this change we observe suggests that the induction of *PABPC1* here is due to starvation stress rather than to ataxin-2 depletion, since higher concentrations of *PABPC1* transcript would otherwise be expected in *ATXN2*-KD cells.

7. CONCLUSION

We have examined the high-throughput transcriptome data of *Atxn2*-KO mice and SCA2 patients from a large Turkish pedigree in parallel to basically understand the native function of ataxin-2 and the expansion-induced pathogenesis, which would eventually lead to the development of molecular diagnostics of disease progression and the identification of molecular targets for therapy.

Possessing the loss- and the toxic-gain-of-function models, we had the chance to combine the findings in both sample sets and make reliable inferences regarding the functional and pathological aspects of ataxin-2. Previously known mechanisms of ataxin-2, such as mRNA stabilization and processing, translational regulation, and stress granule formation, were strengthened by several findings both in the *Atxn2*-KO and the SCA2 patient transcriptome data. Some shared novel functions and downstream effects of ataxin-2 have also been identified in *Atxn2*-KO mice and SCA2 patients, such as the biogenesis and transport of the lipids, and the dysregulated levels of apolipoproteins and other members of the extracellular region gene set.

The overall recurrence of previously known ataxin-2 mechanisms and the emergence of shared novel effects between the knock-out mouse model and the SCA2 patients, is a proof of principle for the theoretical and the experimental approach we employed in the filtration and evaluation of the high-throughput transcriptome data. Some factors identified in this study to be differentially altered among patients, but showing stable expression in controls, might actually be biomarkers of disease progression representing a specific stage, however getting shaded due to the distinct phenotypic and expression features presented by other patients. The number of patients examined in this study, although they possess very little genetic and epigenetic background differences, may not be large enough to dissect such changes. Further investigation of these dysregulated genes in larger cohorts with clinically well-defined progression states would provide better correlation between the stages of the disease and the dysregulation of certain transcripts.

Altogether, we investigated the general function and the expansion-based pathogenicity of ataxin-2 with the long-term goal of paving the way for a cause-targeted treatment. Starting with the dissection of the progression stages at the molecular level, explaining the selective vulnerability of certain cell types and assembling the pieces of complex neural networks, we hope to gain a thorough understanding of ataxin-2 pathology and cure SCA2, hopefully together with other neurodegenerative disorders that ataxin-2 is widely involved in.

APPENDIX A: SUPPLEMENTARY TABLES

Table A1. List of all known spinocerebellar ataxias (Kobayashi *et al.*, 2011; McMurray, 2010; Rüb *et al.*, 2013; Sato *et al.*, 2009; Todd and Paulson, 2010).

Disease	Gene	Chr.	Repeat Unit	Location	Repeat # (Normal)	Repeat # (Disease)
SCA1	*ATXN1*	6p22	CAG	exon	6 – 44	49 – 91
SCA2	*ATXN2*	12q24	CAG	exon	14 – 32	33 – >200
SCA3	*ATXN3*	14q32	CAG	exon	12 – 44	52 – 89
SCA4		16q22				
SCA5	*SPTBN2*	11q13				
SCA6	*CACNA1A*	19p13	CAG	exon	3 – 18	20 – 33
SCA7	*ATXN7*	3p21	CAG	exon	4 – 35	36 – 460
SCA8	*ATXN8OS*	13q21	CTG	3'-UTR	15 – 50	71 – 1300
SCA9						
SCA10	*ATXN10*	22q13	ATTCT	intron	10 – 29	800 – 4500
SCA11	*TTBK2*	15q14				
SCA12	*PPP2R2B*	5q31	CAG	5'-UTR	< 32	51 – 78
SCA13	*KCNC3*	19q13.33				
SCA14	*PRKCG*	19q13.42				
SCA15	*ITPR1*	3p26				
SCA16	*ITPR1*	3p26				
SCA17	*TBP*	6q27	CAG	exon	25 – 44	47 – 63
SCA18		7q31				
SCA19	*KCND3*	1p13				
SCA20		11q12				
SCA21	*TMEM240*	1p36				
SCA22	*KCND3*	1p13				
SCA23	*PDYN*	20p13				
SCA24						
SCA25		2p15-p21				
SCA26	*EEF2*	19p13				
SCA27	*FGF14*	13q33				

Table A1. List of all known spinocerebellar ataxias (Kobayashi *et al.*, 2011; McMurray, 2010; Rüb *et al.*, 2013; Sato *et al.*, 2009; Todd and Paulson, 2010) (cont.).

Disease	**Gene**	**Chr.**	**Repeat Unit**	**Location**	**Repeat # (Normal)**	**Repeat # (Disease)**
SCA28	*AFG3L2*	18p11				
SCA29		3p26				
SCA30		4q34				
SCA31	*BEAN*	16q22	TGGAA	intron		> 110
SCA32		7q32				
SCA33						
SCA34	*ELOVL4*	6q14				
SCA35	*TGM6*	20p13				
SCA36	*NOP56*	20p13	GGCCTG	intron		3 – 8
SCA37		1p32				
SCA38	*ELOVL5*	6p12				
SCA39						
SCA40	*CCDC88C*	14q32				

Table A2. Significantly upregulated pathways in the blood RNA-sequencing data of SCA2 patients.

	GENE SET	SIZE	ES	NES	NOM p-val	FDR q-val	FWER p-val
1	KEGG_OXIDATIVE_PHOSPHORYLATION	110	0.45	5.53	0.000	0.000	0.000
2	REACTOME_METABOLISM_OF_PROTEINS	397	0.23	5.40	0.000	0.000	0.000
3	REACTOME_TRANSLATION	144	0.38	5.28	0.000	0.000	0.000
4	REACTOME_METABOLISM_OF_MRNA	207	0.32	5.21	0.000	0.000	0.000
5	REACTOME_RESPIRATORY_ELECTRON_TRANSPORT_ATP_SYNTHESIS_BY_CHEMIOSMOTIC_COUPLING_AND_HEAT_PRODUCTION_BY_UNCOUPLING_PROTEINS_	79	0.49	5.13	0.000	0.000	0.000
6	REACTOME_INFLUENZA_VIRAL_RNA_TRANSCRIPTION_AND_REPLICATION	100	0.43	5.09	0.000	0.000	0.000
7	REACTOME_SRP_DEPENDENT_COTRANSLATIONAL_PROTEIN_TARGETING_TO_MEMBRANE	107	0.41	5.02	0.000	0.000	0.000
8	KEGG_RIBOSOME	85	0.46	4.95	0.000	0.000	0.000
9	REACTOME_3_UTR_MEDIATED_TRANSLATIONAL_REGULATION	104	0.41	4.94	0.000	0.000	0.000
10	REACTOME_PEPTIDE_CHAIN_ELONGATION	84	0.46	4.93	0.000	0.000	0.000
11	REACTOME_TCA_CYCLE_AND_RESPIRATORY_ELECTRON_TRANSPORT	114	0.39	4.67	0.000	0.000	0.000
12	KEGG_HUNTINGTONS_DISEASE	157	0.32	4.64	0.000	0.000	0.000
13	REACTOME_METABOLISM_OF_RNA	252	0.25	4.55	0.000	0.000	0.000
14	REACTOME_RESPIRATORY_ELECTRON_TRANSPORT	63	0.48	4.51	0.000	0.000	0.000
15	REACTOME_NONSENSE_MEDIATED_DECAY_ENHANCED_BY_THE_EXON_JUNCTION_COMPLEX	105	0.38	4.37	0.000	0.000	0.000

Table A2. Significantly upregulated pathways in the blood RNA-sequencing data of SCA2 patients (cont.).

	GENE SET	SIZE	ES	NES	NOM p-val	FDR q-val	FWER p-val
16	KEGG_PARKINSONS_DISEASE	105	0.37	4.31	0.000	0.000	0.000
17	REACTOME_DEFENSINS	45	0.53	4.15	0.000	0.000	0.000
18	REACTOME_INFLUENZA_LIFE_CYCLE	134	0.29	3.89	0.000	0.000	0.000
19	REACTOME_BETA_DEFENSINS	39	0.52	3.81	0.000	0.000	0.000
20	REACTOME_FORMATION_OF_THE_TERNARY_COMPLEX_AND_SUBSEQUENTLY_THE_43S_COMPLEX	48	0.46	3.76	0.000	0.000	0.000
21	REACTOME_ACTIVATION_OF_THE_MRNA_UPON_BINDING_OF_THE_CAP_BINDING_COMPLEX_AND_EIFS_AND_SUBSEQUENT_BINDING_TO_43S	56	0.41	3.69	0.000	0.000	0.000
22	REACTOME_ER_PHAGOSOME_PATHWAY	57	0.41	3.68	0.000	0.000	0.000
23	KEGG_ALZHEIMERS_DISEASE	144	0.26	3.63	0.000	0.000	0.000
24	KEGG_PROTEASOME	42	0.46	3.54	0.000	0.000	0.000
25	REACTOME_ANTIGEN_PROCESSING_CROSS_PRESENTATION	70	0.36	3.51	0.000	0.000	0.000
26	REACTOME_AUTODEGRADATION_OF_THE_E3_UBIQUITIN_LIGASE_COP1	46	0.43	3.49	0.000	0.000	0.000
27	KEGG_LYSOSOME	118	0.28	3.48	0.000	0.000	0.000
28	REACTOME_CDK_MEDIATED_PHOSPHORYLATION_AND_REMOVAL_OF_CDC6	45	0.43	3.37	0.000	0.000	0.000
29	REACTOME_INNATE_IMMUNE_SYSTEM	254	0.18	3.34	0.000	0.000	0.000
30	REACTOME_P53_INDEPENDENT_G1_S_DNA_DAMAGE_CHECKPOINT	47	0.40	3.24	0.000	0.000	0.000
31	REACTOME_APOPTOSIS	134	0.24	3.23	0.000	0.000	0.000
32	REACTOME_VIF_MEDIATED_DEGRADATION_OF_APOBEC3G	48	0.40	3.23	0.000	0.000	0.000

Table A2. Significantly upregulated pathways in the blood RNA-sequencing data of SCA2 patients (cont.).

	GENE SET	SIZE	ES	NES	NOM p-val	FDR q-val	FWER p-val
33	REACTOME_DESTABILIZATION_OF_MRNA_BY_AUF1_HNRNP_D0	49	0.39	3.22	0.000	0.000	0.000
34	REACTOME_HIV_INFECTION	186	0.20	3.22	0.000	0.000	0.000
35	REACTOME_ACTIVATION_OF_CHAPERONE_GENES_BY_XBP1S	43	0.42	3.22	0.000	0.000	0.000
36	REACTOME_REGULATION_OF_MRNA_STABILITY_BY_PROTEINS_THAT_BIND_AU_RICH_ELEMENTS	80	0.31	3.20	0.000	0.000	0.000
37	REACTOME_APC_C_CDH1_MEDIATED_DEGRADATION_OF_CDC20_AND_OTHER_APC_C_CDH1_TARGETED_PROTEINS_IN_LATE_MITOSIS_EARLY_G1	63	0.34	3.17	0.000	0.000	0.000
38	REACTOME_CROSS_PRESENTATION_OF_SOLUBLE_EXOGENOUS_ANTIGENS_ENDOSOMES	45	0.41	3.15	0.000	0.000	0.001
39	REACTOME_HOST_INTERACTIONS_OF_HIV_FACTORS	119	0.25	3.14	0.000	0.000	0.001
40	KEGG_SYSTEMIC_LUPUS_ERYTHEMATOSUS	113	0.25	3.12	0.000	0.000	0.002
41	REACTOME_SCF_BETA_TRCP_MEDIATED_DEGRADATION_OF_EMI1	48	0.38	3.12	0.000	0.000	0.002
42	REACTOME_REGULATION_OF_APOPTOSIS	53	0.37	3.11	0.000	0.000	0.002
43	REACTOME_P53_DEPENDENT_G1_DNA_DAMAGE_RESPONSE	52	0.36	3.10	0.000	0.000	0.002
44	REACTOME_APC_C_CDC20_MEDIATED_DEGRADATION_OF_MITOTIC_PROTEINS	64	0.33	3.07	0.000	0.000	0.002
45	REACTOME_AUTODEGRADATION_OF_CDH1_BY_CDH1_APC_C	56	0.35	3.02	0.000	0.000	0.002
46	REACTOME_REGULATION_OF_ORNITHINE_DECARBOXYLASE_ODC	47	0.37	3.01	0.000	0.000	0.002

Table A2. Significantly upregulated pathways in the blood RNA-sequencing data of SCA2 patients (cont.).

	GENE SET	SIZE	ES	NES	NOM p-val	FDR q-val	FWER p-val
47	REACTOME_CDT1_ASSOCIATION_WITH_THE_CDC6_ORC_ORIGIN_COMPLEX	53	0.35	3.01	0.000	0.000	0.002
48	REACTOME_ADAPTIVE_IMMUNE_SYSTEM	484	0.12	2.99	0.000	0.000	0.002
49	REACTOME_ASSEMBLY_OF_THE_PRE_REPLICATIVE_COMPLEX	62	0.32	2.96	0.000	0.000	0.002
50	REACTOME_SCFSKP2_MEDIATED_DEGRADATION_OF_P27_P21	53	0.33	2.94	0.000	0.000	0.003
51	KEGG_NEUROACTIVE_LIGAND_RECEPTOR_INTERACTION	189	0.18	2.88	0.000	0.000	0.004
52	REACTOME_HEMOSTASIS	388	0.13	2.85	0.000	0.000	0.005
53	REACTOME_UNFOLDED_PROTEIN_RESPONSE	75	0.28	2.84	0.000	0.000	0.005
54	REACTOME_NEURONAL_SYSTEM	202	0.17	2.83	0.000	0.000	0.005
55	REACTOME_THE_ROLE_OF_NEF_IN_HIV1_REPLICATION_AND_DISEASE_PATHOGENESIS	27	0.47	2.83	0.000	0.000	0.006
56	REACTOME_LATENT_INFECTION_OF_HOMO_SAPIENS_WITH_MYCOBACTERIUM_TUBERCULOSIS	30	0.43	2.83	0.000	0.000	0.006
57	REACTOME_SIGNALING_BY_WNT	61	0.31	2.82	0.000	0.000	0.006
58	REACTOME_ORC1_REMOVAL_FROM_CHROMATIN	64	0.30	2.81	0.000	0.000	0.006
59	REACTOME_ACTIVATION_OF_NF_KAPPAB_IN_B_CELLS	60	0.31	2.79	0.000	0.000	0.006
60	REACTOME_PLATELET_ACTIVATION_SIGNALING_AND_AGGREGATION	176	0.18	2.78	0.000	0.000	0.007
61	REACTOME_POTASSIUM_CHANNELS	64	0.30	2.76	0.000	0.000	0.009
62	REACTOME_PEPTIDE_LIGAND_BINDING_RECEPTORS	133	0.20	2.73	0.000	0.000	0.010

Table A2. Significantly upregulated pathways in the blood RNA-sequencing data of SCA2 patients (cont.).

	GENE SET	SIZE	ES	NES	NOM p-val	FDR q-val	FWER p-val
63	REACTOME_CYCLIN_E_ASSOCIATED_EVENTS_DURING_G1_S_TRANSITION_	62	0.30	2.72	0.000	0.000	0.010
64	REACTOME_GPCR_LIGAND_BINDING	288	0.14	2.68	0.000	0.000	0.010
65	REACTOME_CELL_CYCLE	378	0.12	2.65	0.000	0.000	0.018
66	KEGG_EPITHELIAL_CELL_SIGNALING_IN_HELICOBACTER_PYLORI_INFECTION	65	0.28	2.63	0.000	0.000	0.018
67	KEGG_CYTOSOLIC_DNA_SENSING_PATHWAY	52	0.31	2.63	0.000	0.000	0.018
68	REACTOME_PROTEIN_FOLDING	48	0.32	2.62	0.000	0.000	0.020
69	REACTOME_AMYLOIDS	68	0.27	2.61	0.000	0.000	0.020
70	KEGG_FRUCTOSE_AND_MANNOSE_METABOLISM	30	0.40	2.59	0.002	0.001	0.025
71	REACTOME_DOWNSTREAM_SIGNALING_EVENTS_OF_B_CELL_RECEPTOR_BCR	91	0.23	2.58	0.000	0.001	0.026
72	KEGG_CARDIAC_MUSCLE_CONTRACTION	56	0.29	2.57	0.000	0.001	0.033
73	REACTOME_GLUCOSE_METABOLISM	57	0.29	2.56	0.000	0.001	0.033
74	PID_CXCR4_PATHWAY	96	0.22	2.56	0.000	0.001	0.033
75	REACTOME_REGULATION_OF_MITOTIC_CELL_CYCLE	76	0.25	2.56	0.000	0.001	0.033
76	REACTOME_SYNTHESIS_OF_DNA	89	0.23	2.55	0.000	0.001	0.037
77	REACTOME_M_G1_TRANSITION	75	0.25	2.55	0.000	0.001	0.037
78	REACTOME_CELL_CYCLE_CHECKPOINTS	109	0.20	2.55	0.000	0.001	0.037
79	REACTOME_INTERFERON_ALPHA_BETA_SIGNALING	61	0.28	2.55	0.000	0.001	0.039

Table A3. Significantly downregulated pathways in the blood RNA-sequencing data of SCA2 patients.

	GENE SET	SIZE	ES	NES	NOM p-val	FDR q-val	FWER p-val
1	REACTOME_OLFACTORY_SIGNALING_PATHWAY	271	-0.48	-9.23	0.000	0.000	0.000
2	KEGG_OLFACTORY_TRANSDUCTION	327	-0.45	-9.21	0.000	0.000	0.000
3	REACTOME_GENERIC_TRANSCRIPTION_PATHWAY	307	-0.30	-6.07	0.000	0.000	0.000
4	REACTOME_SLC_MEDIATED_TRANSMEMBRANE_TRANSPORT	185	-0.24	-3.71	0.000	0.000	0.000
5	KEGG_UBIQUITIN_MEDIATED_PROTEOLYSIS	130	-0.21	-2.84	0.000	0.001	0.004
6	REACTOME_SIGNALING_BY_BMP	17	-0.56	-2.76	0.000	0.001	0.008
7	REACTOME_TRANSPORT_OF_MATURE_TRANSCRIPT_TO_CYTOPLASM	52	-0.31	-2.71	0.000	0.001	0.012
8	REACTOME_TRANSPORT_OF_GLUCOSE_AND_OTHER_SUGARS_BILE_SALTS_AND_ORGANIC_ACIDS_METAL_IONS_AND_AMINE_COMPOUNDS	67	-0.28	-2.65	0.000	0.002	0.024
9	KEGG_PAT HWAY S_IN_CANCER	275	-0.14	-2.59	0.002	0.003	0.032

APPENDIX B: PUBLICATIONS

Two scientific papers published during this thesis are:

Halbach MV, Stehning T, Damrath E, Jendrach M, Şen NE, Başak AN, Auburger G. "Both ubiquitin ligases FBXW8 and PARK2 are sequestrated into insolubility by ATXN2 PolyQ expansions, but only FBXW8 expression is dysregulated." *Public Library of Science One,* 2015 Mar 19;10(3):e0121089.

Özoğuz A, Uyan Ö, Birdal G, Iskender C, Kartal E, Lahut S, Ömür Ö, Agim ZS, Eken AG, Sen NE, Kavak P, Saygı C, Sapp PC, Keagle P, Parman Y, Tan E, Koç F, Deymeer F, Oflazer P, Hanağası H, Gürvit H, Bilgiç B, Durmuş H, Ertaş M, Kotan D, Akalın MA, Güllüoğlu H, Zarifoğlu M, Aysal F, Döşoğlu N, Bilguvar K, Günel M, Keskin Ö, Akgün T, Özçelik H, Landers JE, Brown RH, Başak AN. "The distinct genetic pattern of ALS in Turkey and novel mutations." *Neurobiology of Aging,* 2015 Apr;36(4):1764.e9-18.

REFERENCES

Adanyeguh, I.M., P.-G. Henry, T.M. Nguyen, D. Rinaldi, C. Jauffret, R. Valabregue, U.E. Emir, D.K. Deelchand, A. Brice, L.E. Eberly, G. Öz, A. Durr and F. Mochel, 2015, "In Vivo Neurometabolic Profiling in Patients with Spinocerebellar Ataxia Types 1, 2, 3, and 7", *Movement Disorders : Official Journal of the Movement Disorder Society*, Vol. 30, No. 5, pp. 662-670.

Aguiar, J., S. Santurlidis, J. Nowok, C. Alexander, D. Rudnicki, S. Gispert, W. Schulz and G. Auburger, 1999, "Identification of the Physiological Promoter for Spinocerebellar Ataxia 2 Gene Reveals a Cpg Island for Promoter Activity Situated into the Exon 1 of This Gene and Provides Data About the Origin of the Nonmethylated State of These Types of Islands", *Biochemical and Biophysical Research Communications*, Vol. 254, No. 2, pp. 315-318.

Al-Mahdawi, S., R.M. Pinto, D. Varshney, L. Lawrence, M.B. Lowrie, S. Hughes, Z. Webster, J. Blake, J.M. Cooper, R. King and M.A. Pook, 2006, "Gaa Repeat Expansion Mutation Mouse Models of Friedreich Ataxia Exhibit Oxidative Stress Leading to Progressive Neuronal and Cardiac Pathology", *Genomics*, Vol. 88, No. 5, pp. 580-590.

Al-Ramahi, I., A.M. Pérez, J. Lim, M. Zhang, R. Sorensen, M. De Haro, J. Branco, S.M. Pulst, H.Y. Zoghbi and J. Botas, 2007, "Dataxin-2 Mediates Expanded Ataxin-1-Induced Neurodegeneration in a Drosophila Model of Sca1", *Public Library of Science Genetics*, Vol. 3, No. 12, pp. 2551-2564.

Albrecht, M., M. Golatta, U. Wüllner and T. Lengauer, 2004, "Structural and Functional Analysis of Ataxin-2 and Ataxin-3", *European Journal of Biochemistry / FEBS*, Vol. 271, No. 15, pp. 3155-3170.

Albrecht, M. and T. Lengauer, 2004, "Survey on the Pabc Recognition Motif Pam2", *Biochemical and Biophysical Research Communications*, Vol. 316, No. 1, pp. 129-138.

Almaguer-Mederos, L.E., N.S. Falcón, Y.R. Almira, Y.G. Zaldivar, D.C. Almarales, E.M. Góngora, M. Herrera, K.E. Batallán, R.R. Armiñán, M.V. Manresa, G.S. Cruz, J. Laffita-Mesa, T.M. Cyuz, V. Chang, G. Auburger, S. Gispert and L.V. Pérez, 2010, "Estimation of the Age at Onset in Spinocerebellar Ataxia Type 2 Cuban Patients by Survival Analysis", *Clinical Genetics*, Vol. 78, No. 4, pp. 169-174.

Apps, R. and M. Garwicz, 2005, "Anatomical and Physiological Foundations of Cerebellar Information Processing", *Nature Reviews. Neuroscience*, Vol. 6, No. 4, pp. 297-311.

Babovic-Vuksanovic, D., K. Snow, M.C. Patterson and V.V. Michels, 1998, "Spinocerebellar Ataxia Type 2 (Sca 2) in an Infant with Extreme Cag Repeat Expansion", *American Journal of Medical Genetics*, Vol. 79, No. 5, pp. 383-387.

Bauer, P.O., A. Zumrova, V. Matoska, K. Mitsui and P. Goetz, 2004, "Can Ataxin-2 Be Down-Regulated by Allele-Specific De Novo DNA Methylation in Sca2 Patients?", *Medical Hypotheses*, Vol. 63, No. 6, pp. 1018-1023.

Biedler, J.L., S. Roffler-Tarlov, M. Schachner and L.S. Freedman, 1978, "Multiple Neurotransmitter Synthesis by Human Neuroblastoma Cell Lines and Clones", *Cancer Research*, Vol. 38, No. 11, pp. 3751-3757.

Brais, B., J.P. Bouchard, Y.G. Xie, D.L. Rochefort, N. Chrétien, F.M. Tomé, R.G. Lafrenière, J.M. Rommens, E. Uyama, O. Nohira, S. Blumen, A.D. Korczyn, P. Heutink, J. Mathieu, A. Duranceau, F. Codère, M. Fardeau, G.A. Rouleau and A.D. Korcyn, 1998, "Short Gcg Expansions in the Pabp2 Gene Cause Oculopharyngeal Muscular Dystrophy", *Nature Genetics*, Vol. 18, No. 2, pp. 164-167.

Cancel, G., A. Dürr, O. Didierjean, G. Imbert, K. Bürk, A. Lezin, S. Belal, A. Benomar, M. Abada-Bendib, C. Vial, J. Guimarães, H. Chneiweiss, G. Stevanin, G. Yvert, N. Abbas, F. Saudou, A.S. Lebre, M. Yahyaoui, F. Hentati, J.C. Vernant, T. Klockgether, J.L. Mandel, Y. Agid and A. Brice, 1997, "Molecular and Clinical Correlations in Spinocerebellar Ataxia 2: A Study of 32 Families", *Human Molecular Genetics*, Vol. 6, No. 5, pp. 709-715.

Cellini, E., P. Forleo, B. Nacmias, A. Tedde, S. Latorraca, S. Piacentini, L. Parnetti, V. Gallai and S. Sorbi, 2001, "Clinical and Genetic Analysis of Hereditary and Sporadic Ataxia in Central Italy", *Brain Research Bulletin*, Vol. 56, No. 3-4, pp. 363-366.

Chakor, R.T. and H. Bharote, 2012, "Inherited Ataxia with Slow Saccades", *Journal of Postgraduate Medicine*, Vol. 58, No. 4, pp. 318-325.

Charles, P., A. Camuzat, N. Benammar, F. Sellal, A. Destée, A.M. Bonnet, S. Lesage, I. Le Ber, G. Stevanin, A. Dürr and A. Brice, 2007, "Are Interrupted Sca2 Cag Repeat Expansions Responsible for Parkinsonism?", *Neurology*, Vol. 69, No. 21, pp. 1970-1975.

Chiò, A., A. Calvo, C. Moglia, A. Canosa, M. Brunetti, M. Barberis, G. Restagno, A. Conte, G. Bisogni, G. Marangi, A. Moncada, S. Lattante, M. Zollino, M. Sabatelli, A. Bagarotti, L. Corrado, G. Mora, E. Bersano, L. Mazzini and S. D'Alfonso, 2015, "Atxn2 Polyq Intermediate Repeats Are a Modifier of Als Survival", *Neurology*, Vol. 84, No. 3, pp. 251-258.

Choudhry, S., M. Mukerji, a.K. Srivastava, S. Jain and S.K. Brahmachari, 2001, "Cag Repeat Instability at Sca2 Locus: Anchoring Caa Interruptions and Linked Single Nucleotide Polymorphisms", *Human Molecular Genetics*, Vol. 10, No. 21, pp. 2437-2446.

Comuzzie, A.G., S.A. Cole, S.L. Laston, V.S. Voruganti, K. Haack, R.A. Gibbs and N.F. Butte, 2012, "Novel Genetic Loci Identified for the Pathophysiology of Childhood

Obesity in the Hispanic Population", *Public Library of Science One*, Vol. 7, No. 12, pp. e51954-e51954.

Costanzi-Porrini, S., D. Tessarolo, C. Abbruzzese, M. Liguori, T. Ashizawa and M. Giacanelli, 2000, "An Interrupted 34-Cag Repeat Sca-2 Allele in Patients with Sporadic Spinocerebellar Ataxia", *Neurology*, Vol. 54, No. 2, pp. 491-493.

Crespo-Barreto, J., J.D. Fryer, C.A. Shaw, H.T. Orr and H.Y. Zoghbi, 2010, "Partial Loss of Ataxin-1 Function Contributes to Transcriptional Dysregulation in Spinocerebellar Ataxia Type 1 Pathogenesis", *Public Library of Science Genetics*, Vol. 6, No. 7, pp. e1001021-e1001021.

Czeredys, M., J. Gruszczynska-Biegala, T. Schacht, A. Methner and J. Kuznicki, 2013, "Expression of Genes Encoding the Calcium Signalosome in Cellular and Transgenic Models of Huntington's Disease", *Frontiers in Molecular Neuroscience*, Vol. 6, pp. 42-42.

DeJesus-Hernandez, M., I.R. Mackenzie, B.F. Boeve, A.L. Boxer, M. Baker, N.J. Rutherford, A.M. Nicholson, N.A. Finch, H. Flynn, J. Adamson, N. Kouri, A. Wojtas, P. Sengdy, G.-Y.R. Hsiung, A. Karydas, W.W. Seeley, K.A. Josephs, G. Coppola, D.H. Geschwind, Z.K. Wszolek, H. Feldman, D.S. Knopman, R.C. Petersen, B.L. Miller, D.W. Dickson, K.B. Boylan, N.R. Graff-Radford and R. Rademakers, 2011, "Expanded Ggggcc Hexanucleotide Repeat in Noncoding Region of C9orf72 Causes Chromosome 9p-Linked Ftd and Als", *Neuron*, Vol. 72, No. 2, pp. 245-256.

DeMille, D., B.D. Badal, J.B. Evans, a.D. Mathis, J.F. Anderson and J.H. Grose, 2014, "Pas Kinase Is Activated by Direct Snf1-Dependent Phosphorylation and Mediates Inhibition of Torc1 through the Phosphorylation and Activation of Pbp1", *Molecular Biology of the Cell*, Vol. 26, No. 3, pp. 569-582.

Egorova, P., E. Popugaeva and I. Bezprozvanny, 2015, "Disturbed Calcium Signaling in Spinocerebellar Ataxias and Alzheimer's Disease", *Seminars in Cell & Developmental Biology*, pp. 1-7.

Elden, A.C., H.-J. Kim, M.P. Hart, A.S. Chen-Plotkin, B.S. Johnson, X. Fang, M. Armakola, F. Geser, R. Greene, M.M. Lu, A. Padmanabhan, D. Clay-Falcone, L. McCluskey, L. Elman, D. Juhr, P.J. Gruber, U. Rüb, G. Auburger, J.Q. Trojanowski, V.M.Y. Lee, V.M. Van Deerlin, N.M. Bonini and A.D. Gitler, 2010, "Ataxin-2 Intermediate-Length Polyglutamine Expansions Are Associated with Increased Risk for Als", *Nature*, Vol. 466, No. 7310, pp. 1069-1075.

Farg, M.a., K.Y. Soo, S.T. Warraich, V. Sundaramoorthy, I.P. Blair and J.D. Atkin, 2013, "Ataxin-2 Interacts with Fus and Intermediate-Length Polyglutamine Expansions Enhance Fus-Related Pathology in Amyotrophic Lateral Sclerosis", *Human Molecular Genetics*, Vol. 22, No. 4, pp. 717-728.

Fecto, F., J. Yan, S.P. Vemula, E. Liu, Y. Yang, W. Chen, J.G. Zheng, Y. Shi, N. Siddique, H. Arrat, S. Donkervoort, S. Ajroud-Driss, R.L. Sufit, S.L. Heller, H.-X. Deng and T. Siddique, 2011, "Sqstm1 Mutations in Familial and Sporadic Amyotrophic Lateral Sclerosis", *Archives of Neurology*, Vol. 68, No. 11, pp. 1440-1446.

Figley, M.D., G. Bieri, R.-M. Kolaitis, J.P. Taylor and A.D. Gitler, 2014, "Profilin 1 Associates with Stress Granules and Als-Linked Mutations Alter Stress Granule Dynamics", *The Journal of Neuroscience*, Vol. 34, No. 24, pp. 8083-8097.

Fittschen, M., I. Lastres-Becker, M.V. Halbach, E. Damrath, S. Gispert, M. Azizov, M. Walter, S. Müller and G. Auburger, 2015, "Genetic Ablation of Ataxin-2 Increases Several Global Translation Factors in Their Transcript Abundance but Decreases Translation Rate", *Neurogenetics*.

Furtado, S., M. Farrer, Y. Tsuboi, M.L. Klimek, R. de la Fuente-Fernández, J. Hussey, P. Lockhart, D.B. Calne, O. Suchowersky, A.J. Stoessl and Z.K. Wszolek, 2002, "Sca-

2 Presenting as Parkinsonism in an Alberta Family: Clinical, Genetic, and Pet Findings", *Neurology*, Vol. 59, No. 10, pp. 1625-1627.

Gal, J., A.-L. Ström, R. Kilty, F. Zhang and H. Zhu, 2007, "P62 Accumulates and Enhances Aggregate Formation in Model Systems of Familial Amyotrophic Lateral Sclerosis", *The Journal of Biological Chemistry*, Vol. 282, No. 15, pp. 11068-11077.

Geschwind, D.H., S. Perlman, C.P. Figueroa, L.J. Treiman and S.M. Pulst, 1997, "The Prevalence and Wide Clinical Spectrum of the Spinocerebellar Ataxia Type 2 Trinucleotide Repeat in Patients with Autosomal Dominant Cerebellar Ataxia", *American Journal of Human Genetics*, Vol. 60, No. 4, pp. 842-850.

Gettins, P.G.W., 2002, "Serpin Structure, Mechanism, and Function", *Chemical Reviews*, Vol. 102, No. 12, pp. 4751-4804.

Gijbels, K., S. Masure, H. Carton and G. Opdenakker, 1992, "Gelatinase in the Cerebrospinal Fluid of Patients with Multiple Sclerosis and Other Inflammatory Neurological Disorders", *Journal of Neuroimmunology*, Vol. 41, No. 1, pp. 29-34.

Gispert, S., R. Twells, G. Orozco, A. Brice, J. Weber, L. Heredero, K. Scheufler, B. Riley, R. Allotey and C. Nothers, 1993, "Chromosomal Assignment of the Second Locus for Autosomal Dominant Cerebellar Ataxia (Sca2) to Chromosome 12q23-24.1", *Nature Genetics*, Vol. 4, No. 3, pp. 295-299.

Goldbaum, O. and C. Richter-Landsberg, 2004, "Proteolytic Stress Causes Heat Shock Protein Induction, Tau Ubiquitination, and the Recruitment of Ubiquitin to Tau-Positive Aggregates in Oligodendrocytes in Culture", *The Journal of Neuroscience*, Vol. 24, No. 25, pp. 5748-5757.

Gorman, G.S., G. Pfeffer, H. Griffin, E.L. Blakely, M. Kurzawa-Akanbi, J. Gabriel, K. Sitarz, M. Roberts, B. Schoser, A. Pyle, A.M. Schaefer, R. McFarland, D.M. Turnbull, R. Horvath, P.F. Chinnery and R.W. Taylor, 2015, "Clonal Expansion of

Secondary Mitochondrial DNA Deletions Associated with Spinocerebellar Ataxia Type 28", *JAMA Neurology*, Vol. 72, No. 1, pp. 106-111.

Halbach, M.V., T. Stehning, E. Damrath, M. Jendrach, N.E. Şen, a.N. Başak and G. Auburger, 2015, "Both Ubiquitin Ligases Fbxw8 and Park2 Are Sequestrated into Insolubility by Atxn2 Polyq Expansions, but Only Fbxw8 Expression Is Dysregulated", *Public Library of Science One*, Vol. 10, No. 3, pp. e0121089-e0121089.

Hallen, L., H. Klein, C. Stoschek, S. Wehrmeyer, U. Nonhoff, M. Ralser, J. Wilde, C. Röhr, M.R. Schweiger, K. Zatloukal, M. Vingron, H. Lehrach, Z. Konthur and S. Krobitsch, 2011, "The Krab-Containing Zinc-Finger Transcriptional Regulator Zbrk1 Activates Sca2 Gene Transcription through Direct Interaction with Its Gene Product, Ataxin-2", *Human Molecular Genetics*, Vol. 20, No. 1, pp. 104-114.

Hansen, S.T., P. Meera, T.S. Otis and S.M. Pulst, 2013, "Changes in Purkinje Cell Firing and Gene Expression Precede Behavioral Pathology in a Mouse Model of Sca2", *Human Molecular Genetics*, Vol. 22, No. 2, pp. 271-283.

Hart, M.P. and A.D. Gitler, 2012, "Als-Associated Ataxin 2 Polyq Expansions Enhance Stress-Induced Caspase 3 Activation and Increase Tdp-43 Pathological Modifications", *The Journal of Neuroscience*, Vol. 32, No. 27, pp. 9133-9142.

Hayes, S., G. Turecki, K. Brisebois, I. Lopes-Cendes, C. Gaspar, O. Riess, L.P. Ranum, S.M. Pulst and G.a. Rouleau, 2000, "Cag Repeat Length in Rai1 Is Associated with Age at Onset Variability in Spinocerebellar Ataxia Type 2 (Sca2)", *Human Molecular Genetics*, Vol. 9, No. 12, pp. 1753-1758.

He, W. and R. Parker, 2000, "Functions of Lsm Proteins in Mrna Degradation and Splicing", *Current Opinion in Cell Biology*, Vol. 12, No. 3, pp. 346-350.

Hekman, K.E. and C.M. Gomez, 2015, "The Autosomal Dominant Spinocerebellar Ataxias: Emerging Mechanistic Themes Suggest Pervasive Purkinje Cell

Vulnerability", *Journal of Neurology, Neurosurgery, and Psychiatry*, Vol. 86, No. 5, pp. 554-561.

Hiji, M., T. Takahashi, H. Fukuba, H. Yamashita, T. Kohriyama and M. Matsumoto, 2008, "White Matter Lesions in the Brain with Frontotemporal Lobar Degeneration with Motor Neuron Disease: Tdp-43-Immunopositive Inclusions Co-Localize with P62, but Not Ubiquitin", *Acta Neuropathologica*, Vol. 116, No. 2, pp. 183-191.

Homma, T., D. Ishibashi, T. Nakagaki, K. Satoh, K. Sano, R. Atarashi and N. Nishida, 2014, "Increased Expression of P62/Sqstm1 in Prion Diseases and Its Association with Pathogenic Prion Protein", *Scientific Reports*, Vol. 4, pp. 4504-4504.

Huynh, D.P., M.R. Del Bigio, D.H. Ho and S.M. Pulst, 1999, "Expression of Ataxin-2 in Brains from Normal Individuals and Patients with Alzheimer's Disease and Spinocerebellar Ataxia 2", *Annals of Neurology*, Vol. 45, No. 2, pp. 232-241.

Huynh, D.P., H.T. Yang, H. Vakharia, D. Nguyen and S.M. Pulst, 2003, "Expansion of the Polyq Repeat in Ataxin-2 Alters Its Golgi Localization, Disrupts the Golgi Complex and Causes Cell Death", *Human Molecular Genetics*, Vol. 12, No. 13, pp. 1485-1496.

Imbert, G., F. Saudou, G. Yvert, D. Devys, Y. Trottier, J.-M. Garnier, C. Weber, J.-L. Mandel, G. Cancel, N. Abbas, A. Dürr, O. Didierjean, G. Stevanin, Y. Agid and A. Brice, 1996, "Cloning of the Gene for Spinocerebellar Ataxia 2 Reveals a Locus with High Sensitivity to Expanded Cag/Glutamine Repeats", *Nature Genetics*, Vol. 14, No. 3, pp. 285-291.

Inuzuka, M., M. Hayakawa and T. Ingi, 2005, "Serinc, an Activity-Regulated Protein Family, Incorporates Serine into Membrane Lipid Synthesis", *The Journal of Biological Chemistry*, Vol. 280, No. 42, pp. 35776-35783.

Jin, S.M. and R.J. Youle, 2012, "Pink1- and Parkin-Mediated Mitophagy at a Glance", *Journal of Cell Science*, Vol. 125, No. Pt 4, pp. 795-799.

Jobling, R.K., M. Assoum, O. Gakh, S. Blaser, J.A. Raiman, C. Mignot, E. Roze, A. Dürr, A. Brice, N. Lévy, C. Prasad, T. Paton, A.D. Paterson, N.M. Roslin, C.R. Marshall, J.-P. Desvignes, N. Roëckel-Trevisiol, S.W. Scherer, G.A. Rouleau, A. Mégarbané, G. Isaya, V. Delague and G. Yoon, 2015, "Pmpca Mutations Cause Abnormal Mitochondrial Protein Processing in Patients with Non-Progressive Cerebellar Ataxia", *Brain.*

Johnson, J.O., E.P. Pioro, A. Boehringer, R. Chia, H. Feit, A.E. Renton, H.A. Pliner, Y. Abramzon, G. Marangi, B.J. Winborn, J.R. Gibbs, M.A. Nalls, S. Morgan, M. Shoai, J. Hardy, A. Pittman, R.W. Orrell, A. Malaspina, K.C. Sidle, P. Fratta, M.B. Harms, R.H. Baloh, A. Pestronk, C.C. Weihl, E. Rogaeva, L. Zinman, V.E. Drory, G. Borghero, G. Mora, A. Calvo, J.D. Rothstein, C. Drepper, M. Sendtner, A.B. Singleton, J.P. Taylor, M.R. Cookson, G. Restagno, M. Sabatelli, R. Bowser, A. Chiò and B.J. Traynor, 2014, "Mutations in the Matrin 3 Gene Cause Familial Amyotrophic Lateral Sclerosis", *Nature Neuroscience*, Vol. 17, No. 5, pp. 664-666.

Juvonen, V., M. Hietala, V. Kairisto and M.L. Savontaus, 2005, "The Occurrence of Dominant Spinocerebellar Ataxias among 251 Finnish Ataxia Patients and the Role of Predisposing Large Normal Alleles in a Genetically Isolated Population", *Acta Neurologica Scandinavica*, Vol. 111, No. 3, pp. 154-162.

Kaneko, M., M. Ishiguro, Y. Niinuma, M. Uesugi and Y. Nomura, 2002, "Human Hrd1 Protects against Er Stress-Induced Apoptosis through Er-Associated Degradation", *FEBS Letters*, Vol. 532, No. 1-2, pp. 147-152.

Kaplan, A., K.J. Spiller, C. Towne, K.C. Kanning, G.T. Choe, A. Geber, T. Akay, P. Aebischer and C.E. Henderson, 2014, "Neuronal Matrix Metalloproteinase-9 Is a Determinant of Selective Neurodegeneration", *Neuron*, Vol. 81, No. 2, pp. 333-348.

Kathiresan, S., A.K. Manning, S. Demissie, R.B. D'Agostino, A. Surti, C. Guiducci, L. Gianniny, N.P. Burtt, O. Melander, M. Orho-Melander, D.K. Arnett, G.M. Peloso, J.M. Ordovas and L.A. Cupples, 2007, "A Genome-Wide Association Study for

Blood Lipid Phenotypes in the Framingham Heart Study", *BioMed Central Medical Genetics*, Vol. 8 Suppl 1, pp. S17-S17.

Kiehl, T.-R., A. Nechiporuk, K.P. Figueroa, M.T. Keating, D.P. Huynh and S.-M. Pulst, 2006, "Generation and Characterization of Sca2 (Ataxin-2) Knockout Mice", *Biochemical and Biophysical Research Communications*, Vol. 339, No. 1, pp. 17-24.

Kitada, T., S. Asakawa, N. Hattori, H. Matsumine, Y. Yamamura, S. Minoshima, M. Yokochi, Y. Mizuno and N. Shimizu, 1998, "Mutations in the Parkin Gene Cause Autosomal Recessive Juvenile Parkinsonism", *Nature*, Vol. 392, No. 6676, pp. 605-608.

Klinkenberg, M., S. Gispert, J.A. Dominguez-Bautista, I. Braun, G. Auburger and M. Jendrach, 2012, "Restriction of Trophic Factors and Nutrients Induces Parkin Expression", *Neurogenetics*, Vol. 13, No. 1, pp. 9-21.

Knight, S.J., A.V. Flannery, M.C. Hirst, L. Campbell, Z. Christodoulou, S.R. Phelps, J. Pointon, H.R. Middleton-Price, A. Barnicoat and M.E. Pembrey, 1993, "Trinucleotide Repeat Amplification and Hypermethylation of a Cpg Island in Fraxe Mental Retardation", *Cell*, Vol. 74, No. 1, pp. 127-134.

Kobayashi, H., K. Abe, T. Matsuura, Y. Ikeda, T. Hitomi, Y. Akechi, T. Habu, W. Liu, H. Okuda and A. Koizumi, 2011, "Expansion of Intronic Ggcctg Hexanucleotide Repeat in Nop56 Causes Sca36, a Type of Spinocerebellar Ataxia Accompanied by Motor Neuron Involvement", *The American Journal of Human Genetics*, Vol. 89, No. 1, pp. 121-130.

Köttgen, A., C. Pattaro, C.a. Böger, C. Fuchsberger, M. Olden, N.L. Glazer, A. Parsa, X. Gao, Q. Yang, A.V. Smith, J.R.O. Connell, M. Li, H. Schmidt and T. Tanaka, 2010, "Multiple Loci Associated with Indices of Renal Function and Chronic Kidney Disease", *Nature Genetics*, Vol. 42, No. 5, pp. 376-384.

Laffita-Mesa, J.M., P.O. Bauer, V. Kourí, L.P. Serrano, J. Roskams, D.A. Gotay, J.C.M. Brown, P.A.M. Rodríguez, Y. González-Zaldívar, L.A. Mederos, D. Cuello-Almarales and J.A. Santiago, 2012, "Epigenetics DNA Methylation in the Core Ataxin-2 Gene Promoter: Novel Physiological and Pathological Implications", *Human Genetics*, Vol. 131, pp. 625-638.

Lagathu, C., C. Christodoulides, S. Virtue, W.P. Cawthorn, C. Franzin, W.A. Kimber, E.D. Nora, M. Campbell, G. Medina-Gomez, B.N.R. Cheyette, A.J. Vidal-Puig and J.K. Sethi, 2009, "Dact1, a Nutritionally Regulated Preadipocyte Gene, Controls Adipogenesis by Coordinating the Wnt/Beta-Catenin Signaling Network", *Diabetes*, Vol. 58, No. 3, pp. 609-619.

Lahut, S., Ö. Ömür, Ö. Uyan, Z.S. Ağim, A. Özoğuz, Y. Parman, F. Deymeer, P. Oflazer, F. Koç, H. Özçelik, G. Auburger and a.N. Başak, 2012, "Atxn2 and Its Neighbouring Gene Sh2b3 Are Associated with Increased Als Risk in the Turkish Population", *Public Library of Science One*, Vol. 7, No. 8,

Lastres-Becker, I., S. Brodesser, D. Lütjohann, M. Azizov, J. Buchmann, E. Hintermann, K. Sandhoff, A. Schürmann, J. Nowock and G. Auburger, 2008a, "Insulin Receptor and Lipid Metabolism Pathology in Ataxin-2 Knock-out Mice", *Human Molecular Genetics*, Vol. 17, No. 10, pp. 1465-1481.

Lastres-Becker, I., U. Rüb and G. Auburger, 2008b, "Spinocerebellar Ataxia 2 (Sca2)", *Cerebellum*, Vol. 7, No. 2, pp. 115-124.

Lee, T., Y.R. Li, C. Ingre, M. Weber, T. Grehl, O. Gredal, M. de Carvalho, T. Meyer, O.-B. Tysnes, G. Auburger, S. Gispert, N.M. Bonini, P.M. Andersen and A.D. Gitler, 2011, "Ataxin-2 Intermediate-Length Polyglutamine Expansions in European Als Patients", *Human Molecular Genetics*, Vol. 20, No. 9, pp. 1697-1700.

Lessing, D. and N.M. Bonini, 2008, "Polyglutamine Genes Interact to Modulate the Severity and Progression of Neurodegeneration in Drosophila", *Public Library of Science Biology*, Vol. 6, No. 2, pp. e29-e29.

Li, S.-H. and X.-J. Li, 2004, "Huntingtin-Protein Interactions and the Pathogenesis of Huntington's Disease", *Trends in Genetics*, Vol. 20, No. 3, pp. 146-154.

Li, Y.R., O.D. King, J. Shorter and A.D. Gitler, 2013, "Stress Granules as Crucibles of Als Pathogenesis", *Journal of Cell Biology*, Vol. 201, No. 3, pp. 361-372.

Lilienbaum, A., 2013, "Relationship between the Proteasomal System and Autophagy", *International Journal of Biochemistry and Molecular Biology*, Vol. 4, No. 1, pp. 1-26.

Lim, J., J. Crespo-Barreto, P. Jafar-Nejad, A.B. Bowman, R. Richman, D.E. Hill, H.T. Orr and H.Y. Zoghbi, 2008, "Opposing Effects of Polyglutamine Expansion on Native Protein Complexes Contribute to Sca1", *Nature*, Vol. 452, No. 7188, pp. 713-718.

Lim, J., T. Hao, C. Shaw, A.J. Patel, G. Szabó, J.-F. Rual, C.J. Fisk, N. Li, A. Smolyar, D.E. Hill, A.-L. Barabási, M. Vidal and H.Y. Zoghbi, 2006, "A Protein-Protein Interaction Network for Human Inherited Ataxias and Disorders of Purkinje Cell Degeneration", *Cell*, Vol. 125, No. 4, pp. 801-814.

Lim, J., M.L. Lachenmayer, S. Wu, W. Liu, M. Kundu, R. Wang, M. Komatsu, Y.J. Oh, Y. Zhao and Z. Yue, 2015, "Proteotoxic Stress Induces Phosphorylation of P62/Sqstm1 by Ulk1 to Regulate Selective Autophagic Clearance of Protein Aggregates", *Public Library of Science Genetics*, Vol. 11, No. 2, pp. e1004987-e1004987.

Lin, X., B. Antalffy, D. Kang, H.T. Orr and H.Y. Zoghbi, 2000, "Polyglutamine Expansion Down-Regulates Specific Neuronal Genes before Pathologic Changes in Sca1", *Nature Neuroscience*, Vol. 3, No. 2, pp. 157-163.

Liu, J., T.-S. Tang, H. Tu, O. Nelson, E. Herndon, D.P. Huynh, S.M. Pulst and I. Bezprozvanny, 2009, "Deranged Calcium Signaling and Neurodegeneration in

Spinocerebellar Ataxia Type 2", *The Journal of Neuroscience*, Vol. 29, No. 29, pp. 9148-9162.

Liu, X., M. Lu, L. Tang, N. Zhang, D. Chui and D. Fan, 2013, "Atxn2 Cag Repeat Expansions Increase the Risk for Chinese Patients with Amyotrophic Lateral Sclerosis", *Neurobiology of Aging*, Vol. 34, No. 9, pp. 2236.e2235-2238.

Livak, K.J. and T.D. Schmittgen, 2001, "Analysis of Relative Gene Expression Data Using Real-Time Quantitative Pcr and the 2(-Delta Delta C(T)) Method", *Methods*, Vol. 25, No. 4, pp. 402-408.

Lopes-Cendes, I., H.G. Teive, M.E. Calcagnotto, J.C. Da Costa, F. Cardoso, E. Viana, J.A. Maciel, J. Radvany, W.O. Arruda, P.C. Trevisol-Bittencourt, P. Rosa Neto, I. Silveira, C.E. Steiner, W. Pinto Júnior, A.S. Santos, Y. Correa Neto, L.C. Werneck, A.Q. Araújo, G. Carakushansky, L.R. Mello, L.B. Jardim and G.A. Rouleau, 1997, "Frequency of the Different Mutations Causing Spinocerebellar Ataxia (Sca1, Sca2, Mjd/Sca3 and Drpla) in a Large Group of Brazilian Patients", *Arquivos de Neuro-psiquiatria*, Vol. 55, No. 3B, pp. 519-529.

Mangus, D.a., M.C. Evans, N.S. Agrin, M. Smith, P. Gongidi, and A. Jacobson, 2004, "Positive and Negative Regulation of Poly (a) Nuclease", *Molecular Cell Biology*, Vol. 24, No. 12, pp. 5521-5533.

Mao, R., A.S. Aylsworth, N. Potter, W.G. Wilson, G. Breningstall, M.J. Wick, D. Babovic-Vuksanovic, M. Nance, M.C. Patterson, C.M. Gomez and K. Snow, 2002, "Childhood-Onset Ataxia: Testing for Large Cag-Repeats in Sca2 and Sca7", *American Journal of Medical Genetics*, Vol. 110, No. 4, pp. 338-345.

Matilla-Dueñas, A., T. Ashizawa, A. Brice, S. Magri, K.N. McFarland, M. Pandolfo, S.M. Pulst, O. Riess, D.C. Rubinsztein, J. Schmidt, T. Schmidt, D.R. Scoles, G. Stevanin, F. Taroni, B.R. Underwood and I. Sánchez, 2014, "Consensus Paper: Pathological Mechanisms Underlying Neurodegeneration in Spinocerebellar Ataxias", *Cerebellum*, Vol. 13, No. 2, pp. 269-302.

Matsumura, R., N. Futamura, N. Ando and S. Ueno, 2003, "Frequency of Spinocerebellar Ataxia Mutations in the Kinki District of Japan", *Acta Neurologica Scandinavica*, Vol. 107, No. 1, pp. 38-41.

McCann, C., E.E. Holohan, S. Das, A. Dervan, A. Larkin, J.A. Lee, V. Rodrigues, R. Parker and M. Ramaswami, 2011, "The Ataxin-2 Protein Is Required for Microrna Function and Synapse-Specific Long-Term Olfactory Habituation", *Proceedings of the National Academy of Sciences of the United States of America*, Vol. 108, No. 36, pp. E655-E662.

McMurray, C., 2010, "Mechanisms of Trinucleotide Repeat Instability During Human Development", *Nature Reviews Genetics*, Vol. 11, No. 11, pp. 786-799.

Mirkin, S.M., 2007, "Expandable DNA Repeats and Human Disease", *Nature*, Vol. 447, No. 7147, pp. 932-940.

Moretti, P., M. Blazo, L. Garcia, D. Armstrong, R.A. Lewis, B. Roa and F. Scaglia, 2004, "Spinocerebellar Ataxia Type 2 (Sca2) Presenting with Ophthalmoplegia and Developmental Delay in Infancy", *American Journal of Medical Genetics. Part A*, Vol. 124A, No. 4, pp. 392-396.

Mueller, B., E.J. Klemm, E. Spooner, J.H. Claessen and H.L. Ploegh, 2008, "Sel1l Nucleates a Protein Complex Required for Dislocation of Misfolded Glycoproteins", *Proceedings of the National Academy of Sciences of the United States of America*, Vol. 105, No. 34, pp. 12325-12330.

Nakamura, K., T. Mieda, N. Suto, S. Matsuura and H. Hirai, 2014, "Mesenchymal Stem Cells as a Potential Therapeutic Tool for Spinocerebellar Ataxia", *The Cerebellum*, Vol. 14, No. 2, pp. 165-170.

Nechiporuk, T., D.P. Huynh, K. Figueroa, S. Sahba, A. Nechiporuk and S.M. Pulst, 1998, "The Mouse Sca2 Gene: Cdna Sequence, Alternative Splicing and Protein Expression", *Human Molecular Genetics*, Vol. 7, No. 8, pp. 1301-1309.

Nielsen, T.T., K. Svenstrup, E. Budtz-Jørgensen, H. Eiberg, L. Hasholt and J.E. Nielsen, 2012, "Atxn2 with Intermediate-Length Cag/Caa Repeats Does Not Seem to Be a Risk Factor in Hereditary Spastic Paraplegia", *Journal of the Neurological Sciences*, Vol. 321, No. 1-2, pp. 100-102.

Nonhoff, U., M. Ralser, F. Welzel, I. Piccini, D. Balzereit, M.-L. Yaspo, H. Lehrach and S. Krobitsch, 2007, "Ataxin-2 Interacts with the Dead/H-Box Rna Helicase Ddx6 and Interferes with P-Bodies and Stress Granules", *Molecular Biology of the Cell*, Vol. 18, No. 4, pp. 1385-1396.

Nonis, D., M.H.H. Schmidt, S. van de Loo, F. Eich, I. Dikic, J. Nowock and G. Auburger, 2008, "Ataxin-2 Associates with the Endocytosis Complex and Affects Egf Receptor Trafficking", *Cellular Signalling*, Vol. 20, No. 10, pp. 1725-1739.

Oka, T., T. Sayano, S. Tamai, S. Yokota, H. Kato, G. Fujii and K. Mihara, 2008, "Identification of a Novel Protein Mics1 That Is Involved in Maintenance of Mitochondrial Morphology and Apoptotic Release of Cytochrome C", *Molecular Biology of the Cell*, Vol. 19, No. 6, pp. 2597-2608.

Orr, H.T., M.Y. Chung, S. Banfi, T.J. Kwiatkowski, A. Servadio, A.L. Beaudet, A.E. McCall, L.A. Duvick, L.P. Ranum and H.Y. Zoghbi, 1993, "Expansion of an Unstable Trinucleotide Cag Repeat in Spinocerebellar Ataxia Type 1", *Nature Genetics*, Vol. 4, No. 3, pp. 221-226.

Orr, H.T. and H.Y. Zoghbi, 2007, "Trinucleotide Repeat Disorders", *Annual Review of Neuroscience*, Vol. 30, pp. 575-621.

Park, J.H., B.R. Yoon, H.J. Kim, P.H. Lee, B.-O. Choi and K.W. Chung, 2014, "Compound Mitochondrial DNA Mutations in a Neurological Patient with Ataxia, Myoclonus and Deafness", *Journal of Genetics*, Vol. 93, No. 1, pp. 173-177.

Payami, H., J. Nutt, S. Gancher, T. Bird, M.G. McNeal, W.K. Seltzer, J. Hussey, P. Lockhart, K. Gwinn-Hardy, A.A. Singleton, A.B. Singleton, J. Hardy and M. Farrer, 2003, "Sca2 May Present as Levodopa-Responsive Parkinsonism", *Movement Disorders*, Vol. 18, No. 4, pp. 425-429.

Phillips, M.C., 2014, "Molecular Mechanisms of Cellular Cholesterol Efflux", *Journal of Biological Chemistry*, Vol. 289, No. 35, pp. 24020-24029.

Planagumà, J., M. Liljeström, F. Alameda, R. Bützow, I. Virtanen, J. Reventós and M. Hukkanen, 2011, "Matrix Metalloproteinase-2 and Matrix Metalloproteinase-9 Codistribute with Transcription Factors Runx1/Aml1 and Etv5/Erm at the Invasive Front of Endometrial and Ovarian Carcinoma", *Human Pathology*, Vol. 42, No. 1, pp. 57-67.

Potter, M.D., A. Buijs, B. Kreider, L. van Rompaey and G.C. Grosveld, 2000, "Identification and Characterization of a New Human Ets-Family Transcription Factor, Tel2, That Is Expressed in Hematopoietic Tissues and Can Associate with Tel1/Etv6", *Blood*, Vol. 95, No. 11, pp. 3341-3348.

Price, N.M., J. Farrar, T.T. Tran, T.H. Nguyen, T.H. Tran and J.S. Friedland, 2001, "Identification of a Matrix-Degrading Phenotype in Human Tuberculosis in Vitro and in Vivo", *Journal of Immunology*, Vol. 166, No. 6, pp. 4223-4230.

Pruijt, J.F., W.E. Fibbe, L. Laterveer, R.A. Pieters, I.J. Lindley, L. Paemen, S. Masure, R. Willemze and G. Opdenakker, 1999, "Prevention of Interleukin-8-Induced Mobilization of Hematopoietic Progenitor Cells in Rhesus Monkeys by Inhibitory Antibodies against the Metalloproteinase Gelatinase B (Mmp-9)", *Proceedings of the National Academy of Sciences of the United States of America*, Vol. 96, No. 19, pp. 10863-10868.

Przedborski, S., M. Vila and V. Jackson-lewis, 2003, "Neurodegeneration : What Is It and Where Are We ?", *Journal of Clinical Investigations*, Vol. 111, No. 1, pp. 3-10.

Pujana, M.A., J. Corral, M. Gratacòs, O. Combarros, J. Berciano, D. Genís, I. Banchs, X. Estivill and V. Volpini, 1999, "Spinocerebellar Ataxias in Spanish Patients: Genetic Analysis of Familial and Sporadic Cases. The Ataxia Study Group", *Human Genetics*, Vol. 104, No. 6, pp. 516-522.

Pulst, S.M., A. Nechiporuk, T. Nechiporuk, S. Gispert, X.N. Chen, I. Lopes-Cendes, S. Pearlman, S. Starkman, G. Orozco-Diaz, A. Lunkes, P. DeJong, G.A. Rouleau, G. Auburger, J.R. Korenberg, C. Figueroa and S. Sahba, 1996, "Moderate Expansion of a Normally Biallelic Trinucleotide Repeat in Spinocerebellar Ataxia Type 2", *Nature Genetics*, Vol. 14, No. 3, pp. 269-276.

Ragothaman, M. and U. Muthane, 2008, "Homozygous Sca 2 Mutations Changes Phenotype and Hastens Progression", *Movement Disorders*, Vol. 23, No. 5, pp. 770-771.

Ralser, M., U. Nonhoff, M. Albrecht, T. Lengauer, E.E. Wanker, H. Lehrach and S. Krobitsch, 2005, "Ataxin-2 and Huntingtin Interact with Endophilin-a Complexes to Function in Plastin-Associated Pathways", *Human Molecular Genetics*, Vol. 14, No. 19, pp. 2893-2909.

Ramachandra, N.B. and L. Kusuma, 2015, "An Understanding of Spinocerebellar Ataxia", *The Indian Journal of Medical Research*, Vol. 141, No. 2, pp. 148-150.

Reddy, K., B. Zamiri, S.Y.R. Stanley, R.B. Macgregor and C.E. Pearson, 2013, "The Disease-Associated R(Ggggcc)N Repeat from the C9orf72 Gene Forms Tract Length-Dependent Uni- and Multimolecular Rna G-Quadruplex Structures", *The Journal of Biological Chemistry*, Vol. 288, No. 14, pp. 9860-9866.

Renton, A.E., A. Chiò and B.J. Traynor, 2014, "State of Play in Amyotrophic Lateral Sclerosis Genetics", *Nature Neuroscience*, Vol. 17, No. 1, pp. 17-23.

Renton, A.E., E. Majounie, A. Waite, J. Simón-Sánchez, S. Rollinson, J.R. Gibbs, J.C. Schymick, H. Laaksovirta, J.C. van Swieten, L. Myllykangas, H. Kalimo, A. Paetau, Y. Abramzon, A.M. Remes, A. Kaganovich, S.W. Scholz, J. Duckworth, J. Ding, D.W. Harmer, D.G. Hernandez, J.O. Johnson, K. Mok, M. Ryten, D. Trabzuni, R.J. Guerreiro, R.W. Orrell, J. Neal, A. Murray, J. Pearson, I.E. Jansen, D. Sondervan, H. Seelaar, D. Blake, K. Young, N. Halliwell, J.B. Callister, G. Toulson, A. Richardson, A. Gerhard, J. Snowden, D. Mann, D. Neary, M.A. Nalls, T. Peuralinna, L. Jansson, V.-M. Isoviita, A.-L. Kaivorinne, M. Hölttä-Vuori, E. Ikonen, R. Sulkava, M. Benatar, J. Wuu, A. Chiò, G. Restagno, G. Borghero, M. Sabatelli, D. Heckerman, E. Rogaeva, L. Zinman, J.D. Rothstein, M. Sendtner, C. Drepper, E.E. Eichler, C. Alkan, Z. Abdullaev, S.D. Pack, A. Dutra, E. Pak, J. Hardy, A. Singleton, N.M. Williams, P. Heutink, S. Pickering-Brown, H.R. Morris, P.J. Tienari and B.J. Traynor, 2011, "A Hexanucleotide Repeat Expansion in C9orf72 Is the Cause of Chromosome 9p21-Linked Als-Ftd", *Neuron*, Vol. 72, No. 2, pp. 257-268.

Riess, O., F.A. Laccone, S. Gispert, L. Schöls, C. Zühlke, A.M. Vieira-Saecker, S. Herlt, K. Wessel, J.T. Epplen, B.H. Weber, F. Kreuz, S. Chahrokh-Zadeh, A. Meindl, A. Lunkes, J. Aguiar, M. Macek, A. Krebsová, K. Bürk, S. Tinschert, I. Schreyer, S.M. Pulst and G. Auburger, 1997, "Sca2 Trinucleotide Expansion in German Sca Patients", *Neurogenetics*, Vol. 1, No. 1, pp. 59-64.

Ross, O.a., N.J. Rutherford, M. Baker, A.I. Soto-Ortolaza, M.M. Carrasquillo, M. DeJesus-Hernandez, J. Adamson, M. Li, K. Volkening, E. Finger, W.W. Seeley, K.J. Hatanpaa, C. Lomen-Hoerth, A. Kertesz, E.H. Bigio, C. Lippa, B.K. Woodruff, D.S. Knopman, C.L. White, J.a. Van Gerpen, J.F. Meschia, I.R. Mackenzie, K. Boylan, B.F. Boeve, B.L. Miller, M.J. Strong, R.J. Uitti, S.G. Younkin, N.R. Graff-Radford, R.C. Petersen, Z.K. Wszolek, D.W. Dickson and R. Rademakers, 2011, "Ataxin-2 Repeat-Length Variation and Neurodegeneration", *Human Molecular Genetics*, Vol. 20, No. 16, pp. 3207-3212.

Rottnek, M., S. Riggio, W. Byne, M. Sano, R.L. Margolis and R.H. Walker, 2008, "Schizophrenia in a Patient with Spinocerebellar Ataxia 2: Coincidence of Two Disorders or a Neurodegenerative Disease Presenting with Psychosis?", *The American Journal of Psychiatry*, Vol. 165, No. 8, pp. 964-967.

Rüb, U., L. Schöls, H. Paulson, G. Auburger, P. Kermer, J.C. Jen, K. Seidel, H.W. Korf and T. Deller, 2013, "Clinical Features, Neurogenetics and Neuropathology of the Polyglutamine Spinocerebellar Ataxias Type 1, 2, 3, 6 and 7", *Progress in Neurobiology*, Vol. 104, pp. 38-66.

Saegusa, H., M. Wakamori, Y. Matsuda, J. Wang, Y. Mori, S. Zong and T. Tanabe, 2007, "Properties of Human Cav2.1 Channel with a Spinocerebellar Ataxia Type 6 Mutation Expressed in Purkinje Cells", *Molecular and Cellular Neurosciences*, Vol. 34, No. 2, pp. 261-270.

Sahba, S., A. Nechiporuk, K.P. Figueroa, T. Nechiporuk and S.M. Pulst, 1998, "Genomic Structure of the Human Gene for Spinocerebellar Ataxia Type 2 (Sca2) on Chromosome 12q24.1", *Genomics*, Vol. 47, No. 3, pp. 359-364.

Sanpei, K., H. Takano, S. Igarashi, T. Sato, M. Oyake, H. Sasaki, A. Wakisaka, K. Tashiro, Y. Ishida, T. Ikeuchi, R. Koide, M. Saito, A. Sato, T. Tanaka, S. Hanyu, Y. Takiyama, M. Nishizawa, N. Shimizu, Y. Nomura, M. Segawa, K. Iwabuchi, I. Eguchi, H. Tanaka, H. Takahashi and S. Tsuji, 1996, "Identification of the Spinocerebellar Ataxia Type 2 Gene Using a Direct Identification of Repeat Expansion and Cloning Technique, Direct", *Nature Genetics*, Vol. 14, No. 3, pp. 277-284.

Sato, N., T. Amino, K. Kobayashi, S. Asakawa, T. Ishiguro, T. Tsunemi, M. Takahashi, T. Matsuura, K.M. Flanigan, S. Iwasaki, F. Ishino, Y. Saito, S. Murayama, M. Yoshida, Y. Hashizume, Y. Takahashi, S. Tsuji, N. Shimizu, T. Toda, K. Ishikawa and H. Mizusawa, 2009, "Spinocerebellar Ataxia Type 31 Is Associated with

"Inserted" Penta-Nucleotide Repeats Containing (Tggaa)N", *American Journal of Human Genetics*, Vol. 85, No. 5, pp. 544-557.

Satterfield, T.F., S.M. Jackson and L.J. Pallanck, 2002, "A Drosophila Homolog of the Polyglutamine Disease Gene Sca2 Is a Dosage-Sensitive Regulator of Actin Filament Formation", *Genetics*, Vol. 162, No. 4, pp. 1687-1702.

Satterfield, T.F. and L.J. Pallanck, 2006, "Ataxin-2 and Its Drosophila Homolog, Atx2, Physically Assemble with Polyribosomes", *Human Molecular Genetics*, Vol. 15, No. 16, pp. 2523-2532.

Scherzed, W., E.R. Brunt, H. Heinsen, R.a. De Vos, K. Seidel, K. Bürk, L. Schöls, G. Auburger, D. Del Turco, T. Deller, H.W. Korf, W.F. Den Dunnen and U. Rüb, 2012, "Pathoanatomy of Cerebellar Degeneration in Spinocerebellar Ataxia Type 2 (Sca2) and Type 3 (Sca3)", *Cerebellum*, Vol. 11, No. 3, pp. 749-760.

Scoles, D.R., L.T. Pflieger, K.K. Thai, S.T. Hansen, W. Dansithong and S.M. Pulst, 2012, "Ets1 Regulates the Expression of Atxn2", *Human Molecular Genetics*, Vol. 21, No. 23, pp. 5048-5065.

Seidel, K., S. Siswanto, E.R.P. Brunt, W. den Dunnen, H.-W. Korf and U. Rüb, 2012, "Brain Pathology of Spinocerebellar Ataxias", *Acta Neuropathologica*, Vol. 124, No. 1, pp. 1-21.

Shibata, H., D.P. Huynh and S.M. Pulst, 2000, "A Novel Protein with Rna-Binding Motifs Interacts with Ataxin-2", *Human Molecular Genetics*, Vol. 9, No. 9, pp. 1303-1313.

Spadafora, P., G. Annesi, M. Liguori, P. Tarantino, N. Cutuli, S. Carrideo, I.C. Cirò Candiano, E.V. De Marco, D. Civitelli, F. Annesi, S. Giuffrida and A. Quattrone, 2007, "Gene Dosage Influences the Age at Onset of Sca2 in a Family from Southern Italy", *Clinical Genetics*, Vol. 72, No. 4, pp. 381-383.

Suriben, R., S. Kivimäe, D.A.C. Fisher, R.T. Moon and B.N.R. Cheyette, 2009, "Posterior Malformations in Dact1 Mutant Mice Arise through Misregulated Vangl2 at the Primitive Streak", *Nature Genetics*, Vol. 41, No. 9, pp. 977-985.

Swarup, V., A.K. Srivastava, M.V. Padma and R.R. Moganty, 2013, "Quantitative Profiling and Identification of Plasma Proteins of Spinocerebellar Ataxia Type 2 Patients", *Neuro-degenerative Diseases*, Vol. 12, No. 4, pp. 199-206.

Takahara, T. and T. Maeda, 2012, "Transient Sequestration of Torc1 into Stress Granules During Heat Stress", *Molecular Cell*, Vol. 47, No. 2, pp. 242-252.

Tian, X., U. Gala, Y. Zhang, W. Shang, S. Nagarkar Jaiswal, A. di Ronza, M. Jaiswal, S. Yamamoto, H. Sandoval, L. Duraine, M. Sardiello, R.V. Sillitoe, K. Venkatachalam, H. Fan, H.J. Bellen and C. Tong, 2015, "A Voltage-Gated Calcium Channel Regulates Lysosomal Fusion with Endosomes and Autophagosomes and Is Required for Neuronal Homeostasis", *Public Library of Science Biology*, Vol. 13, No. 3, pp. e1002103-e1002103.

Todd, P.K. and H.L. Paulson, 2010, "Rna-Mediated Neurodegeneration in Repeat Expansion Disorders", *Annals of Neurology*, Vol. 67, No. 3, pp. 291-300.

Tolosano, E., S. Fagoonee, N. Morello, F. Vinchi and V. Fiorito, 2010, "Heme Scavenging and the Other Facets of Hemopexin", *Antioxidants and Redox Signaling*, Vol. 12, No. 2, pp. 305-320.

van Blitterswijk, M., B. Mullen, M.G. Heckman, M.C. Baker, M. DeJesus-Hernandez, P.H. Brown, M.E. Murray, G.Y.R. Hsiung, H. Stewart, A.M. Karydas, E. Finger, A. Kertesz, E.H. Bigio, S. Weintraub, M. Mesulam, K.J. Hatanpaa, C.L. White, M. Neumann, M.J. Strong, T.G. Beach, Z.K. Wszolek, C. Lippa, R. Caselli, L. Petrucelli, K.a. Josephs, J.E. Parisi, D.S. Knopman, R.C. Petersen, I.R. Mackenzie, W.W. Seeley, L.T. Grinberg, B.L. Miller, K.B. Boylan, N.R. Graff-Radford, B.F. Boeve, D.W. Dickson and R. Rademakers, 2014, "Ataxin-2 as Potential Disease Modifier in C9orf72 Expansion Carriers", *Neurobiology of Aging*, Vol. 35, pp. 1-5.

Van den Heuvel, D.M.a., O. Harschnitz, L.H. van den Berg and R.J. Pasterkamp, 2014, "Taking a Risk: A Therapeutic Focus on Ataxin-2 in Amyotrophic Lateral Sclerosis?", *Trends in Molecular Medicine*, Vol. 20, No. 1, pp. 25-35.

Velázquez-Perez, L., R. Rodríguez-Labrada, N. Canales-Ochoa, G. Sanchez-Cruz, J. Fernandez-Ruiz, J.M. Montero, R. Aguilera-Rodríguez, R. Diaz, L.E. Almaguer-Mederos and A.P. Truitz, 2010, "Progression Markers of Spinocerebellar Ataxia 2. A Twenty Years Neurophysiological Follow up Study", *Journal of the Neurological Sciences*, Vol. 290, No. 1-2, pp. 22-26.

Wadia, N.H. and R.K. Swami, 1971, "A New Form of Heredo-Familial Spinocerebellar Degeneration with Slow Eye Movements (Nine Families)", *Brain*, Vol. 94, No. 2, pp. 359-374.

Wang, S., B. Wang, N. Pan, L. Fu, C. Wang, G. Song, J. An, Z. Liu, W. Zhu, Y. Guan, Z.-Q.D. Xu, P. Chan, Z. Chen and Y.A. Zhang, 2015, "Differentiation of Human Induced Pluripotent Stem Cells to Mature Functional Purkinje Neurons", *Scientific Reports*, Vol. 5, pp. 9232-9232.

Wang, Y.-C., C.-M. Lee, L.-C. Lee, L.-C. Tung, H.-M. Hsieh-Li, G.-J. Lee-Chen and M.-T. Su, 2011, "Mitochondrial Dysfunction and Oxidative Stress Contribute to the Pathogenesis of Spinocerebellar Ataxia Type 12 (Sca12)", *The Journal of Biological Chemistry*, Vol. 286, No. 24, pp. 21742-21754.

Wiedemeyer, R., F. Westermann, I. Wittke, J. Nowock and M. Schwab, 2003, "Ataxin-2 Promotes Apoptosis of Human Neuroblastoma Cells", *Oncogene*, Vol. 22, No. 3, pp. 401-411.

Wong, Y.C. and E.L.F. Holzbaur, 2015, "Autophagosome Dynamics in Neurodegeneration at a Glance", *Journal of Cell Science*, Vol. 128, No. 7, pp. 1259-1267.

Yokoshi, M., Q. Li, M. Yamamoto, H. Okada, Y. Suzuki and Y. Kawahara, 2014, "Direct Binding of Ataxin-2 to Distinct Elements in 3' Utrs Promotes Mrna Stability and Protein Expression", *Molecular Cell*, Vol. 55, No. 2, pp. 186-198.

Yu, Z., Y. Zhu, A.S. Chen-Plotkin, D. Clay-Falcone, L. McCluskey, L. Elman, R.G. Kalb, J.Q. Trojanowski, V.M.Y. Lee, V.M. van Deerlin, A.D. Gitler and N.M. Bonini, 2011, "Polyq Repeat Expansions in Atxn2 Associated with Als Are Caa Interrupted Repeats", *Public Library of Science One*, Vol. 6, No. 3, pp. 14-19.

Zeitlin, S., J.P. Liu, D.L. Chapman, V.E. Papaioannou and A. Efstratiadis, 1995, "Increased Apoptosis and Early Embryonic Lethality in Mice Nullizygous for the Huntington's Disease Gene Homologue", *Nature Genetics*, Vol. 11, No. 2, pp. 155-163.

Zhang, F., G. Wang, Y.Y. Shugart, Y. Xu, C. Liu, L. Wang, T. Lu, H. Yan, Y. Ruan, Z. Cheng, L. Tian, C. Jin, J. Yuan, Z. Wang, W. Zhu, L. Cao, Y. Liu, W. Yue and D. Zhang, 2014, "Association Analysis of a Functional Variant in Atxn2 with Schizophrenia", *Neuroscience Letters*, Vol. 562, pp. 24-27.